FLP-type Nitrile Activation and Cyclic Ether Ring Opening by Halo-Borane Nonagermanide-Cluster Lewis Acid-Base-Pairs

Supporting Information

Content

Experimental details

General. All manipulations were performed under oxygen-free, dry conditions under argon atmosphere using standard Schlenk or glove box techniques. Glassware was dried prior to use by heating it *in vacuo*. The solvents used were obtained from an MBraun Grubbs apparatus. All other commercially available chemicals were used without further purification. K_4Ge_9 was prepared by fusion of stoichiometric amounts of the elements in stainless-steel tubes at 650 °C. The silylated $[Ge_9]$ clusters $[Ge_9\{Si(TMS)_3\}_2]^{2-}$,[1] the halo-diazaborolidines DAB^R-Br (DAB = 2-bromo-1,3,2-diazaborolidine; R = *o*-tol. *o*-xyl, Mes, Dipp),[2] 2-bromo-1,3,2-diazaborole $DAB(II)^{Dipp}$-Br,[2] and $(^iPr_2N)_2B$-*X* (*X*: Cl, Br) were synthesized according to modified literature procedures.[3]

Single crystal structure determination. The air- and moisture-sensitive crystals of **3** to **6** were transferred from the mother liquor into perfluoroalkyl ether oil under inert gas atmosphere in a glove box. For diffraction data collection, the single crystals were fixed on a glass capillary and positioned in a 150 K cold N_2 gas stream using the crystal cap system. Data collection was performed with a STOE StadiVari diffractometer ($Mo_{K\alpha}$ radiation) equipped with a DECTRIS PILATUS 300K detector. Structures were solved by Direct Methods (SHELXS-97) and refined by full-matrix least-squares calculations against F^2 (SHELXL-2014 or SHELXL-2018).[4] The positions of the hydrogen atoms were calculated and refined using a riding model. Unless stated otherwise, all non-hydrogen atoms were treated with anisotropic displacement parameters. The supplementary crystallographic data for this paper have been deposited with the Cambridge Structural database and are available free of charge *via* www.ccdc.cam.ac.uk/data_request/cif. The crystallographic data for compounds **3** to **6** are summarized in Table S3. In compound **4** disordered solvent molecules have been taken care of by the Platon squeeze function.[5]

NMR spectroscopy. NMR spectra were measured on a Bruker Avance Ultrashield 400 MHz spectrometer. Chemical shifts are reported in parts per million (ppm) relative to TMS, with the solvent peaks serving as internal reference.[6] Abbreviations for signal multiplicities are: singlet (s), doublet (d), triplet (t), heptet (hept), broad signal (brs).

Elemental analysis. Elemental analyses were carried out in the microanalytical laboratory of the Chemistry Department of Technische Universität München. Analyses of C, H, N were performed in a combustion analyzer (EURO EA, HEKA tech).

Electron Spray Ionization Mass Spectrometry (ESI MS). Sample preparation was performed under inert conditions using a glove box. Data collection was performed using a Bruker Daltronic HTC mass spectrometer (dry gas temperature: 300 °C; injection speed 240 μl/h), and the data were processed using the Bruker Compass Data Analysis 4.0 SP 5 program (Bruker). The spectra were plotted using Excel 2016 (Microsoft) and OriginPro2016G (Origin Lab). Simulated spectra are always shown as black bars.

Syntheses.

K[Ge₉{Si(TMS)₃}₂DAB^{o-tol}] (1): In a typical experiment equimolar amounts of $K_2[Ge_9\{Si(TMS)_3\}_2]$ (92 mg, 0.075 mmol. 1 equiv.) and DAB^{o-tol}-Br (24.7 mg, 0.075 mmol, 1 equiv.) were weighted into a Schlenk tube in the glove box, and dioxane (3 mL) was added to obtain a deep red solution. After stirring for 5 h at room temperature, the solvent was removed *in vacuo* yielding an ochre solid. Subsequent dissolution in toluene (15 mL) gave a dark red solution, which was filtered. Upon concentration, the product precipitated as microcrystalline solid from the solution. The mother liquor was filtered-off, and the solid was dried *in vacuo* to yield the product as a dark yellow microcrystalline powder (65 mg, 0.045 mmol,

60 % yield). **¹H NMR** (400 MHz, 298 K, thf-d_8): δ [ppm] = 7.16-7.11 (m, 2H, CH$_{Ph}$), 7.08-7.04 (m, 2H, CH$_{Ph}$), 7.01-6.90 (m, 4H, CH$_{Ph}$), 3.65 (s, 4H, CH$_{2(Bb)}$), 2.35 (s, 6H, Me), 0.18 (s, 54H, Me$_{TMS}$). **¹³C NMR** (101 MHz, 298 K, thf-d_8): δ [ppm] = 147.03 (s, C$_{Ph(N)}$), 137.19 (s, C$_{Ph(Me)}$), 131.38 (s, CH$_{Ph}$), 130.60 (s, CH$_{Ph}$), 127.08 (s, CH$_{Ph}$), 125.66 (s, CH$_{Ph}$), 53.93 (s, CH$_{2(Bb)}$), 20.14 (s, Me), 3.28 (s, Me$_{TMS}$). **²⁹Si-INEPT NMR** (79 MHz, 298 K, thf-d_8): δ [ppm] = -9.99 (s, Si$_{TMS}$), -108.80 (s, Si$_{Ge9}$). **¹¹B NMR** (128 MHz, 298 K, thf-d_8): δ [ppm] = 42.92 (brs, B$_{Ge9}$). **Elemental analysis**: anal. calcd. for Ge$_9$Si$_8$BC$_{34}$H$_{72}$N$_2$K: C, 28.41; H, 5.05; N,1.95; found: C, 27.53; H, 4.87; N, 2.02. **ESI MS**: m/z 1398.7 [Ge$_9${Si(TMS)$_3$}$_2$DAB$^{o\text{-tol}}$]⁻.

K[Ge$_9${Si(TMS)$_3$}$_2$(CH$_2$)$_4$O-DAB$^{o\text{-tol}}$] (2): In a typical experiment DAB$^{o\text{-tol}}$-Br (24.7 mg, 0.075 mmol, 1 equiv.) was weighted into a Schlenk tube in the glove box, and thf (1.5 mL) was added to obtain a colorless solution, which was stirred for 2 h at room temperature, before equimolar amounts of K$_2$[Ge$_9${Si(TMS)$_3$}$_2$] (92 mg, 0.075 mmol. 1 equiv.) were added, and then the solution was stirred for another 3 h at room temperature. Subsequently, the solvent was removed *in vacuo*, and hexane (2 · 5 mL) was added to the residue and removed *in vacuo*. Thereafter, the residue was dissolved in toluene (3 mL) and filtered. Removal of toluene yielded the product as a dark-brown oily solid. Purification by recrystallization from toluene solution was not successful so far. **¹H NMR** (400 MHz, 298 K, thf-d_8): δ [ppm] = 7.22-7.18 (m, 2H, CH$_{Ph}$), 7.15-7.09 (m, 4H, CH$_{Ph}$), 6.95-6.91 (m, 2H, CH$_{Ph}$), 3.61 (s, 4H, CH$_{2(Bb)}$), 3.25-3.22 (m, 2H, CH$_2$-O), 2.34 (s, 6H, Me), 1.25-1.20 (m, 4H, CH$_2$), 1.12-1.07 (m, 2H, CH$_2$-Ge), 0.24 (s, 54H, Me$_{TMS}$).**¹³C NMR** (101 MHz, 298 K, thf-d_8): Due to the presence of impurities a reliable assignment of the signals was not possible. **²⁹Si-INEPT NMR** (79 MHz, 298 K, thf-d_8): δ [ppm] = -9.65 (s, Si$_{TMS}$), -108.65 (s, Si$_{Ge9}$).**¹¹B NMR** (128 MHz, 298 K, thf-d_8): δ [ppm] = 23.14 (brs, B$_O$). **ESI MS**: m/z 1470.8 [Ge$_9${Si(TMS)$_3$}$_2$(CH$_2$)$_4$O-DAB$^{o\text{-tol}}$]⁻, 1478.8 [Ge$_9${Si(TMS)$_3$}(CD$_2$)$_4$O-DAB$^{o\text{-tol}}$]⁻.

Synthesis of K[Ge$_9${Si(TMS)$_3$}$_2$(CH$_2$)$_4$O-DAB^{Mes}] (3): In a typical experiment equimolar amounts of K$_2$[Ge$_9${Si(TMS)$_3$}$_2$] (92 mg, 0.075 mmol. 1 equiv.) and DAB^{Mes}-Br (29 mg, 0.075 mmol, 1 equiv.) were weighted into a glass vial in the glove box, and thf (3 mL) was added to obtain a deep red solution. After stirring for 3 h at room temperature, the solvent was removed *in vacuo* yielding a brown oil. Addition and subsequent removal of hexane (2 · 4 mL) yielded a brownish/red solid. Dissolution in toluene (3 mL) gave a dark red solution, which was filtered and concentrated to one third of its original volume. Placement in a freezer at -40 °C yielded the product as a red microcrystalline powder (45 mg, 0.028 mmol, 38 % yield). **¹H NMR** (400 MHz, 298 K, thf-d_8): δ [ppm] = 6.84 (s, 4H, CH$_{Ph}$), 3.42 (s, 4H, CH$_{2(Bb)}$), 3.14 (m, 2H, CH$_2$-O), 2.30 (s, 12H, Me$_{(o)}$), 2.23 (s, 6H Me$_{(p)}$), 1.19-1.14 (m, 4H, CH$_2$), 1.09-1.03 (m, 2H, CH$_2$-Ge), 0.24 (s, 54H, Me$_{TMS}$). **¹³C NMR** (101 MHz, 298 K, thf-d_8): δ [ppm] = 140.98 (s, C$_{Ph(N)}$), 137.09 (s, C$_{Ph(o)}$), 134.91 (s, C$_{Ph(p)}$), 129.65 (s, CH$_{Ph}$), 64.32 (s, CH$_2$-O), 49.34 (s, CH$_{2(Bb)}$), 36.66 (s, CH$_2$), 31.79 (s, CH$_2$), 21.37 (s, Me$_{Ph(p)}$), 18.75 (s, Me$_{Ph(o)}$), 11.14 (s, CH$_2$-Ge) 3.23 (s, Me$_{TMS}$). **²⁹Si-INEPT NMR** (79 MHz, 298 K, thf-d_8): δ [ppm] = -9.67 (s, Si$_{TMS}$), -108.69 (s, Si$_{Ge9}$). **¹¹B NMR** (128 MHz, 298 K, thf-d_8): δ [ppm] = 23.82 (brs, B$_O$). **Elemental analysis**: anal. calcd. for Ge$_9$Si$_8$BC$_{42}$H$_{88}$N$_2$OK: C, 32.22; H, 5.67; N,1.79; found: C, 32.25; H, 5.40, N, 1.78. **ESI MS**: m/z 1526.8 [Ge$_9${Si(TMS)$_3$}$_2$(CH$_2$)$_4$O-DAB^{Mes}]⁻ or 1534.8 [Ge$_9${Si(TMS)$_3$}$_2$(CD$_2$)$_4$O-DAB^{Mes}]⁻.

Synthesis of K[Ge$_9${Si(TMS)$_3$}$_2$(CH$_2$)$_4$O-DAB(II)^{Dipp}] (4): In a typical experiment equimolar amounts of K$_2$[Ge$_9${Si(TMS)$_3$}$_2$] (92 mg, 0.075 mmol. 1 equiv.) and DAB(II)^{Dipp}-Br (35 mg, 0.075 mmol, 1 equiv.) were weighted into a Schlenk tube in the glove box, and thf (2 mL) was added to obtain a deep red solution. After stirring for three weeks at 35 °C, the solvent was removed *in vacuo*, yielding a brown oil. Addition and subsequent removal of hexane (3 · 6 mL) yielded a brown solid. Dissolution in toluene (2 mL) gave a dark red solution, which was filtered. The solution was concentrated to half of its original volume and stored in a freezer at -40 °C for crystallization, yielding the product as red block-shaped crystals (18.5 mg, 0.011 mmol, 15 % yield). **¹H NMR** (400 MHz, 298 K, thf-d_8): δ [ppm] = 7.23-7.18 (s, 2H, CH$_{Ph(p)}$), 7.16-7.13 (m, 4H, CH$_{Ph(m)}$), 5.87 (s, 2H, CH$_{Bb}$), 3.25-3.16 (m, 6H, CH$_{iPr}$ + CH$_2$-O), 1.22 (d, $^3J_{HH}$ = 6.8 Hz, 12H, Me$_{iPr}$), 1.18 (d, $^3J_{HH}$ = 6.8 Hz, 12H, Me$_{iPr}$), 1.16-1.14 (m, 4H, CH$_2$), 1.07-1.03 (m, 2H, CH$_2$-Ge), 0.22 (s, 54H, Me$_{TMS}$). **¹³C NMR** (101 MHz, 298 K, thf-d_8): δ [ppm] = 147.24 (s, C$_{Ph(N)}$), 139.49 (s, CH$_{Ph(p)}$),

127.84 (s, $C_{Ph(iPr)}$), 123.82 (s, $CH_{Ph(m)}$), 117.57 (s, CH_{Bb}), 65.47(s, CH_2-O), 36.43 (s, CH_2), 31.57 (s, CH_2), 29.28 (s, CH_{iPr}), 26.43 (s, Me_{iPr}) , 24.46 (s, Me_{iPr}), 11.17 (s, CH_2-Ge), 3.23 (s, Me_{TMS}). **^{29}Si-INEPT NMR** (79 MHz, 298 K, thf-d_8): δ [ppm] = -9.67 (s, Si_{TMS}), -108.72 (s, Si_{Ge9}). **^{11}B NMR** (128 MHz, 298 K, thf-d_8): δ [ppm] = 20.66 (brs, B_O). **ESI MS**: *m/z* 1608.8 [Ge_9{Si(TMS)$_3$}$_2$(CH$_2$)$_4$O-DAB(II)^{Dipp}]$^-$ or *m/z* 1616.8 [Ge_9{Si(TMS)$_3$}$_2$(CD$_2$)$_4$O-DAB(II)^{Dipp}]$^-$.

Synthesis of K[Ge$_9${Si(TMS)$_3$}$_2$(CH$_2$)$_3$O-DAB^{Mes}] (5): In a typical experiment equimolar amounts of K$_2$[Ge$_9${Si(TMS)$_3$}$_2$] (123 mg, 0.100 mmol. 1 equiv.) and DAB^{Mes}-Br (38.5 mg, 0.100 mmol, 1 equiv.) were weighted into a Schlenk tube in the glove box, and trimethyleneoxide (1.5 mL) was added to obtain a deep red solution. After stirring for 3.5 h at room temperature, the solvent was removed *in vacuo* yielding a brown oil. Addition and subsequent removal of hexane (4 · 4 mL) yielded a brown solid. Dissolution in toluene (2 · 5 mL) gave a dark red solution, which was filtered and concentrated to half of its original volume, before it was placed in a freezer at -40 °C. Overnight a brown oil separated from the solution, which was removed by filtering-off the supernatant solution. The latter was placed in the freezer at -40 °C again, yielding orange block-shaped crystals of the product (26 mg, 0.017 mmol, 17 %). **^{1}H NMR** (400 MHz, 298 K, thf-d_8): δ [ppm] = 6.82 (s, 4H, CH_{Ph}), 3.40 (s, 4H, $CH_{2(Bb)}$), 3.04 (t, $^3J_{HH}$ = 7.0 Hz, 2H, CH_2-O), 2.29 (s, 12H, $Me_{(o)}$), 2.21 (s, 6H $Me_{(p)}$), 1.39-1.29 (m, 2H, CH_2), 0.83-0.77 (m, 2H, CH_2-Ge), 0.23 (s, 54H, Me_{TMS}). **^{13}C NMR** (101 MHz, 298 K, thf-d_8): δ [ppm] = 140.98 (s, $C_{Ph(N)}$), 138.46 (s, $C_{Ph(o)}$), 134.79 (s, $C_{Ph(p)}$), 129.63 (s, CH_{Ph}), 68.59 (s, CH_2-O), 49.35 (s, $CH_{2(Bb)}$), 38.73 (s, CH_2), 31.33 (s, CH_2), 21.54 (s, $Me_{Ph(p)}$), 18.81 (s, $Me_{Ph(o)}$), 6.87 (s, CH_2-Ge) 3.23 (s, Me_{TMS}). **^{29}Si-INEPT NMR** (79 MHz, 298 K, thf-d_8): δ [ppm] = -9.66 (s, Si_{TMS}), -108.69 (s, Si_{Ge9}). **^{11}B NMR** (128 MHz, 298 K, thf-d_8): δ [ppm] = 23.06 (brs, B_O). **Elemental analysis:** anal. calcd. for Ge$_9$Si$_8$BC$_{41}$H$_{86}$N$_2$OK · 0.9 tol: C, 34.62; H, 5.75; N,1.72; found: C, 34.25; H; 5.68, N, 1.71 (toluene content of the microcrystalline solid was determined by ^{1}H NMR spectroscopy). **ESI MS**: *m/z* 1512.8 [Ge$_9${Si(TMS)$_3$}$_2$(CH$_2$)$_3$O-DAB^{Mes}]$^-$.

Synthesis of K[Ge$_9${Si(TMS)$_3$}$_2$CH$_3$C=N-DAB^{Mes}] (6): In a typical experiment equimolar amounts of K$_2$[Ge$_9${Si(TMS)$_3$}$_2$] (92 mg, 0.075 mmol. 1 equiv.) and DAB^{Mes}-Br (38.5 mg, 0.100 mmol, 1 equiv.) were weighted into a Schlenk tube in the glove box, and MeCN (3 mL) was added. After stirring for 5 h at room temperature, the solvent was removed *in vacuo* yielding a brown oil. Addition and subsequent removal of hexane (2 · 5 mL) yielded a brown solid. Dissolution in toluene (2 mL) gave a dark red solution, which was filtered. The solution was concentrated to half of its original volume and stored at room temperature yielding orange needle-shaped crystals. The supernatant solution was filtered-off, and the solid was washed with hexane (5 · 2 mL) and dried *in vacuo* (49 mg, 0.032 mmol, 43 %). **^{1}H NMR** (400 MHz, 298 K, thf-d_8): δ [ppm] = 6.74 (s, 4H, CH_{Ph}), 3.49 (s, 4H, $CH_{2(Bb)}$), 2.32 (s, 12H, $Me_{(o)}$), 2.20 (s, 6H $Me_{(p)}$), 1.78 (s, 3H, Me_{MeCN}), 0.25 (s, 54H, Me_{TMS}). **^{13}C NMR** (101 MHz, 298 K, thf-d_8): δ [ppm] = 141.07 (s, $C_{Ph(N)}$), 137.22 (s, $C_{Ph(o)}$), 134.08 (s, $C_{Ph(p)}$), 129.59 (s, CH_{Ph}), 50.21 (s, $CH_{2(Bb)}$), 20.08 (s, $Me_{Ph(o)}$), 19.29 (s, $Me_{Ph(p)}$), 3.24 (s, Me_{TMS}). Signal of C=N could not be detected probably due to low concentration of sample. **^{29}Si-INEPT NMR** (79 MHz, 298 K, thf-d_8): δ [ppm] = -9.53 (s, Si_{TMS}), -107.27 (s, Si_{Ge9}). **^{11}B NMR** (128 MHz, 298 K, thf-d_8): δ [ppm] = 18.38 (brs, B_O). **Elemental analysis**: anal. calcd. for Ge$_9$Si$_8$BC$_{40}$H$_{83}$N$_3$K: C, 31.31; H, 5.45; N, 2.74; found: C, 31.90; H, 5.41; N, 2.71. **ESI MS**: *m/z* 1495.7 [Ge$_9${Si(TMS)$_3$}$_2$(CH$_3$)C=N-BN$_{Mes}$]$^-$, 1498.7 [Ge$_9${Si(TMS)$_3$}$_2$(CD$_3$)C=N-BN$_{Mes}$]$^-$.

Activation of thf with DAB^R-Br and (^{i}Pr$_2$N)$_2$B-Br

In a typical experiment 100 µmol of the diazaborolidine DAB^R-Br, DAB(II)^{Dipp}-Br or (^{i}Pr$_2$N)$_2$B-Br was weighted into a Schlenk tube, and thf (2 mL) was added. After the reaction time (Table S1) the solvent was removed *in vacuo* yielding a colorless or light brown (DAB^{Dipp}-Br and DAB(II)^{Dipp}-Br) oil, which was dissolved in C$_6$D$_6$ and investigated by NMR spectroscopy (^{1}H, ^{11}B). Respective NMR spectra are presented below (see Figures S5-S16).

Table S1. Reaction conditions for thf ring-opening reactions induced by different bromo-boranes.

	[mg]	reaction time [h]	temperature
(^{i}Pr$_2$N)$_2$B-Br	29.1	3	r.t.
DAB$^{o\text{-}tol}$-Br	32.9	1	r.t.
DAB$^{o\text{-}xyl}$-Br	35.7	3	r.t.
DAB^{Mes}-Br	38.5	3	r.t.
DAB^{Dipp}-Br	46.9	69	70 °C
DAB(II)^{Dipp}-Br	46.7	69	70 °C

(^{i}Pr$_2$N)$_2$B-O-(CH$_2$)$_4$-Br

^{1}H NMR (400 MHz, 298 K, C$_6$D$_6$): δ [ppm] = 3.63 (t, $^3J_{HH}$ = 6.7 Hz, 2H, CH$_2$-O), 3.34 (hept, $^3J_{HH}$ = 6.6 Hz, 4H, CH$_{iPr}$), 3.03 (t, $^3J_{HH}$ = 6.7 Hz, 2H, CH$_2$-Br), 1.81-1.73 (m, 2H, CH$_2$), 1.56-1.49 (m, 2H, CH$_2$), 1.13 (d, $^3J_{HH}$ = 6.6 Hz, 24H, CH$_{3iPr}$). **^{11}B NMR** (128 MHz, 298 K, C$_6$D$_6$): δ [ppm] = 26.00 (brs).

DAB$^{o\text{-}tol}$-O-(CH$_2$)$_4$-Br

^{1}H NMR (400 MHz, 298 K, C$_6$D$_6$): δ [ppm] = 7.14-7.06 (m, 4H, CH$_{Ph}$), 7.00-6.96 (m, 2H, CH$_{Ph}$), 6.79-6.73 (m, 2H, CH$_{Ph}$), 3.34 (s, 4H, CH$_{2(Bb)}$), 3.26 (t, $^3J_{HH}$ = 6.8 Hz, 2H, CH$_2$-O), 2.72 (t, $^3J_{HH}$ = 6.8 Hz, 2H, CH$_2$-Br), 2.36 (s, 6H, Me), 1.38-1.29 (m, 2H, CH$_2$), 1.13-1.04 (m, 2H, CH$_2$). **^{11}B NMR** (128 MHz, 298 K, C$_6$D$_6$): δ [ppm] = 23.71 (brs).

DAB$^{o\text{-}xyl}$-O-(CH$_2$)$_4$-Br

^{1}H NMR (400 MHz, 298 K, C$_6$D$_6$): δ [ppm] = 7.04-6.97 (m, 6H, CH$_{Ph}$), 3.26 (s, 4H, CH$_{(Bb)}$), 3.19 (t, $^3J_{HH}$ = 6.9 Hz, 2H, CH$_2$-O), 2.67 (t, $^3J_{HH}$ = 6.9 Hz, 2H, CH$_2$-Br), 2.37 (s, 12H, CH$_{3(o)}$), 1.35-1.27 (m, 2H, CH$_2$), 1.05-0.98 (m, 2H, CH$_2$). **^{11}B NMR** (128 MHz, 298 K, C$_6$D$_6$): δ [ppm] = 23.42 (brs).

DAB^{Mes}-O-(CH$_2$)$_4$-Br

^{1}H NMR (400 MHz, 298 K, C$_6$D$_6$): δ [ppm] = 6.85 (s, 4H, CH$_{Ph}$), 3.31 (s, 4H, CH$_{2(Bb)}$), 3.26 (t, $^3J_{HH}$ = 6.8 Hz, 2H, CH$_2$-O), 2.69 (t, $^3J_{HH}$ = 6.8 Hz, 2H, CH$_2$-Br), 2.39 (s, 12H, Me$_{(o)}$), 2.16 (s, 6H, Me$_{(p)}$), 1.41-1.32 (m, 2H, CH$_2$), 1.10-1.01 (m, 2H, CH$_2$). **^{11}B NMR** (128 MHz, 298 K, C$_6$D$_6$): δ [ppm] = 23.58 (brs).

DAB^{Dipp}-O-(CH$_2$)$_4$-Br

^{1}H NMR (400 MHz, 298 K, C$_6$D$_6$): δ [ppm] = 7.21-7.17 (m, 4H, CH$_{(m)}$), 7.16-7.13 (m, 2H, CH$_{(p)}$), 3.61 (hept, $^3J_{HH}$ = 6.8 Hz, 4H, CH$_{iPr}$), 3.43 (s, 4H, CH$_{(Bb)}$), 3.29 (t, $^3J_{HH}$ = 6.9 Hz, 2H, CH$_2$-O), 2.67 (t, $^3J_{HH}$ = 6.9 Hz, 2H, CH$_2$-Br), 1.37 (d, $^3J_{HH}$ = 6.9 Hz, 12H, CH$_{3iPr}$), 1.33 (d, $^3J_{HH}$ = 6.9 Hz, 12H, CH$_{3iPr}$), 1.27-1.23 (m, 2H, CH$_2$), 1.11-1.03 (m, 2H, CH$_2$). **^{11}B NMR** (128 MHz, 298 K, C$_6$D$_6$): δ [ppm] = 23.69 (brs).

DAB(II)^{Dipp}-O-(CH$_2$)$_4$-Br

^{1}H NMR (400 MHz, 298 K, CDCl$_3$): δ [ppm] = 7.44-7.28 (m, 4H, CH$_{(m)}$), 7.24 (s, 2H, CH$_{(p)}$), 5.98 (s, 2H, CH$_{(Bb)}$), 3.39 (t, $^3J_{HH}$ = 6.2 Hz, 2H, CH$_2$-O), 3.29-3.21 (m, 4H, CH$_{iPr}$), 3.20-3.16 (m, CH$_2$-Br, 2H), 1.66 (pent, $^3J_{HH}$ = 7.0 Hz, 2H, CH$_2$), 1.44-1.38 (m, 2H, CH$_2$), 1.29 (d, $^3J_{HH}$ = 5.2 Hz, 12H, CH$_{3iPr}$), 1.28 (d, $^3J_{HH}$ = 5.2 Hz, 12H, CH$_{3iPr}$). **^{11}B NMR** (128 MHz, 298 K, CDCl$_3$): δ [ppm] = 20.94 (brs).

Reactivity of DAB^{Mes}-Br towards MeCN

In a typical experiment 100 µmol of the diazaborolidine DAB^{Mes}-Br was weighted into a Schlenk tube, and MeCN (2 mL) was added. After the reaction time (Table S2), the solvent was removed *in vacuo*, yielding a colorless solid, which was dissolved in C_6D_6 and investigated by NMR spectroscopy (^{1}H, ^{11}B). Furthermore, 100 µmol of the diazaborolidine DAB^{Mes}-Br and 100 µmol MeCN were combined in a *J-Young* NMR tube, and the reaction was monitored directly in C_6D_6. Respective NMR spectra (including the spectrum of pure reactant DAB^{Mes}-Br) are presented below (see Figures S17-S20).

Table S2. Reaction conditions for investigating the reactivity of DAB^{Mes}-Br towards MeCN.

	[mg]	reaction time [h]	temperature
DAB^{Mes}-Br	38.5	16	r.t.
DAB^{Mes}-Br	38.5	16	70 °C

DAB^{Mes}-Br

^{1}H NMR (400 MHz, 298 K, C_6D_6): δ [ppm] = 6.83 (s, 4H, CH$_{Ph}$), 3.31 (s, 4H, CH$_{2(Bb)}$), 2.33 (s, 12H, Me$_{(o)}$), 2.14 (s, 6H, Me$_{(p)}$). **^{11}B NMR** (128 MHz, 298 K, C_6D_6): δ [ppm] = 25.97 (brs).

The residues of the reaction of DAB^{Mes}-Br with MeCN at r. t. or 70 °C as well as the *in situ* investigation of the borane and MeCN in C_6D_6 show no additional or shifted signals in the NMR spectra, manifesting that no reaction occurs (in absence of [Ge$_9$] cluster; Figures S19 and S20).

ESI MS sample preparation

Insertion of tetrahydrofurane (thf) and trimethyleneoxide (tmo)

Equimolar amounts of K$_2$[Ge$_9${Si(TMS)$_3$}$_2$] and DAB$^{o\text{-}xyl}$-Br or (^{i}Pr$_2$N)$_2$B-Br (0.020 mmol) were weighted into a glass vial in the glove box, and thf / thf-d_8 or tmo (0.5 mL) was added to obtain a deep red solution. The mixture was stirred for 3 h at room temperature, before it was transferred to a Schlenk tube, and the solvent was removed *in vacuo*. Subsequently, the obtained residues were diluted with thf and investigated by ESI MS. The respective spectra are presented below.

Equimolar amounts of K$_2$[Ge$_9${Si(TMS)$_3$}$_2$] and DAB(II)^{Dipp}-Br or DAB^{Dipp}-Br (0.020 mmol) were dissolved in thf / thf-d_8 or tmo (0.5 mL) and stirred at 35 °C for 3 weeks. Alternatively, a solution of the respective bromo-borane in thf can be heated to 60 °C for 2 d before K$_2$[Ge$_9${Si(TMS)$_3$}$_2$] is added. In this case complete conversion of the reactants occurs overnight. Subsequently, the solvent was removed *in vacuo*, and the obtained residues were diluted with thf and investigated by ESI MS. The respective spectra are presented below.

Activation of acetonitrile

Equimolar amounts of K$_2$[Ge$_9${Si(TMS)$_3$}$_2$] and DAB$^{o\text{-}xyl}$-Br or (^{i}Pr$_2$N)$_2$B-Br (0.020 mmol) were weighted into a glass vial in the glove box, and MeCN / MeCN-d_3 (0.5 mL) was added to obtain a deep red solution. The mixture was stirred for 3 h at room temperature, before it was transferred to a Schlenk tube, and the solvent was removed *in vacuo*. Subsequently, the obtained residues were diluted with MeCN and investigated by ESI MS. The respective spectra are presented below.

Equimolar amounts of K$_2$[Ge$_9${Si(TMS)$_3$}$_2$] and DAB(II)^{Dipp}-Br or DAB^{Dipp}-Br (0.020 mmol) were dissolved in MeCN / MeCN-d_3 (0.5 mL) and stirred at 40 °C for 4 d. Subsequently, the solvent was removed *in vacuo*, and the obtained residues were diluted with MeCN and investigated by ESI MS. The respective spectra are presented below.

Crystallographic data of compounds 3 – 6

Table S3. Crystallographic data of compounds **3** - **6**.

Compound	3	4	5	6
formula	$Ge_9Si_8BC_{42}H_{88}N_2OK \cdot 1.5tol$	$Ge_9Si_8BC_{48}H_{98}N_2OK \cdot 2tol$	$Ge_9Si_8BC_{48}H_{94}N_2OK$	$Ge_9Si_8BC_{40}H_{83}N_3K \cdot 1tol$
fw [g·mol^{-1}]	1703.28	1831.49	1643.19	1626.16
space group	$P\bar{1}$	$P\bar{1}$	$P\bar{1}$	$P2_1$
a [Å]	14.7094(7)	16.402(1)	14.666(1)	13.7573(4)
b [Å]	16.9327(6)	16.841(1)	15.460(2)	9.2613(3)
c [Å]	18.7377(9)	17.542(1)	18.062(2)	28.424(1)
α [deg]	65.966(3)	92.419(6)	65.417(7)	90
β [deg]	67.528(4)	107.892(5)	82.365(7)	94.438(3)
γ [deg]	88.951(3)	102.920(6)	88.648(8)	90
V [Å^3]	3886.2(3)	4462.2(6)	3688.9(6)	3610.6(2)
Z	2	2	2	2
T [K]	150	150	150	150
λ [Å]	Mo $K\alpha$	Mo $K\alpha$	Mo $K\alpha$	Mo $K\alpha$
ρ_{calcd} [g·cm^{-3}]	1.456	1.363	1.479	1.496
μ [mm^{-1}]	3.638	3.174	3.830	3.911
collected reflections	74106	96277	77184	78148
indep. reflections	15237	17531	14484	14199
R_{int} / R_δ	0.0695/0.0482	0.0848/0.1019	0.0878/0.0599	0.0405/0.0258
parameters / restraints	682/6	785/0	656/0	648/1
R_1 [$I > 2\,\sigma(I)$ / all data]	0.0435/0.0836	0.0443/0.1025	0.0475/0.0915	0.0253/0.0296
wR_2 [$I > 2\,\sigma(I)$ / all data]	0.0880/0.1113	0.0727/0.0871	0.0937/0.1195	0.0556/0.0574
goodness of fit	1.115	0.901	1.084	1.031
max./min. diff. el. density [e · Å^{-3}]	1.45/-1.26	0.78/-0.61	0.81/-0.89	0.43/-0.36
CCDC	1993875	1993876	1993877	1993878
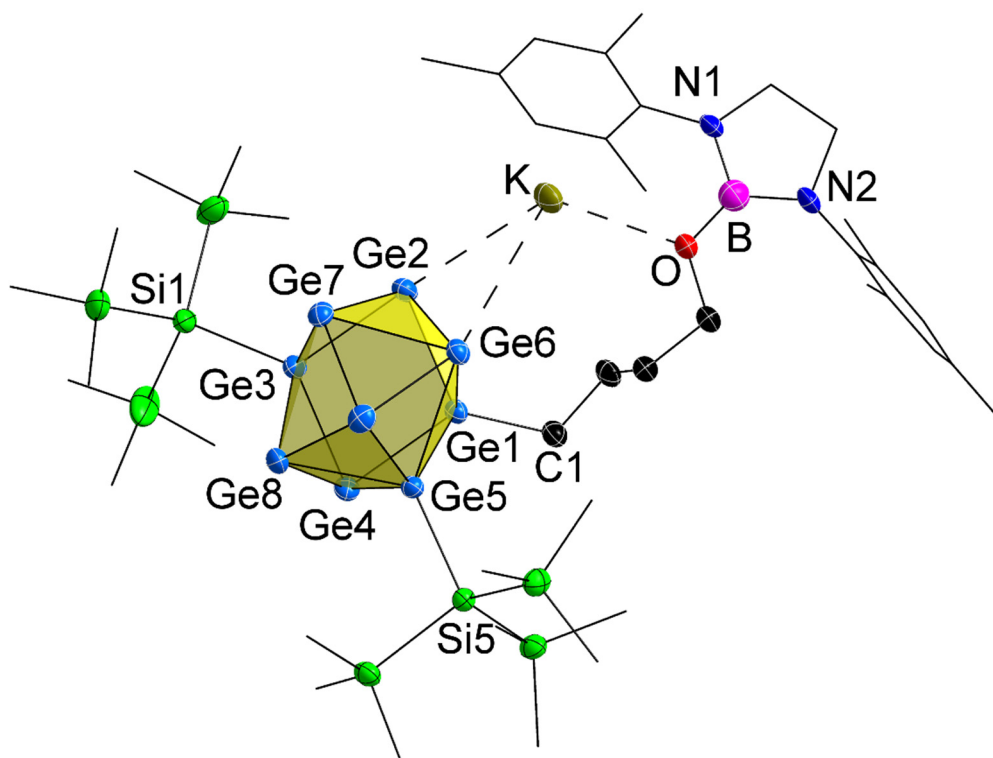
Figure S1. Molecular structure of compound **3**. All ellipsoids are shown at a 50 % probability level. For clarity, protons and co-crystallized solvent molecules are omitted. Carbon atoms of silyl groups and of the DAB[Mes] moiety are presented as black wire sticks. For crystallographic data and selected bond lengths of **3** see Tables S3 and S4.

Table S4. Selected bond lengths in compound **3**.

bond	distance [Å]
Ge1-Ge2	2.5038(8)
Ge1-Ge4	2.5675(7)
Ge1-Ge5	2.5339(8)
Ge1-Ge6	2.7612(8)
Ge2-Ge3	2.5503(8)
Ge2-Ge6	2.6985(9)
Ge2-Ge7	2.6740(8)
Ge3-Ge4	2.5460(8)
Ge3-Ge7	2.6127(8)
Ge3-Ge8	2.5899(8)
Ge4-Ge5	2.6750(8)
Ge4-Ge8	2.7432(8)
Ge5-Ge6	2.7587(8)
Ge5-Ge8	2.6063(8)
Ge5-Ge9	2.5437(8)
Ge6-Ge7	2.6926(8)
Ge6-Ge9	2.6077(8)
Ge7-Ge8	2.9322(8)
Ge7-Ge9	2.5900(9)
Ge8-Ge9	2.6804(9)
Ge1-C1	1.995(5)
Ge3-Si1	2.396(2)
Ge5-Si5	2.395(2)
Ge2-Ge4	3.976(1)
Ge5-Ge6	2.759(2)
Ge7-Ge8	2.932(1)
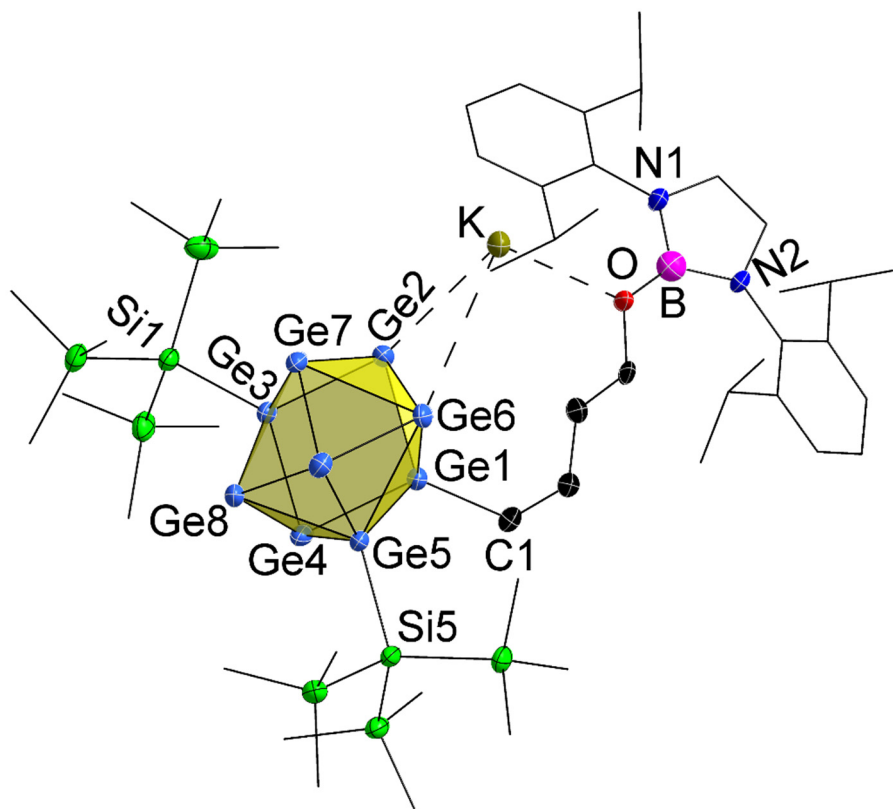
Figure S2. Molecular structure of compound **4**. All ellipsoids are shown at a 50 % probability level. For clarity, protons and co-crystallized solvent molecules are omitted. Carbon atoms of silyl groups and the DAB(II)^Dipp moiety are presented as black wire sticks. For crystallographic data and selected bond lengths of **4** see Tables S3 and S5.

Table S5. Selected bond lengths in compound **4**.

bond	distance [Å]
Ge1–Ge2	2.5046(8)
Ge1–Ge4	2.5577(8)
Ge1–Ge5	2.5334(8)
Ge1–Ge6	2.7429(9)
Ge2–Ge3	2.5394(7)
Ge2–Ge6	2.6699(8)
Ge2–Ge7	2.6825(9)
Ge3–Ge4	2.5361(8)
Ge3–Ge7	2.6202(8)
Ge3–Ge8	2.5758(8)
Ge4–Ge5	2.6690(8)
Ge4–Ge8	2.7555(9)
Ge5–Ge6	2.8140(8)
Ge5–Ge8	2.6048(7)
Ge5–Ge9	2.5188(8)
Ge6–Ge7	2.6876(7)
Ge6–Ge9	2.6027(8)
Ge7–Ge8	2.9324(8)
Ge7–Ge9	2.5919(8)
Ge8–Ge9	2.6825(8)
Ge1–C1	2.007(5)
Ge3–Si1	2.392(1)
Ge5–Si5	2.403(2)
Ge2–Ge4	3.918(1)
Ge5–Ge6	2.815(2)
Ge7–Ge8	2.934(1)
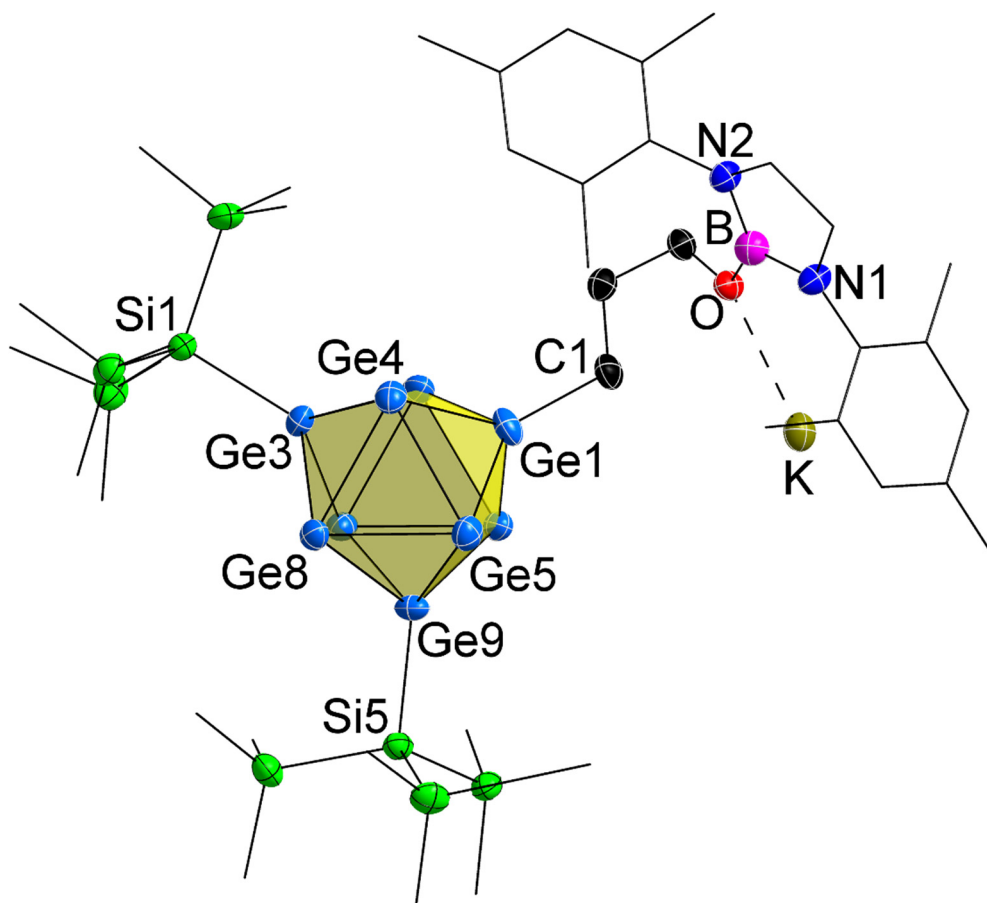
Figure S3. Molecular structure of compound **5**. All ellipsoids are shown at a 50 % probability level. For clarity, protons and co-crystallized solvent molecules are omitted. Carbon atoms of silyl groups and the DAB^{Mes} moiety are presented as black wire sticks. For crystallographic data and selected bond lengths of **5** see Tables S3 and S6.

Table S6. Selected bond lengths in compound **5**.

bond	distance [Å]
Ge1-Ge2	2.528(1)
Ge1-Ge4	2.5237(9)
Ge1-Ge5	2.524(1)
Ge1-Ge6	2.519(1)
Ge2-Ge3	2.5074(9)
Ge2-Ge6	2.692(1)
Ge2-Ge7	2.692(1)
Ge3-Ge4	2.5516(9)
Ge3-Ge7	2.5473(9)
Ge3-Ge8	2.5326(9)
Ge4-Ge5	2.665(1)
Ge4-Ge8	2.715(1)
Ge5-Ge8	2.6612(9)
Ge5-Ge9	2.555(1)
Ge6-Ge7	2.6825(9)
Ge6-Ge9	2.5031(9)
Ge7-Ge9	2.5563(9)
Ge8-Ge9	2.5518(9)
Ge1-C1	1.984(6)
Ge3-Si1	2.381(2)
Ge9-Si5	2.383(2)
Ge2-Ge4	3.429(1)
Ge5-Ge6	3.525(1)
Ge7-Ge8	3.295(1)
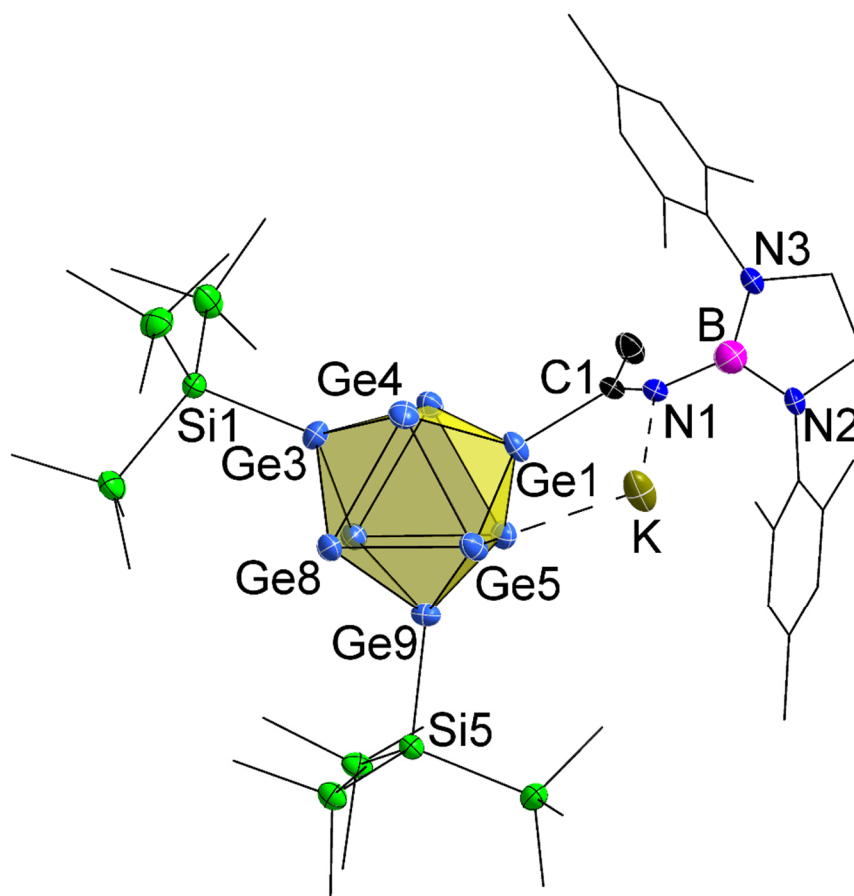
Figure S4. Molecular structure of compound **6**. All ellipsoids are shown at a 50 % probability level. For clarity, protons and co-crystallized solvent molecules are omitted. Carbon atoms of silyl groups and the DAB^{Mes} moiety are presented as black wire sticks. For crystallographic data and selected bond lengths of **6** see Tables S3 and S7.

Table S7. Selected bond lengths in compound **6**.

bond	distance [Å]
Ge1-Ge2	2.5332(7)
Ge1-Ge4	2.5360(7)
Ge1-Ge5	2.5573(7)
Ge2-Ge3	2.5232(7)
Ge2-Ge6	2.6599(7)
Ge2-Ge7	2.7213(7)
Ge3-Ge4	2.5267(7)
Ge3-Ge7	2.5128(7)
Ge3-Ge8	2.5532(7)
Ge4-Ge5	2.6679(7)
Ge4-Ge8	2.7396(7)
Ge5-Ge8	2.6347(7)
Ge5-Ge9	2.5308(7)
Ge6-Ge7	2.6637(7)
Ge6-Ge9	2.5300(7)
Ge7-Ge9	2.5541(7)
Ge8-Ge9	2.5619(7)
Ge1-C1	1.997(4)
Ge3-Si1	2.369(1)
Ge9-Si5	2.381(1)
Ge2-Ge4	3.370(1)
Ge5-Ge6	3.663(1)
Ge7-Ge8	3.201(1)

NMR spectra
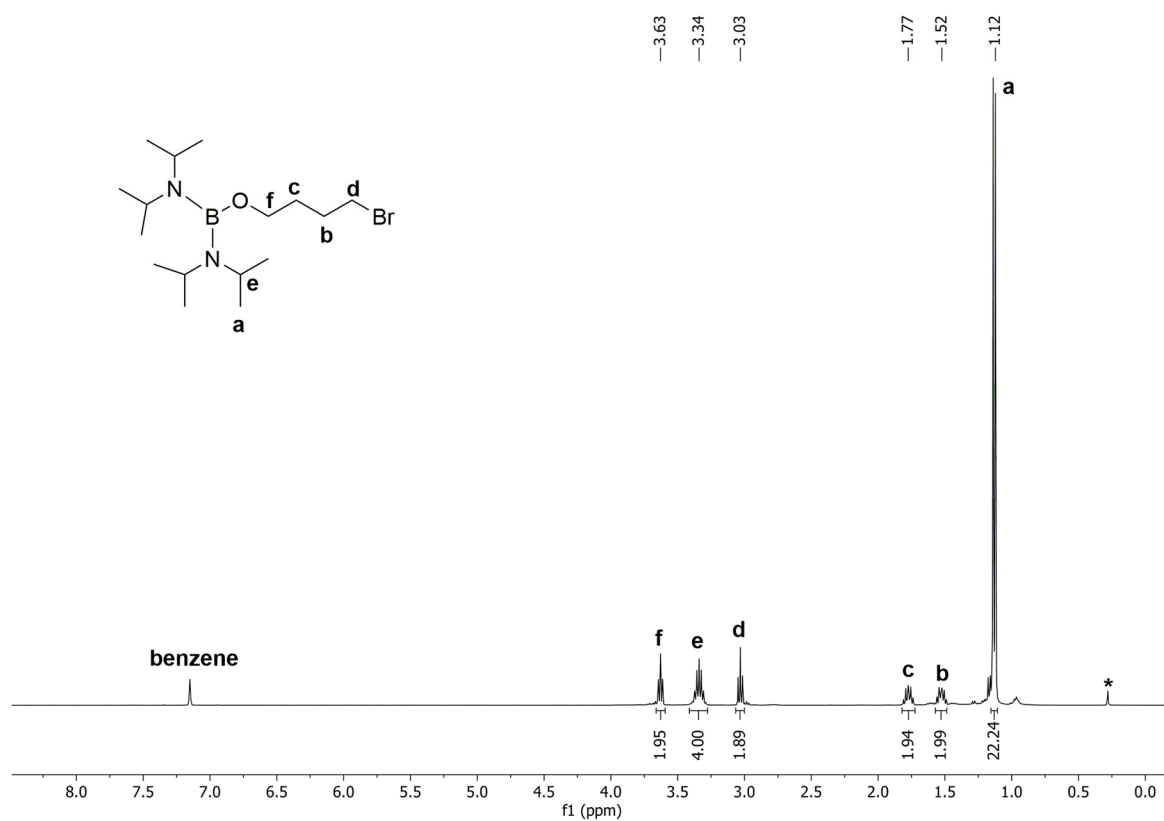
Figure S5. ^{1}H NMR spectrum of (^{i}Pr$_2$N)$_2$B-(CH$_2$)$_4$-Br acquired in C$_6$D$_6$.* silicon grease.
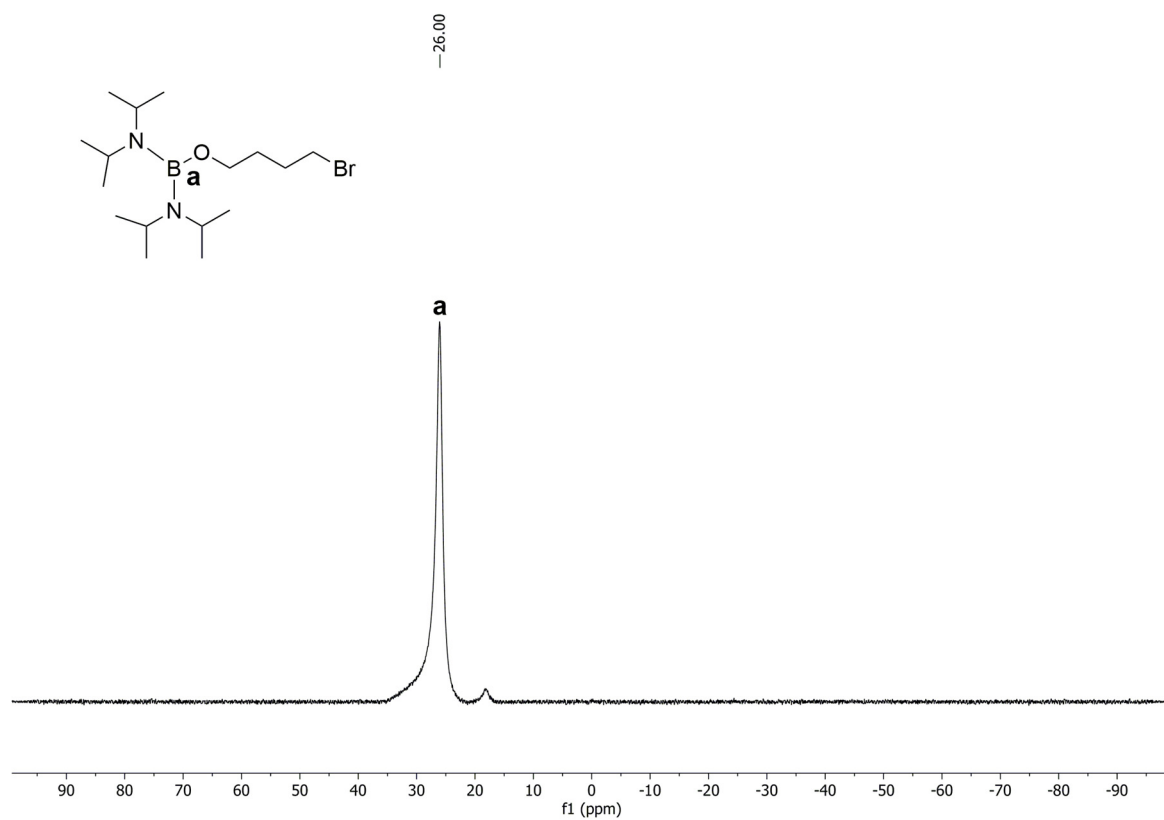
Figure S6. ^{11}B NMR spectrum of (^{i}Pr$_2$N)$_2$B-O-(CH$_2$)$_4$-Br acquired in C$_6$D$_6$.
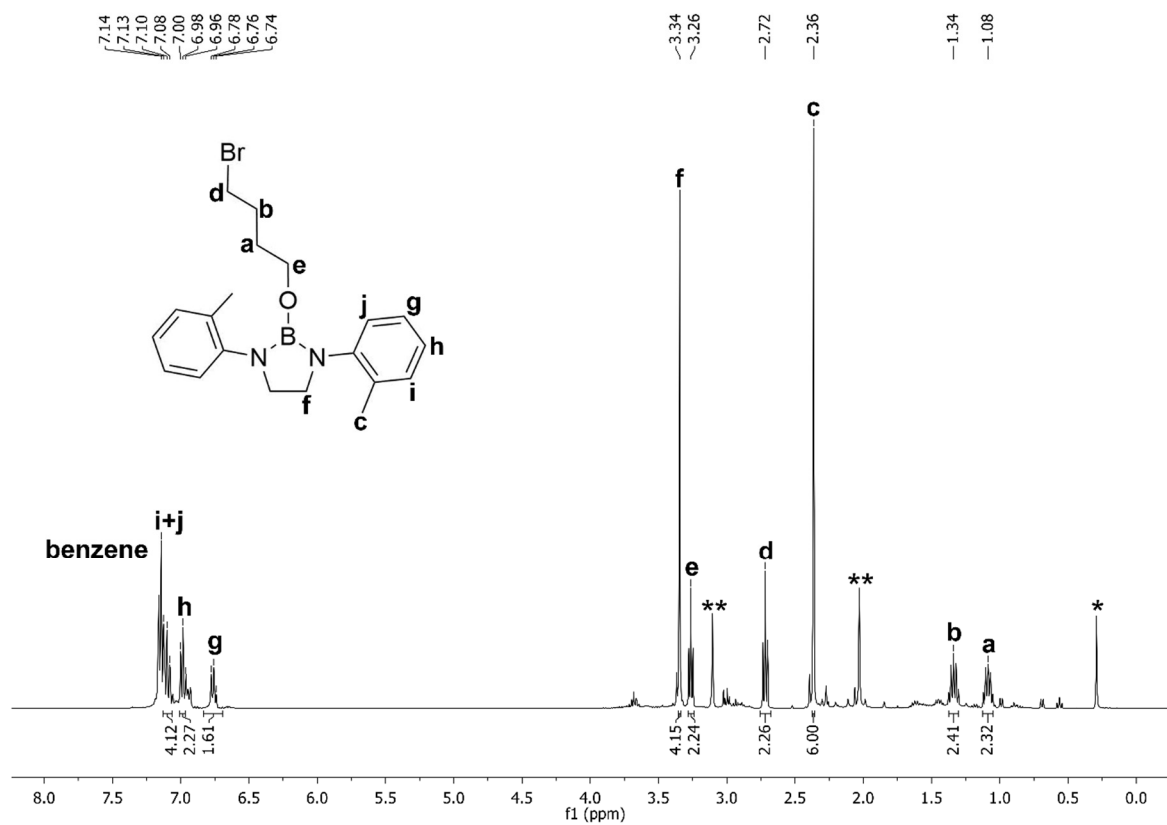
Figure S7. ^{1}H NMR spectrum of DAB$^{o\text{-}tol}$-O-(CH$_2$)$_4$-Br acquired in C$_6$D$_6$.* silicon grease; ** unknown side product(s).
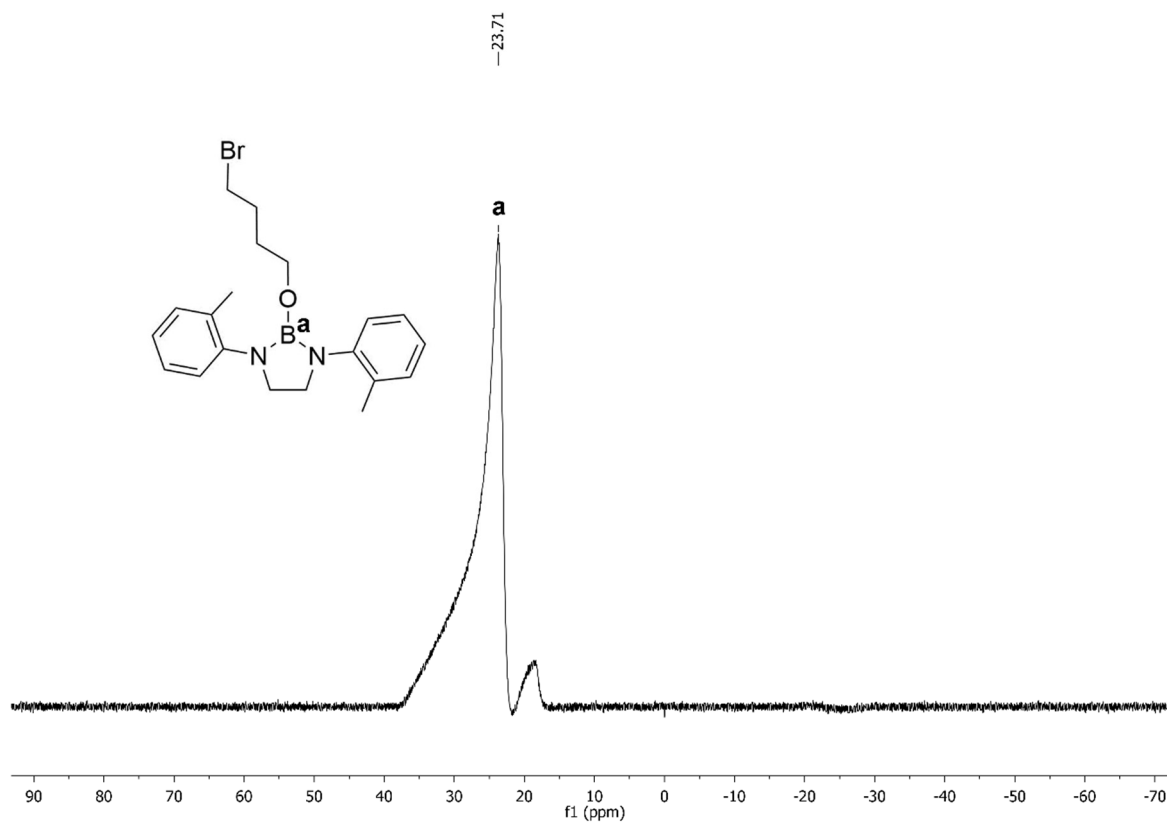
Figure S8. ^{11}B NMR spectrum of DAB$^{o\text{-}tol}$-O-(CH$_2$)$_4$-Br acquired in C$_6$D$_6$. Impurity is caused by unidentified species.
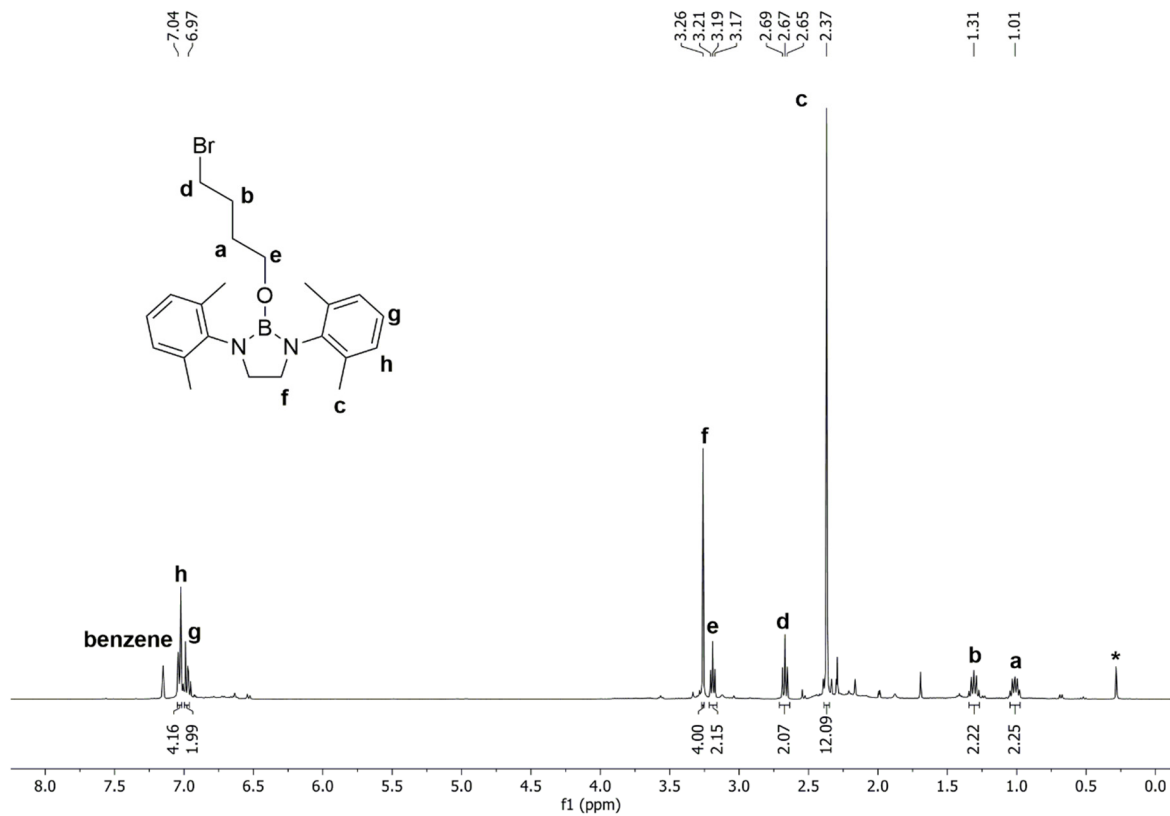
Figure S9. ^1H NMR spectrum of DAB$^{o\text{-xyl}}$-O-(CH$_2$)$_4$-Br acquired in C$_6$D$_6$.* silicon grease.
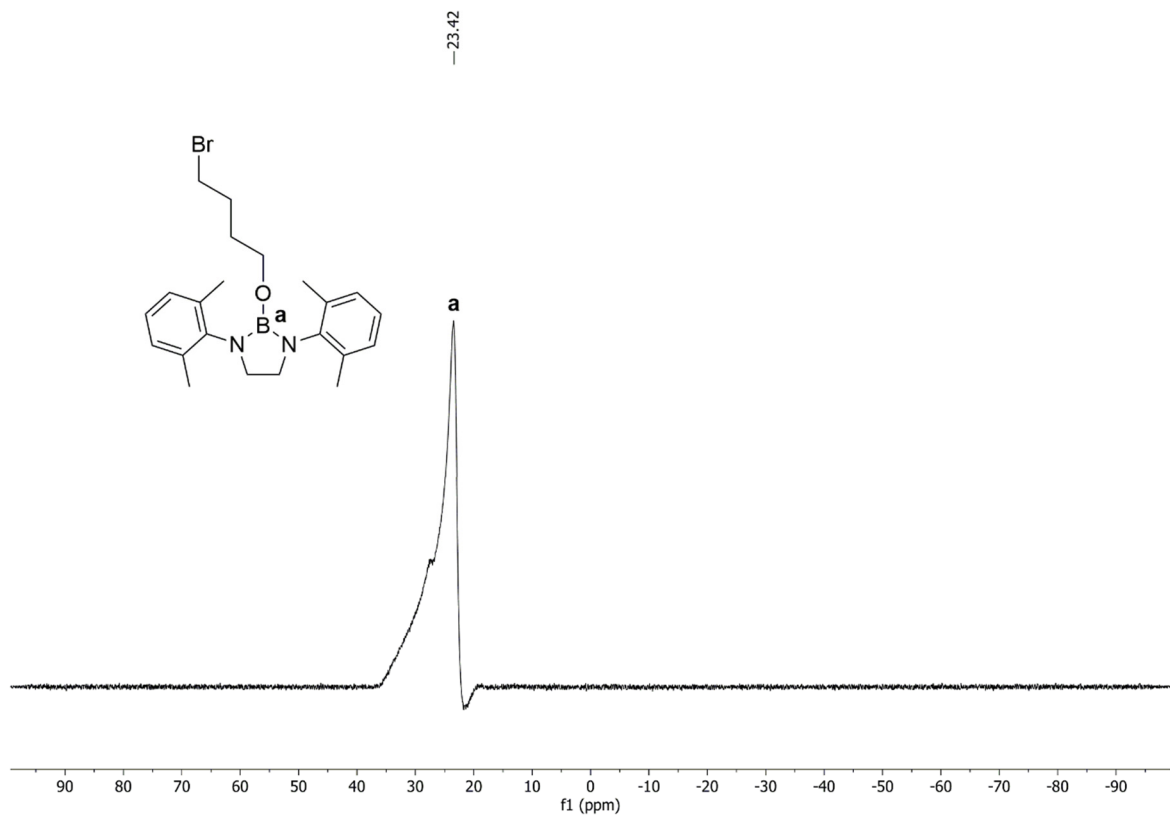
Figure S10. ^{11}B NMR spectrum of DAB$^{o\text{-xyl}}$-O-(CH$_2$)$_4$-Br acquired in C$_6$D$_6$. Impurity is caused by an unidentified species.
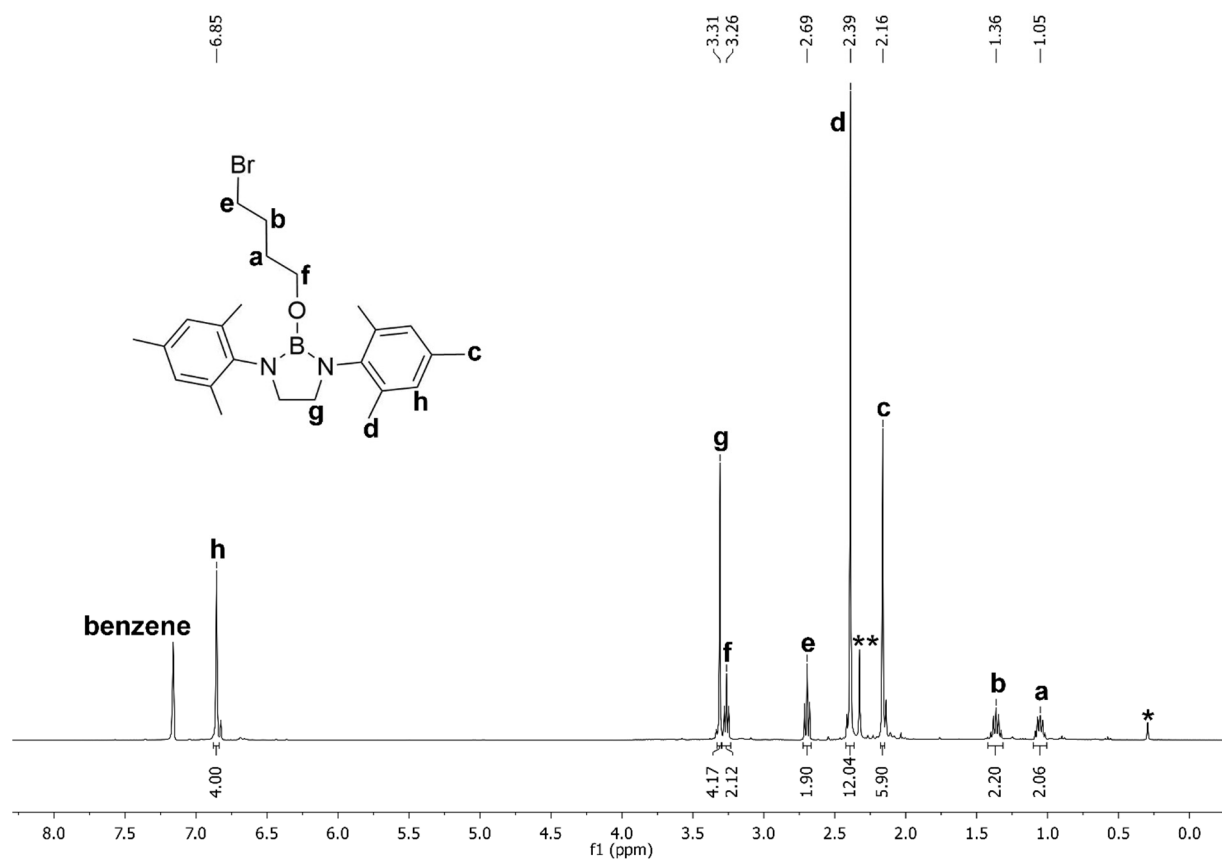
Figure S11. ^{1}H NMR spectrum of DAB^{Mes}-O-(CH$_2$)$_4$-Br acquired in C$_6$D$_6$. * silicon grease; ** unknown side product(s).
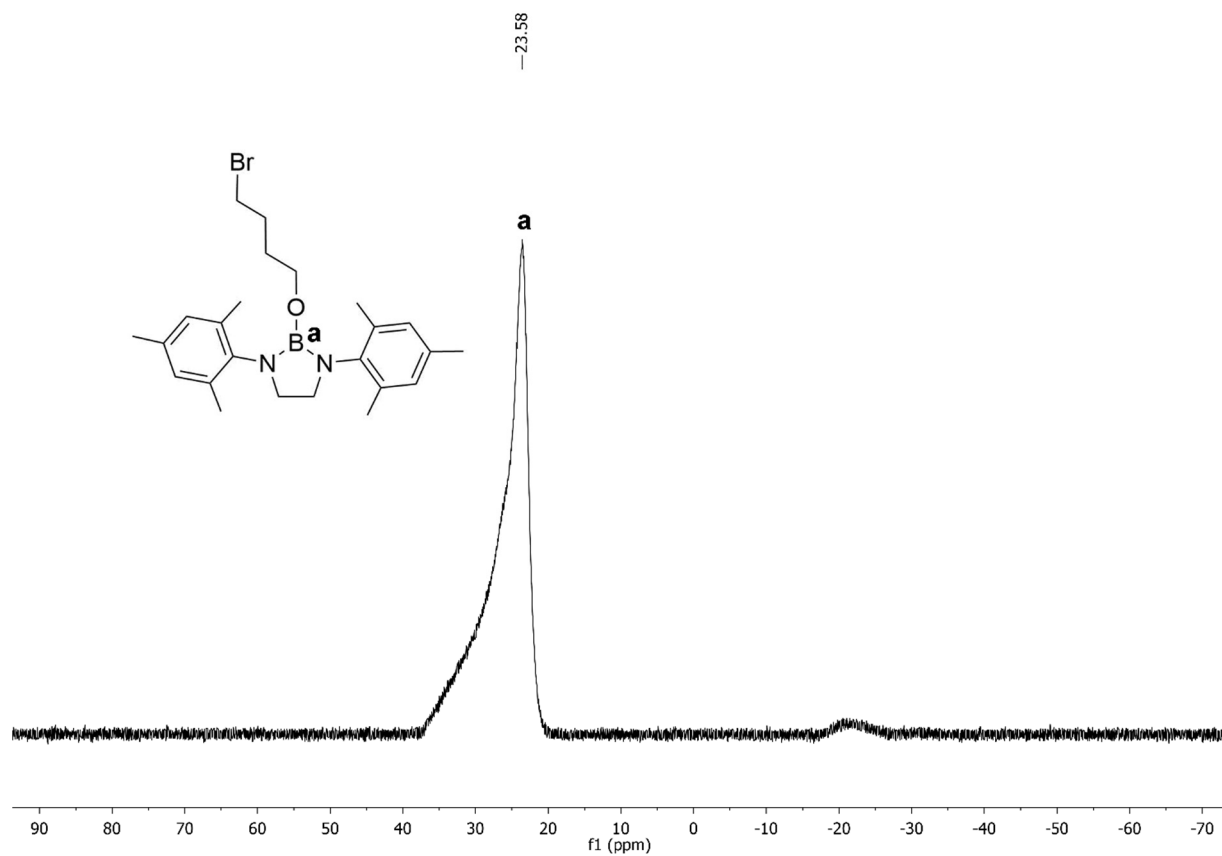
Figure S12. ^{11}B NMR spectrum of DAB^{Mes}-O-(CH$_2$)$_4$-Br acquired in C$_6$D$_6$. Impurity is caused by an unidentified species.
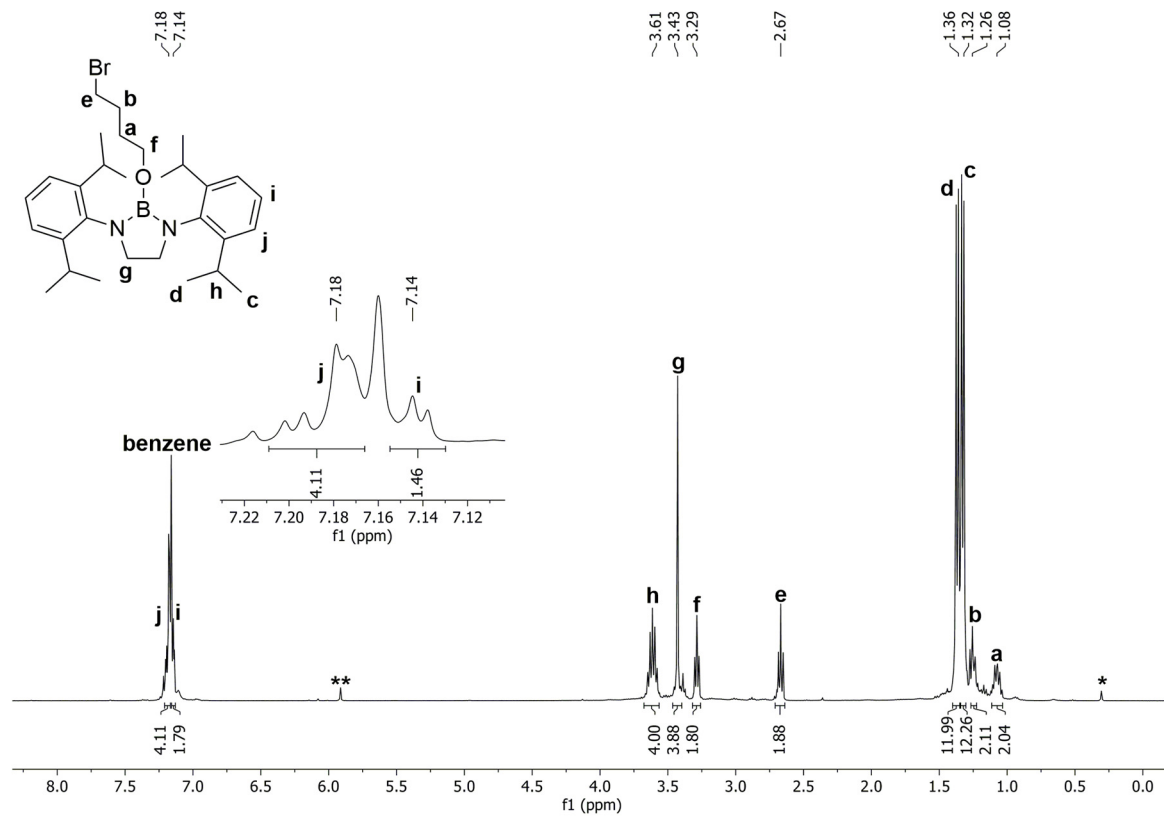
Figure S13. ^1H NMR spectrum of DAB^{Dipp}-O-(CH$_2$)$_4$-Br acquired in C$_6$D$_6$. * silicon grease; ** unknown side product.
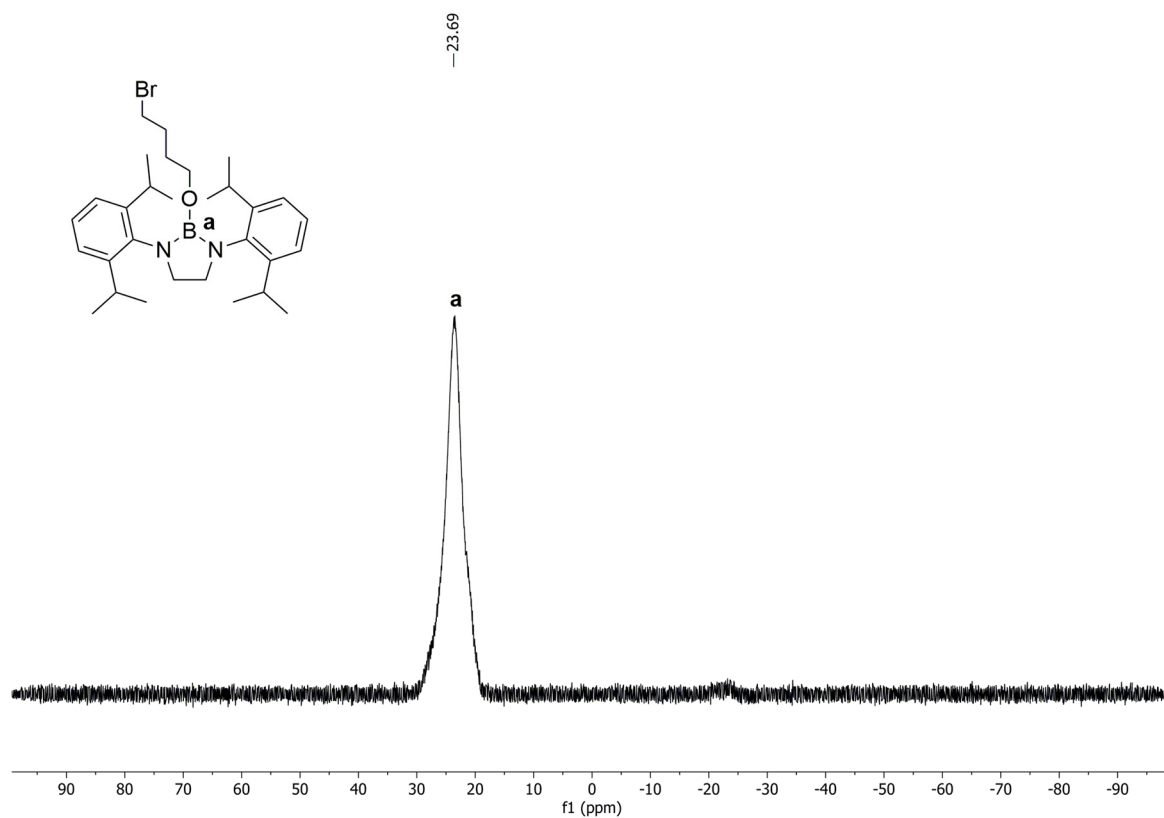
Figure S14. ^{11}B NMR spectrum of DAB^{Dipp}-O-(CH$_2$)$_4$-Br acquired in C$_6$D$_6$.
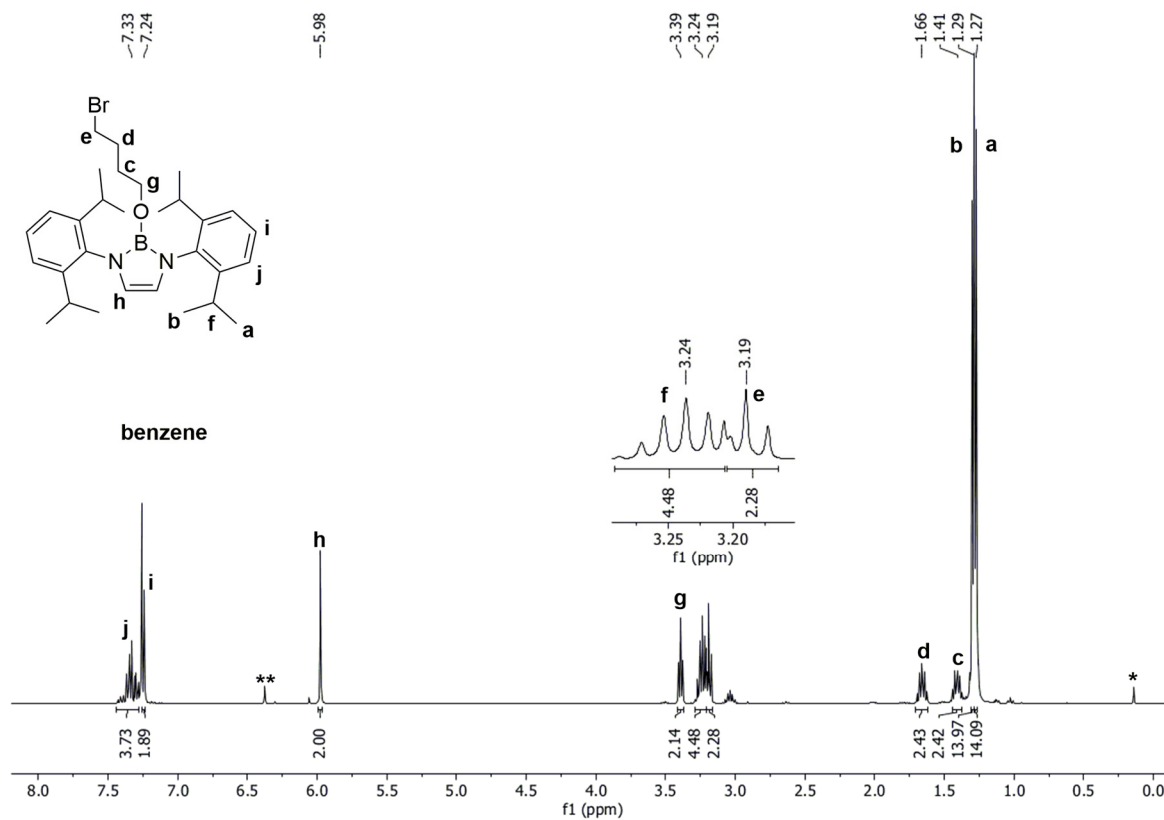
Figure S15.^{1}H NMR spectrum of DAB(II)^{Dipp}-O-(CH$_2$)$_4$-Br acquired in C$_6$D$_6$. * silicon grease; ** unknown side product.
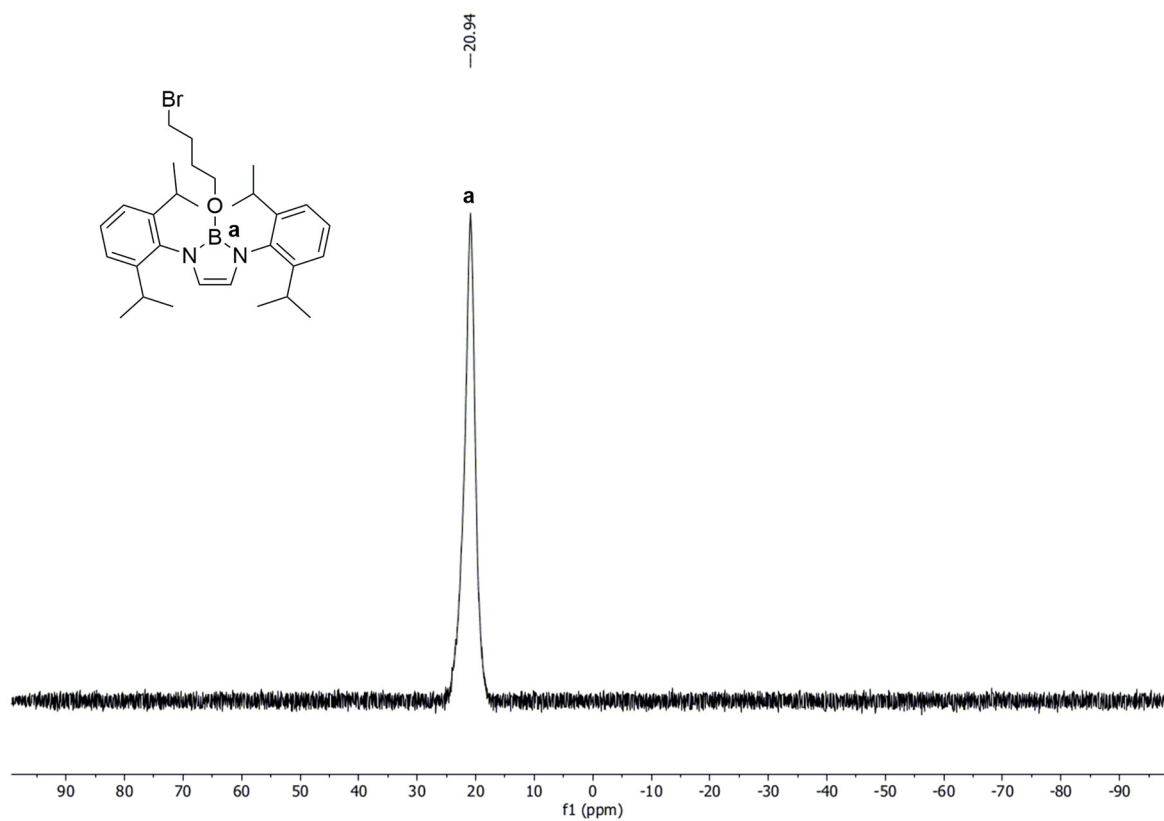
Figure S16.^{11}B NMR spectrum of DAB(II)^{Dipp}-O-(CH$_2$)$_4$-Br acquired in C$_6$D$_6$.
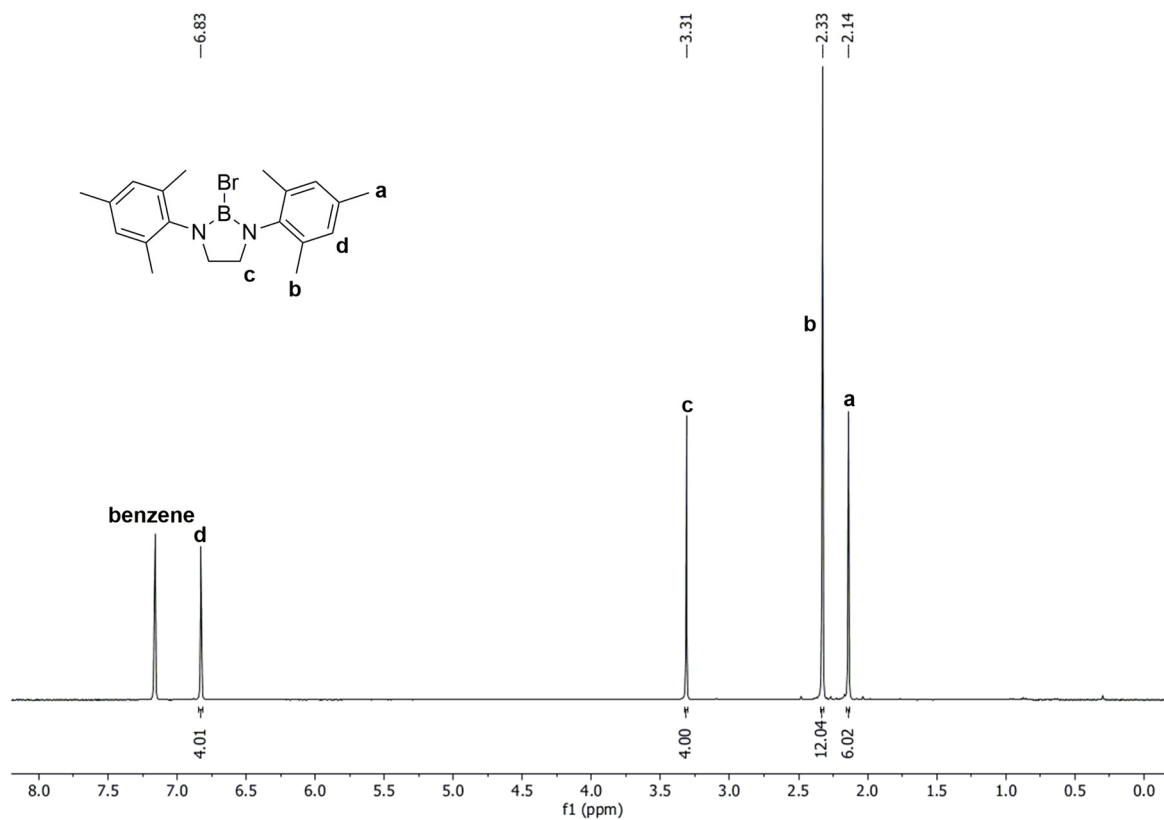
Figure S17.^{1}H NMR spectrum of DAB^{Mes}-Br acquired in C$_6$D$_6$ (before MeCN application).
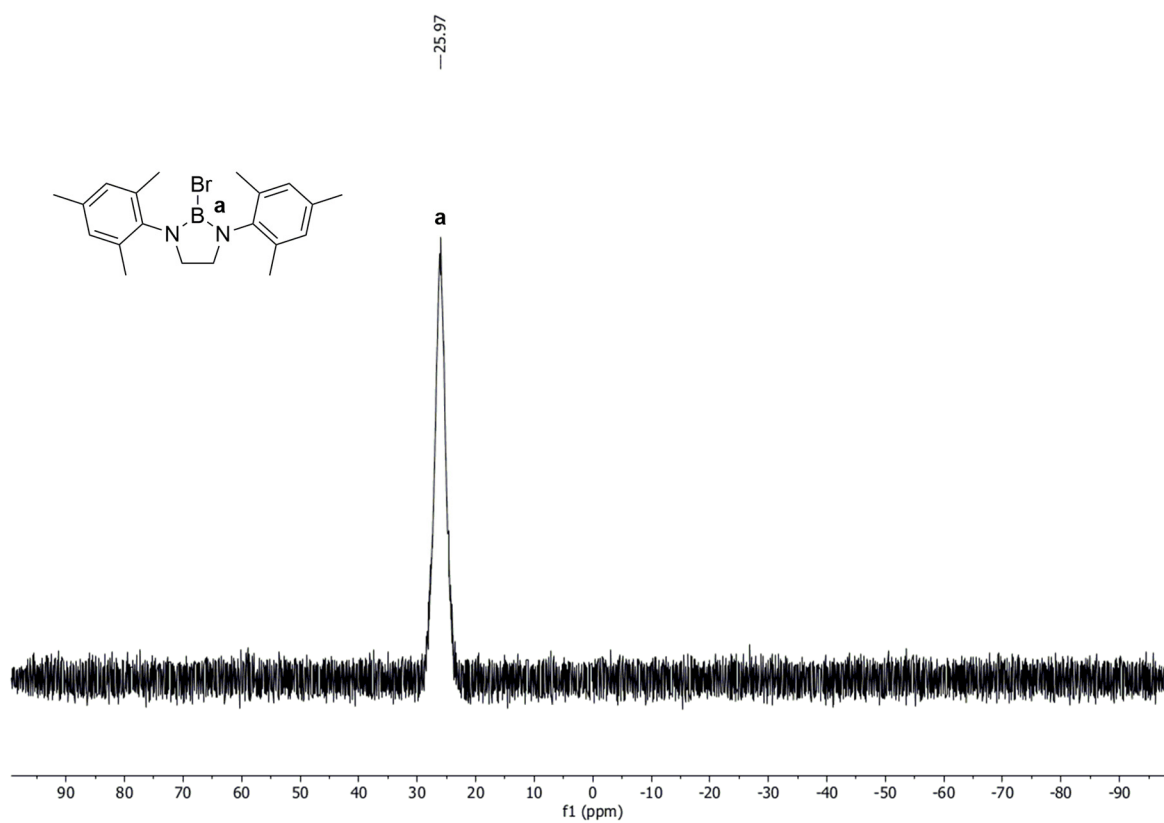
Figure S18.^{11}B NMR spectrum of DAB^{Mes}-Br acquired in C$_6$D$_6$ (before MeCN application).
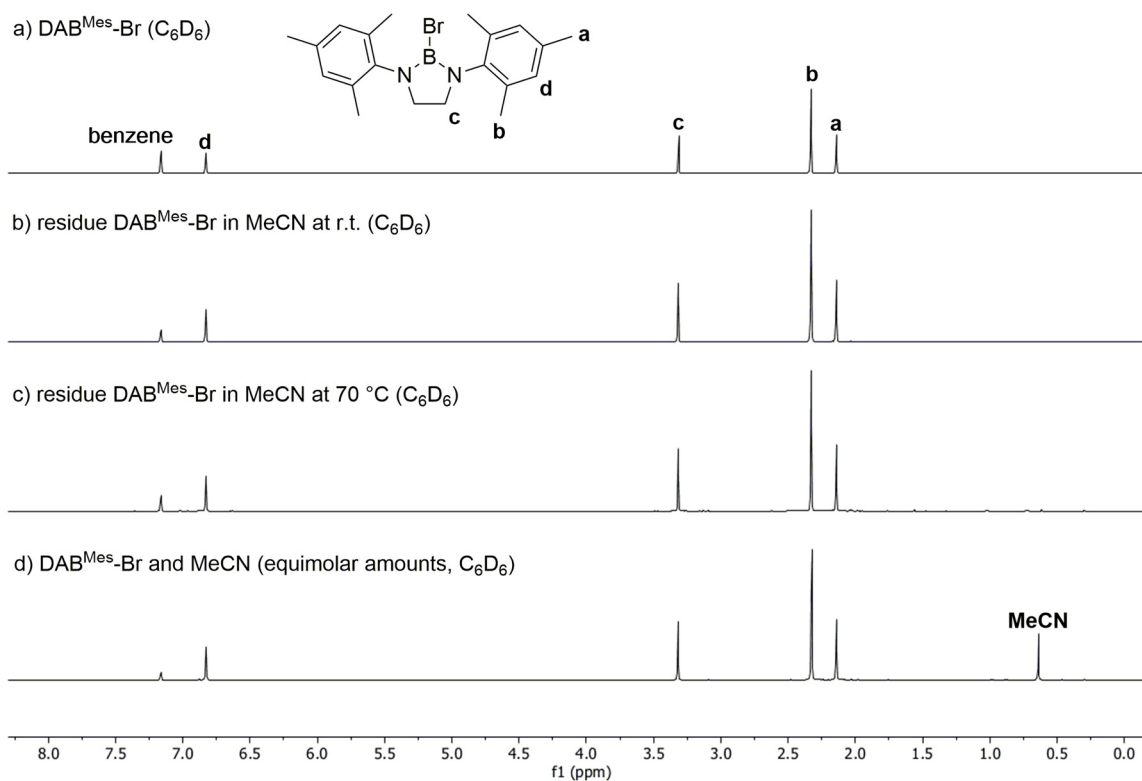
Figure S19. ^{1}H NMR spectra of DAB[Mes]-Br acquired in C6D6: a) pure reactant DAB[Mes]-Br; b) residue of the reaction of DAB[Mes]-Br and MeCN at r.t. for 16 h; c) residue of the reaction of DAB[Mes]-Br and MeCN at 70 °C for 16 h; d) *in situ* monitoring of a combination of DAB[Mes]-Br and MeCN (equimolar amounts). Signal integration according to Figure S17.
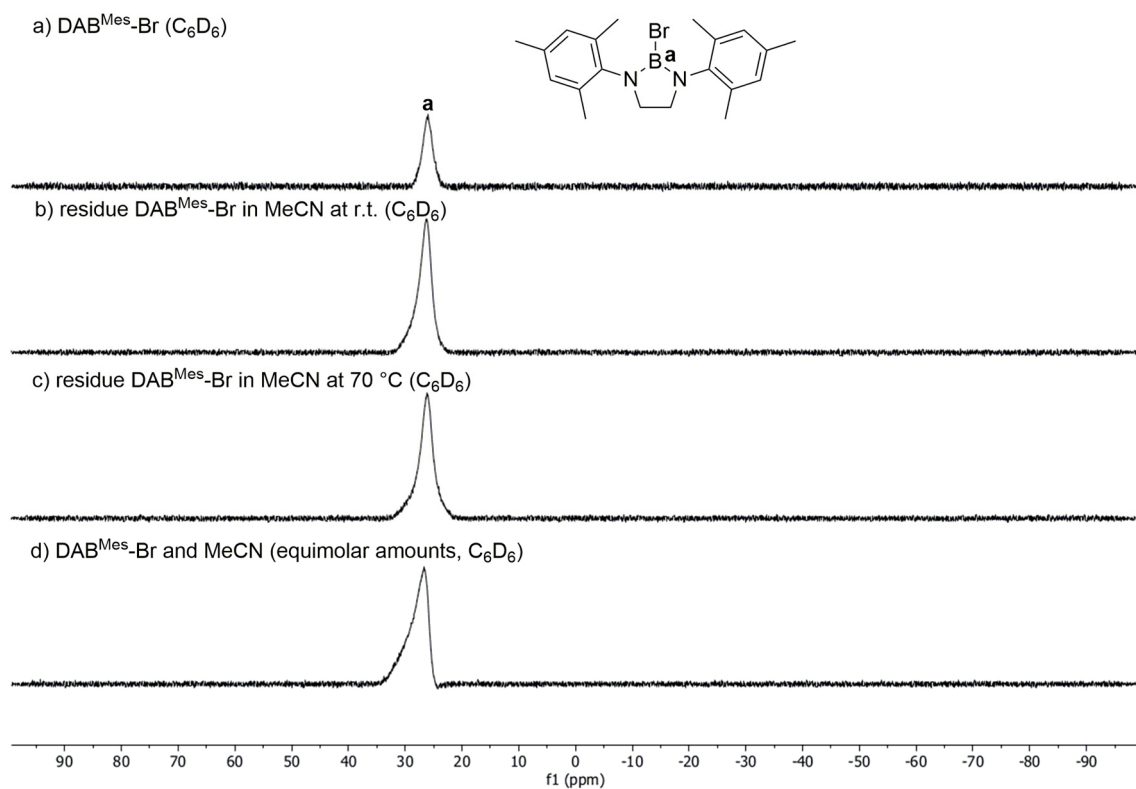
Figure S20. ^{11}B NMR spectra of DAB[Mes]-Br acquired in C6D6: a) pure reactant DAB[Mes]-Br; b) residue of the reaction of DAB[Mes]-Br and MeCN at r.t. for 16 h; c) residue of the reaction of DAB[Mes]-Br and MeCN at 70 °C for 16 h; d) *in situ* monitoring of a combination of DAB[Mes]-Br and MeCN (equimolar amounts).
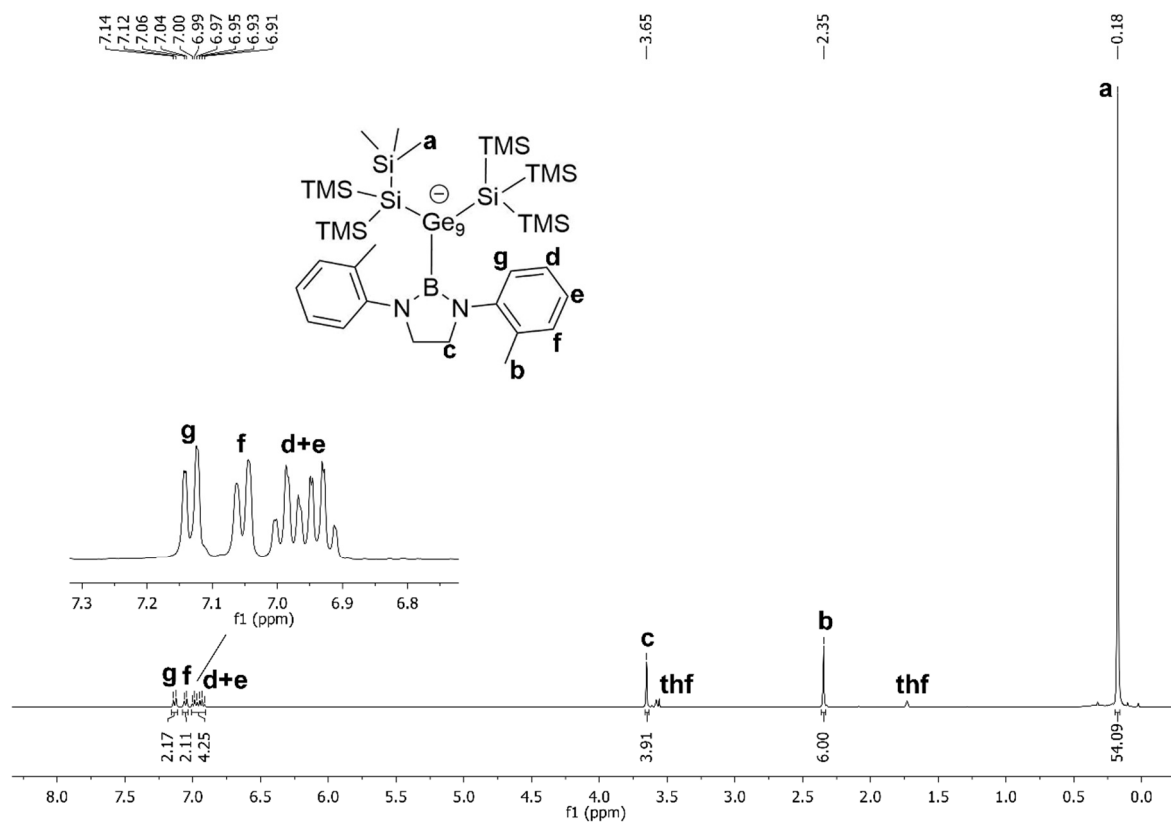
Figure S21. ^{1}H NMR spectrum of compound **1** acquired in thf-d_8.
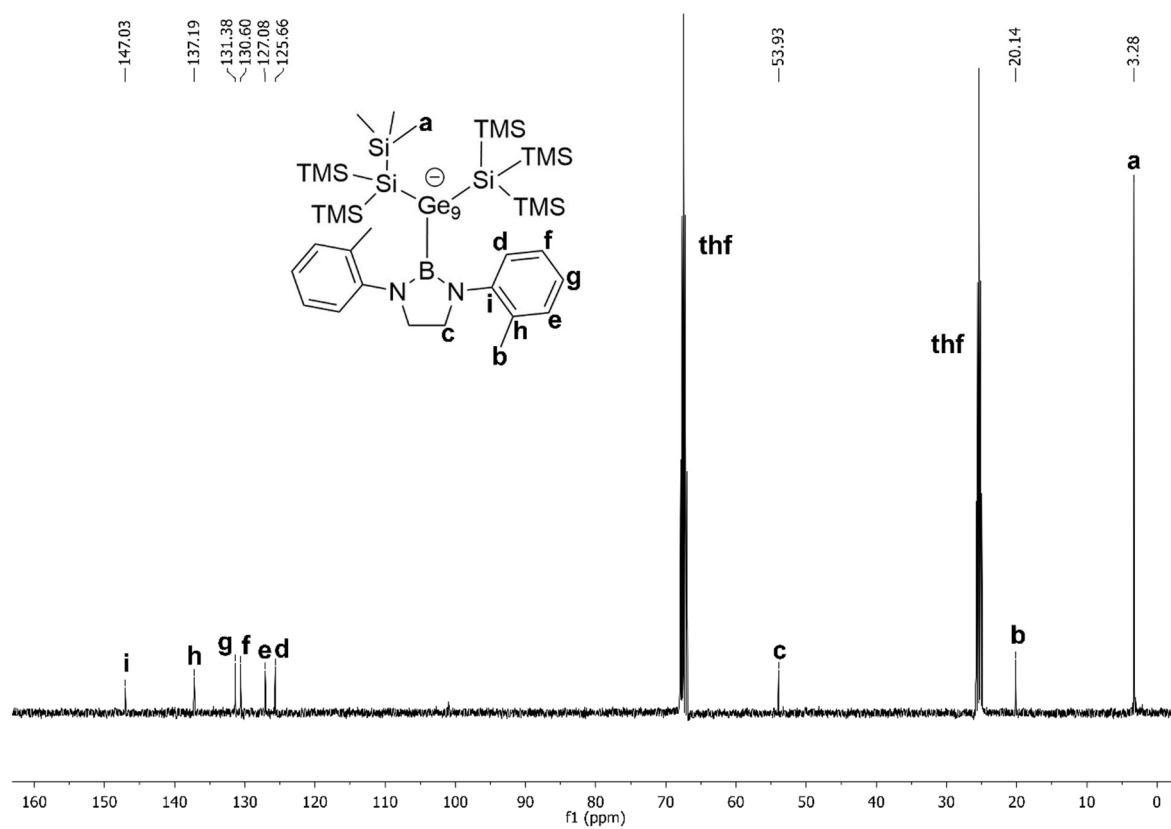
Figure S22. ^{13}C NMR spectrum of compound **1** acquired in thf-d_8.

—9.99

—108.80

b

a
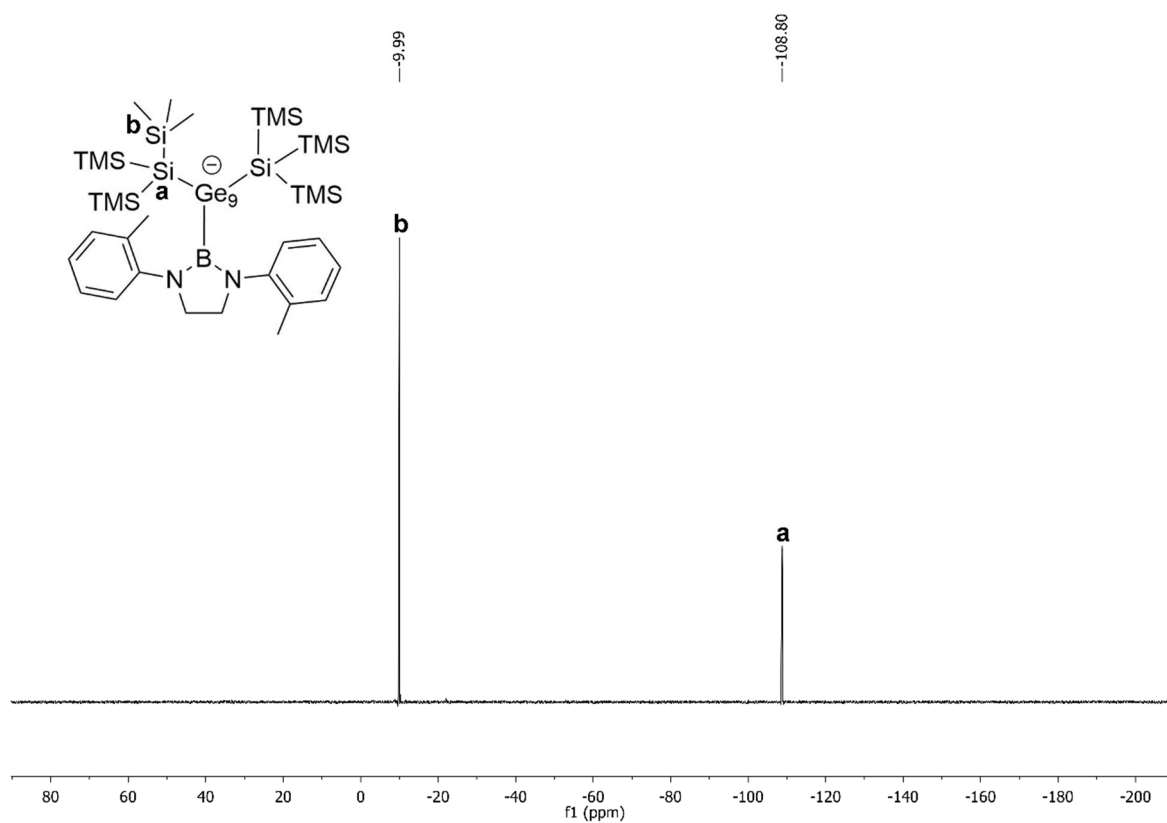
Figure S23. ^{29}Si-INEPT NMR spectrum of compound **1** acquired in thf-d_8.

—42.92

a
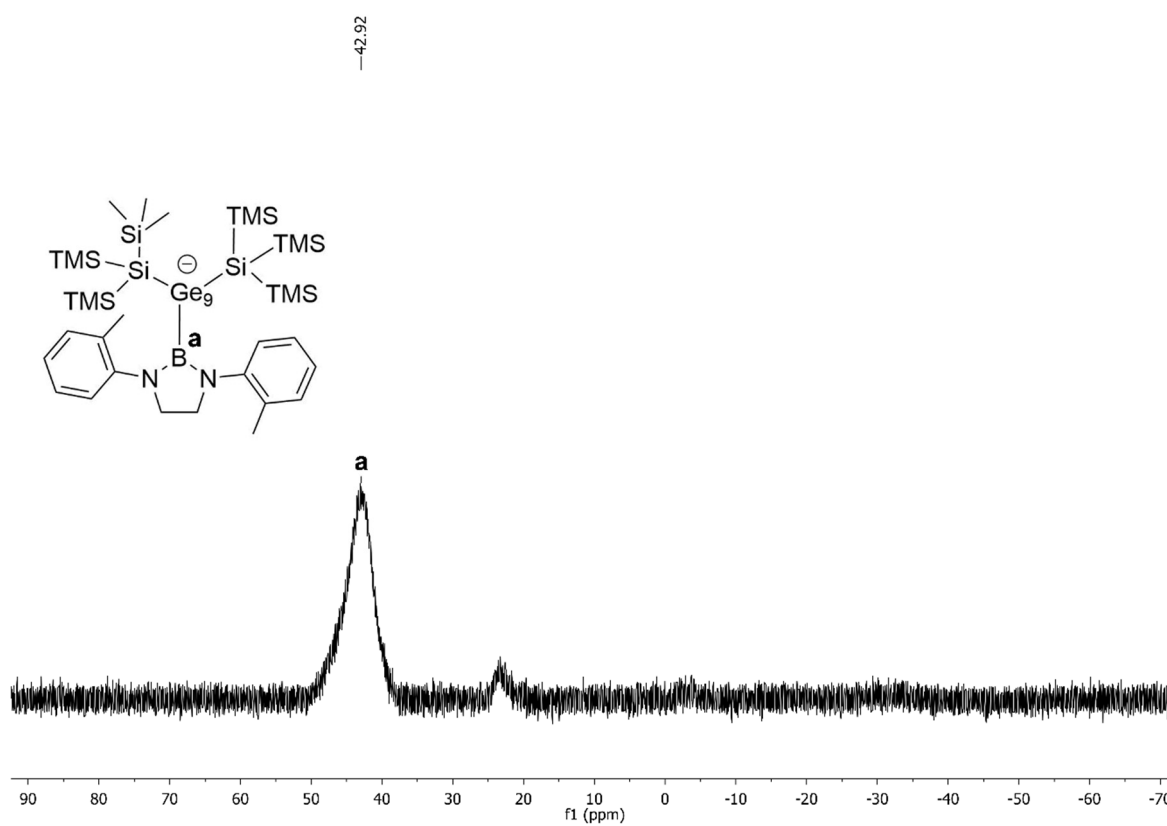
Figure S24. ^{11}B NMR spectrum of compound **1** acquired in thf-d_8. Impurity is caused by an unidentified species.
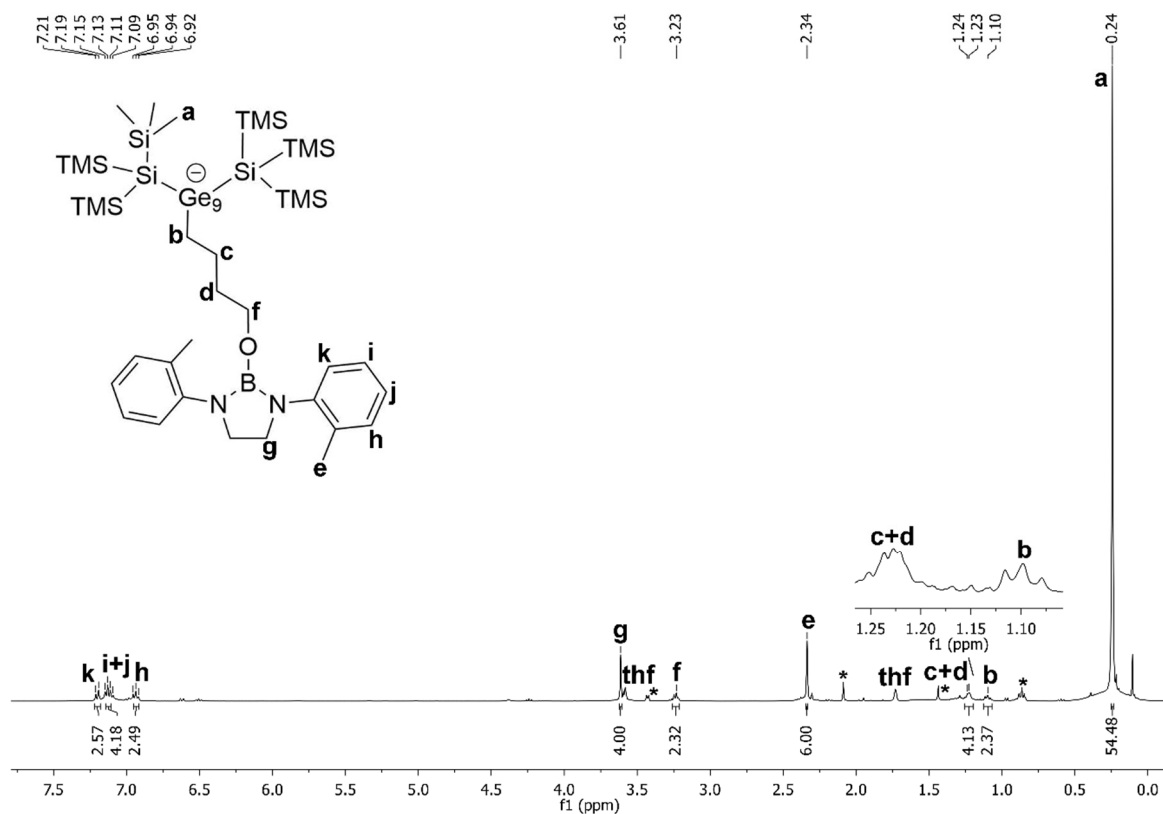
Figure S25. ^{1}H NMR spectrum of compound **2** acquired in thf-d_8. Asterisked signals are caused by unknown impurities.
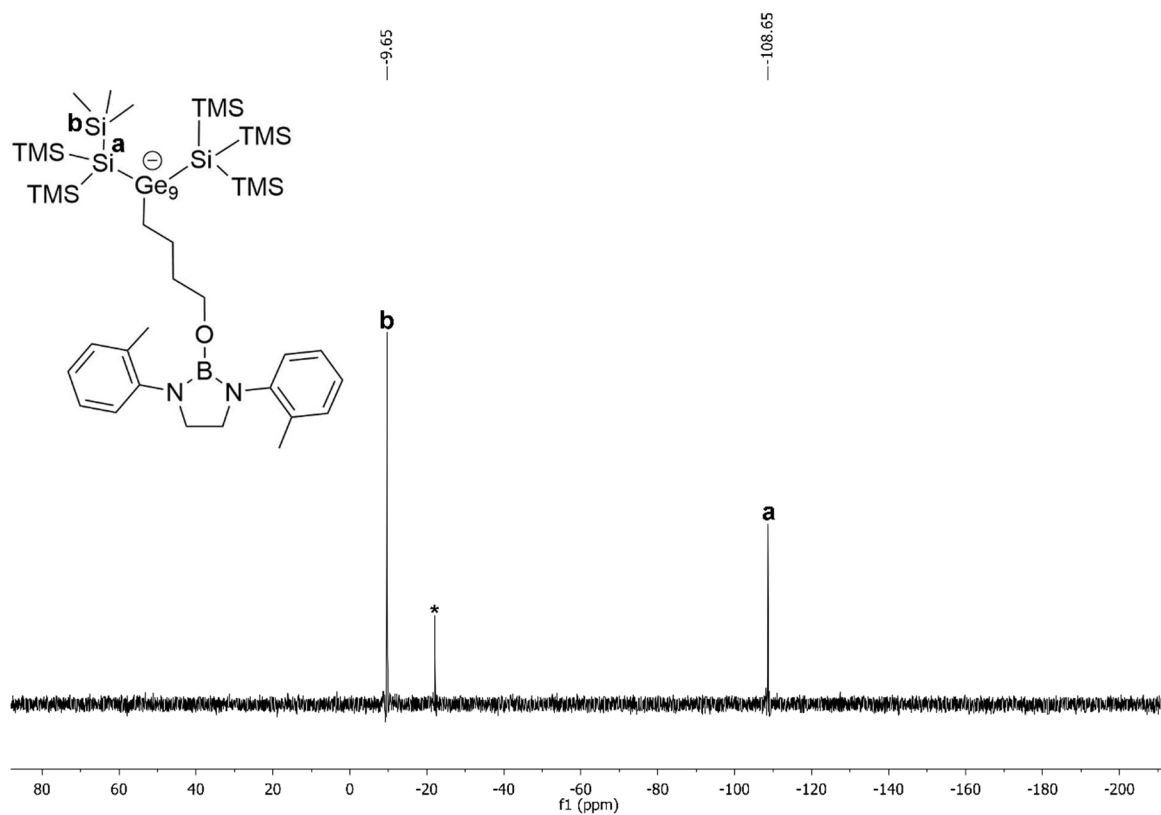
Figure S26. ^{29}Si-INEPT NMR spectrum of compound **2** acquired in thf-d_8. Asterisked signal caused by silicon grease.

S21
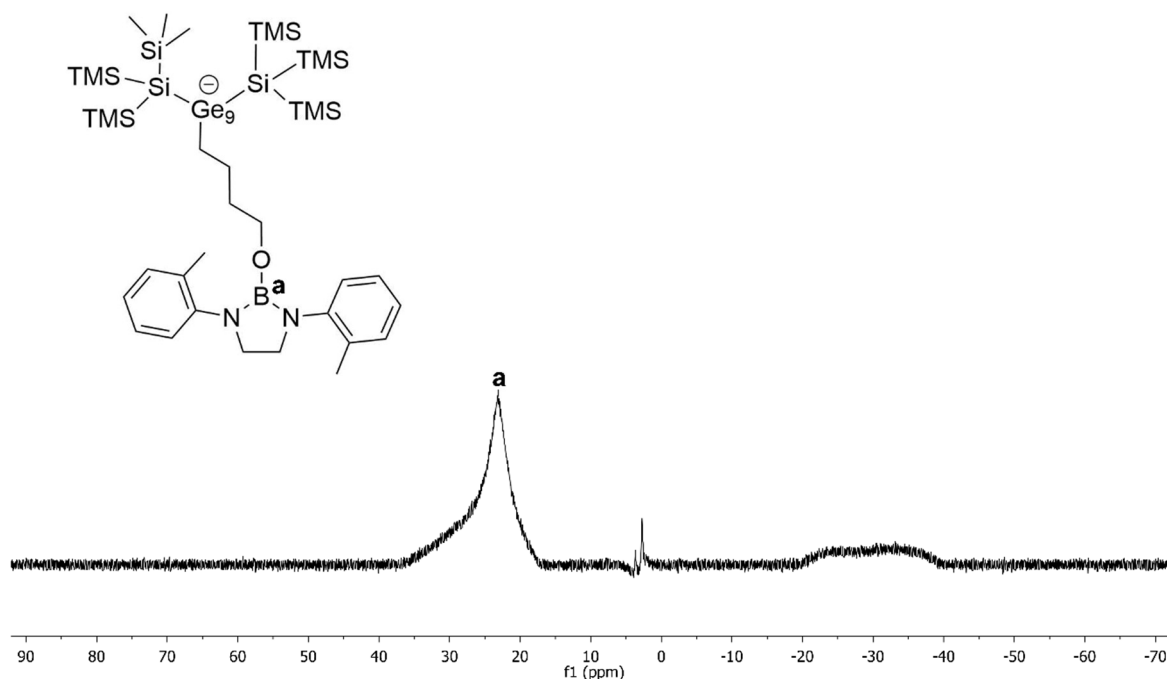
Figure S27. ^{11}B NMR spectrum of compound **2** acquired in thf-d_8. Impurity is caused by unidentified species.
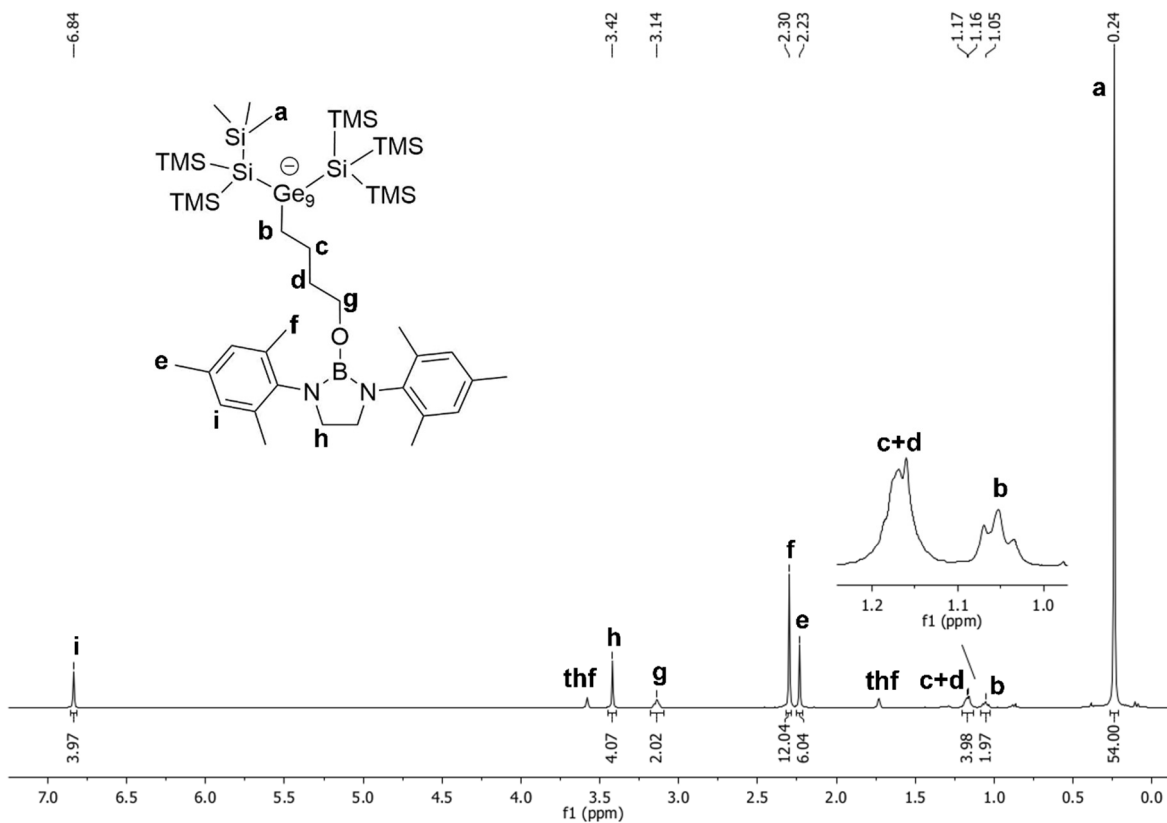
Figure S28. ^1H NMR spectrum of compound **3** acquired in thf-d_8.
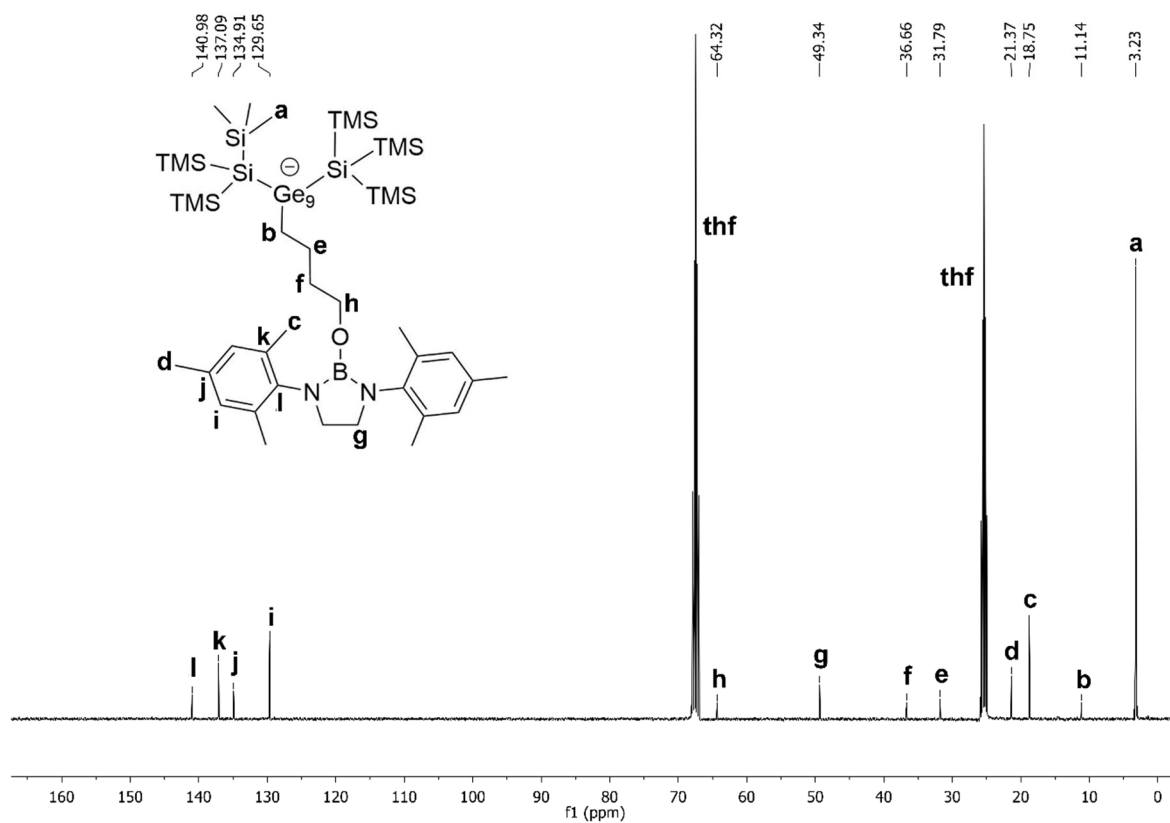
Figure S29. ^{13}C NMR spectrum of compound **3** acquired in thf-d_8.
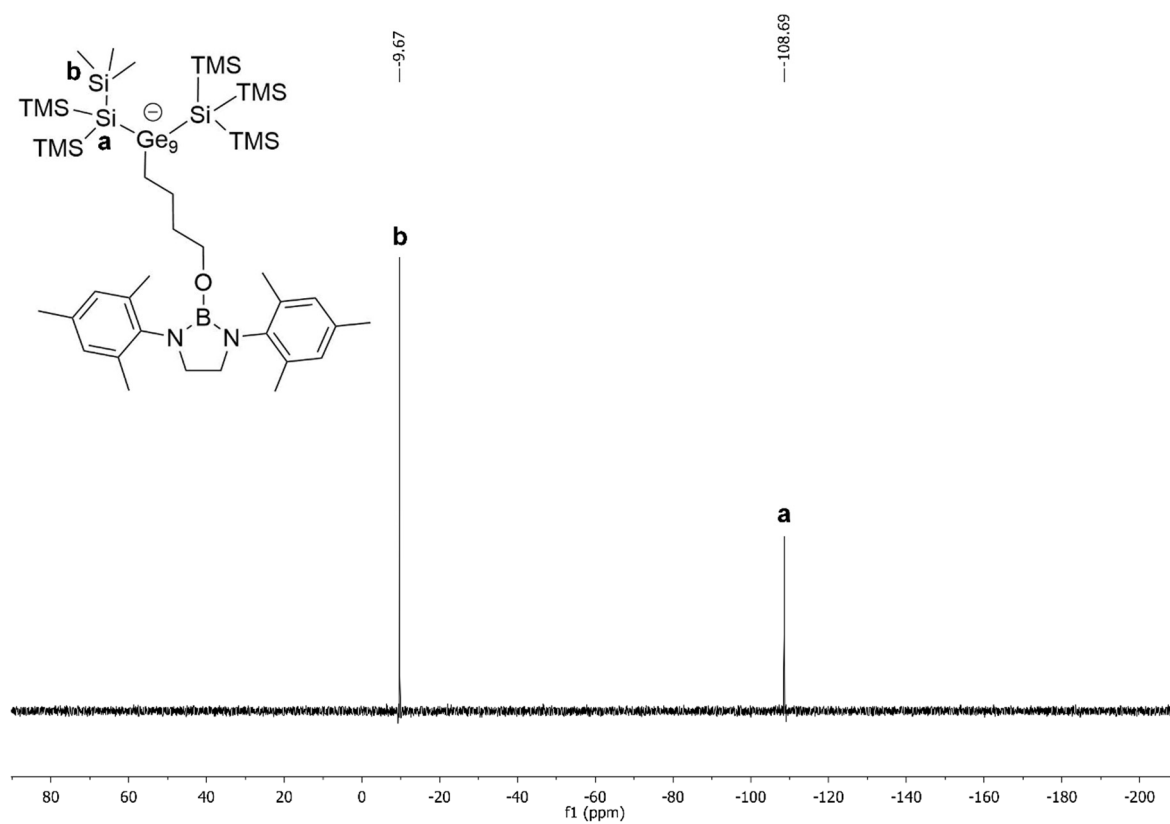
Figure S30. ^{29}Si-INEPT NMR spectrum of compound **3** acquired in thf-d_8.

S23

−23.82

a
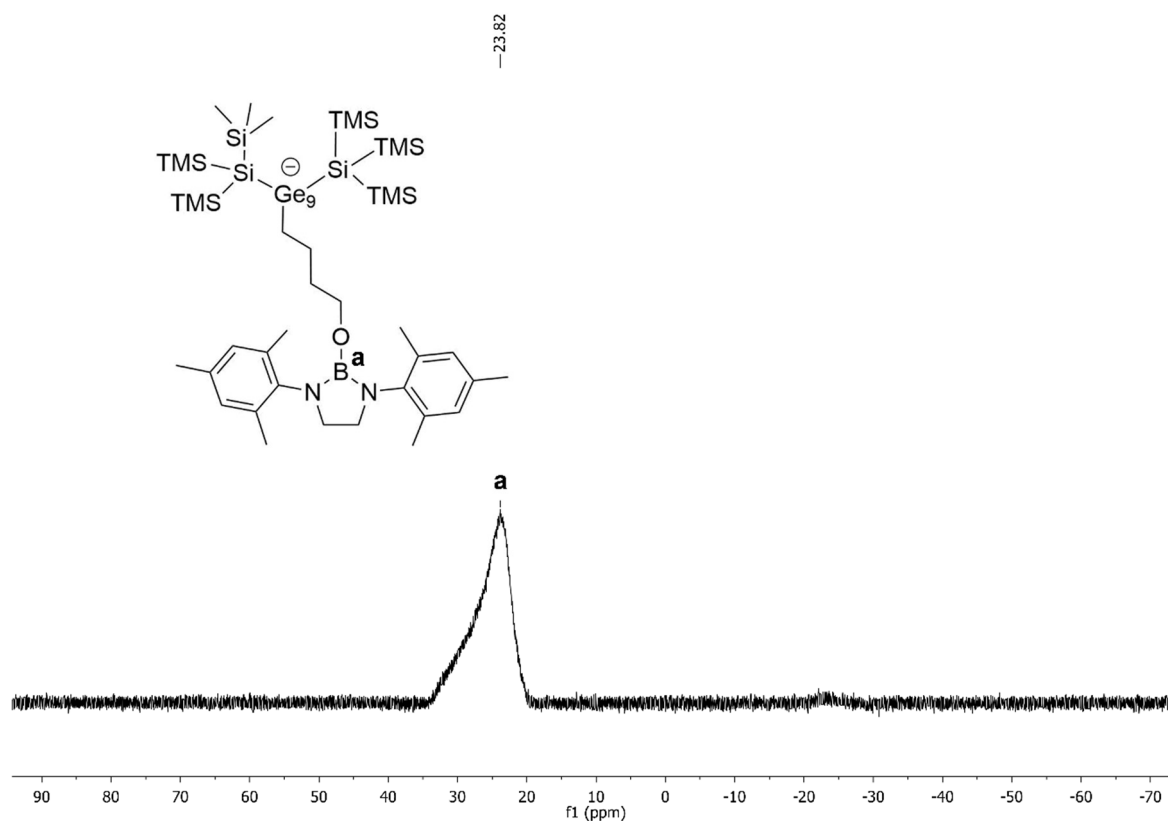
Figure S31. ^{11}B NMR spectrum of compound **3** acquired in thf-d_8. Impurity is caused by an unidentified species.

90 °C
70 °C
50 °C
30 °C
23°C
0 °C
-10 °C
-30 °C
-50 °C
-70 °C
-80 °C
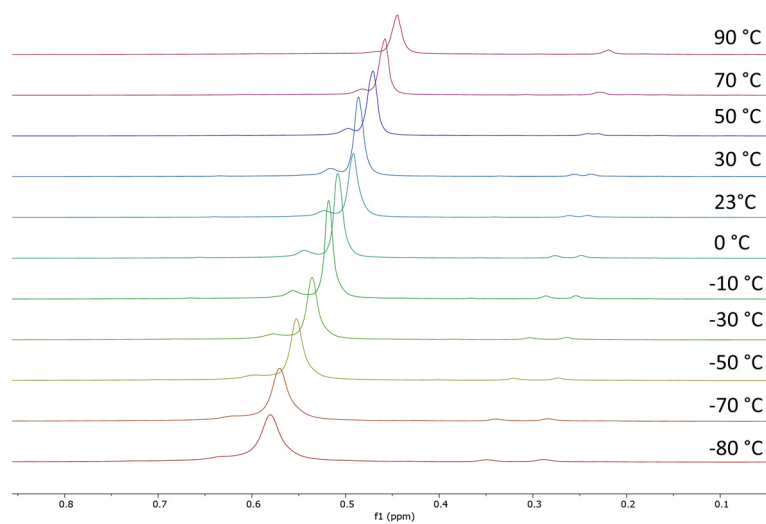
Figure S32. Selected area of VT (variable temperature) ^{1}H NMR spectra of compound **3** acquired in tol-d_8.
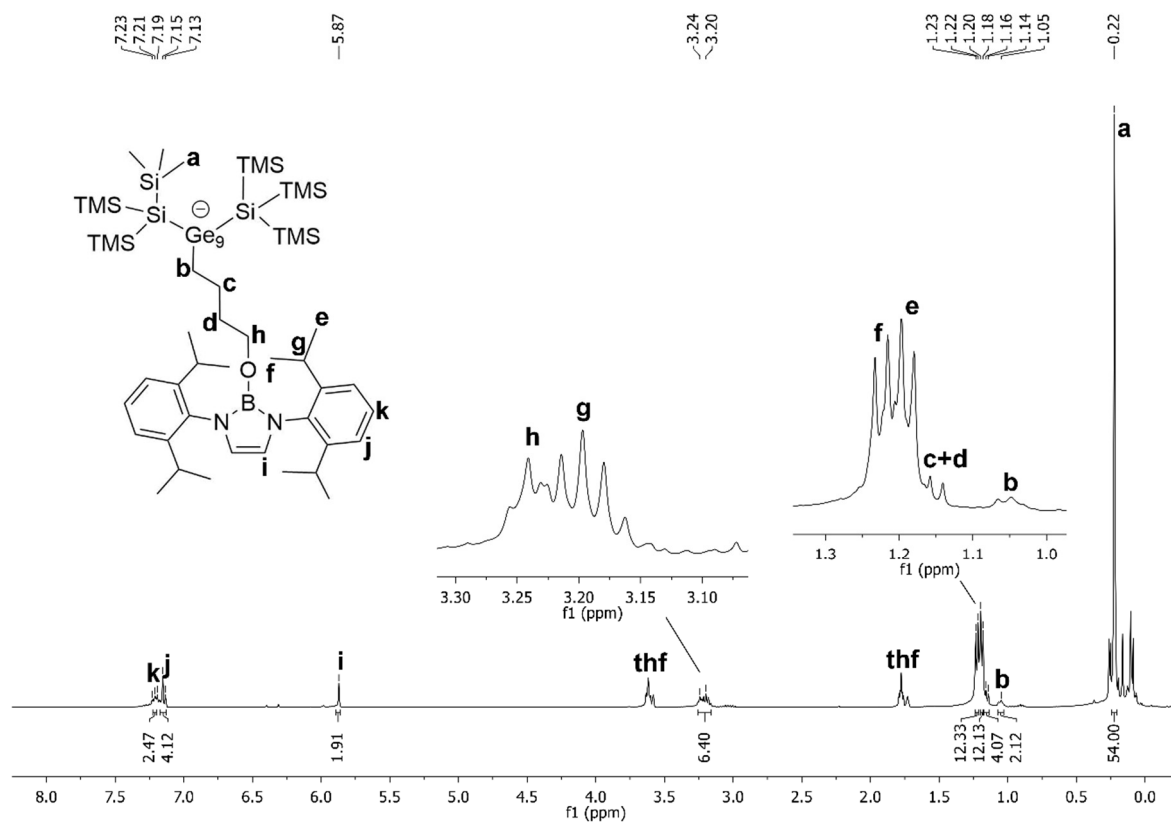
Figure S33. ^{1}H NMR spectrum of compound **4** acquired in thf-d_8.
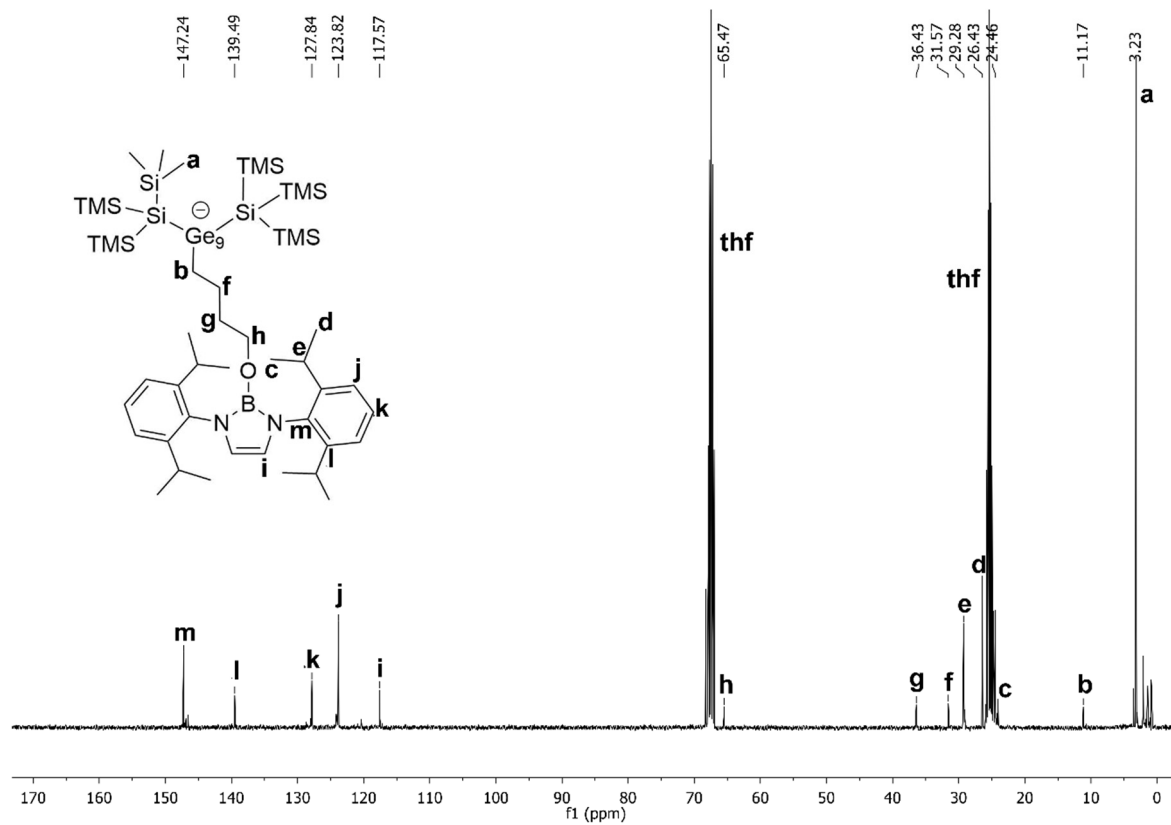
Figure S34. ^{13}C NMR spectrum of compound **4** acquired in thf-d_8.

−9.67

−108.72

b

a

80 60 40 20 0 -20 -40 -60 -80 -100 -120 -140 -160 -180 -200
f1 (ppm)
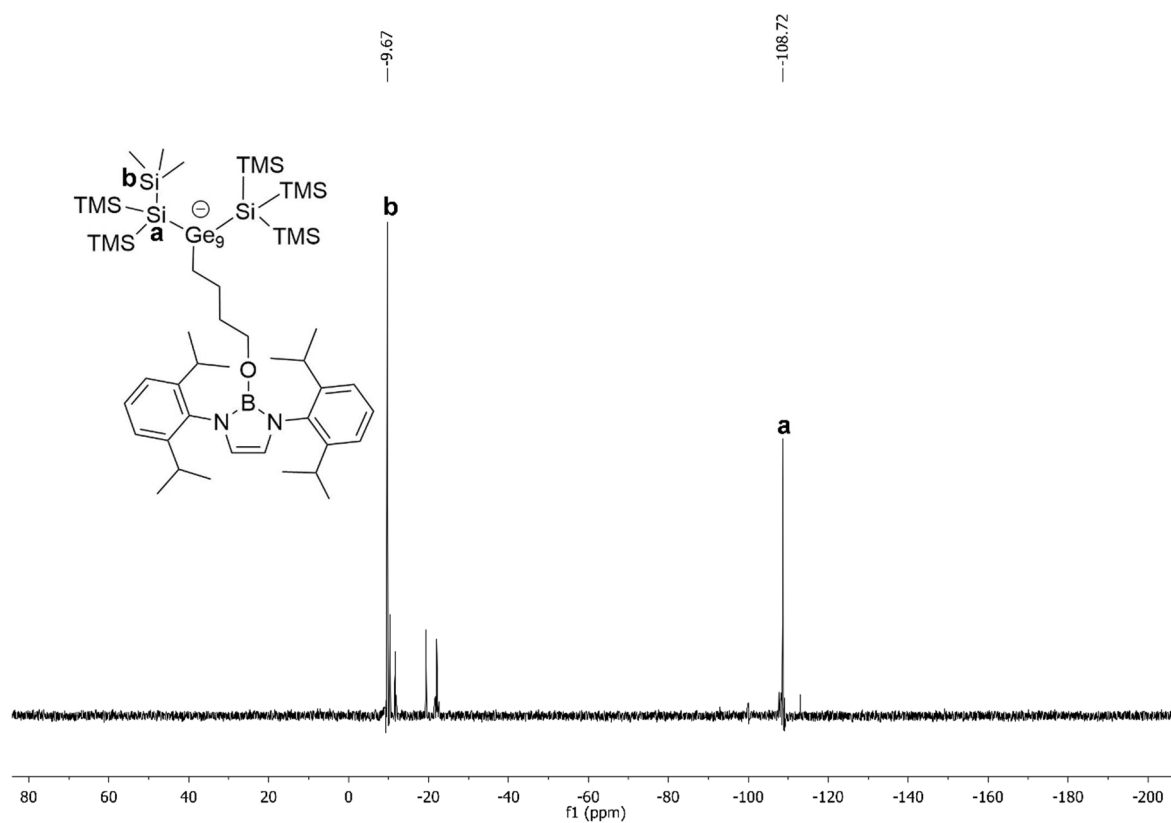
Figure S35.^{29}Si-INEPT NMR spectrum of compound **4** acquired in thf-d_8. Impurity is caused by unidentified species.

−20.66

a

a

90 80 70 60 50 40 30 20 10 0 -10 -20 -30 -40 -50 -60 -70 -80 -90
f1 (ppm)
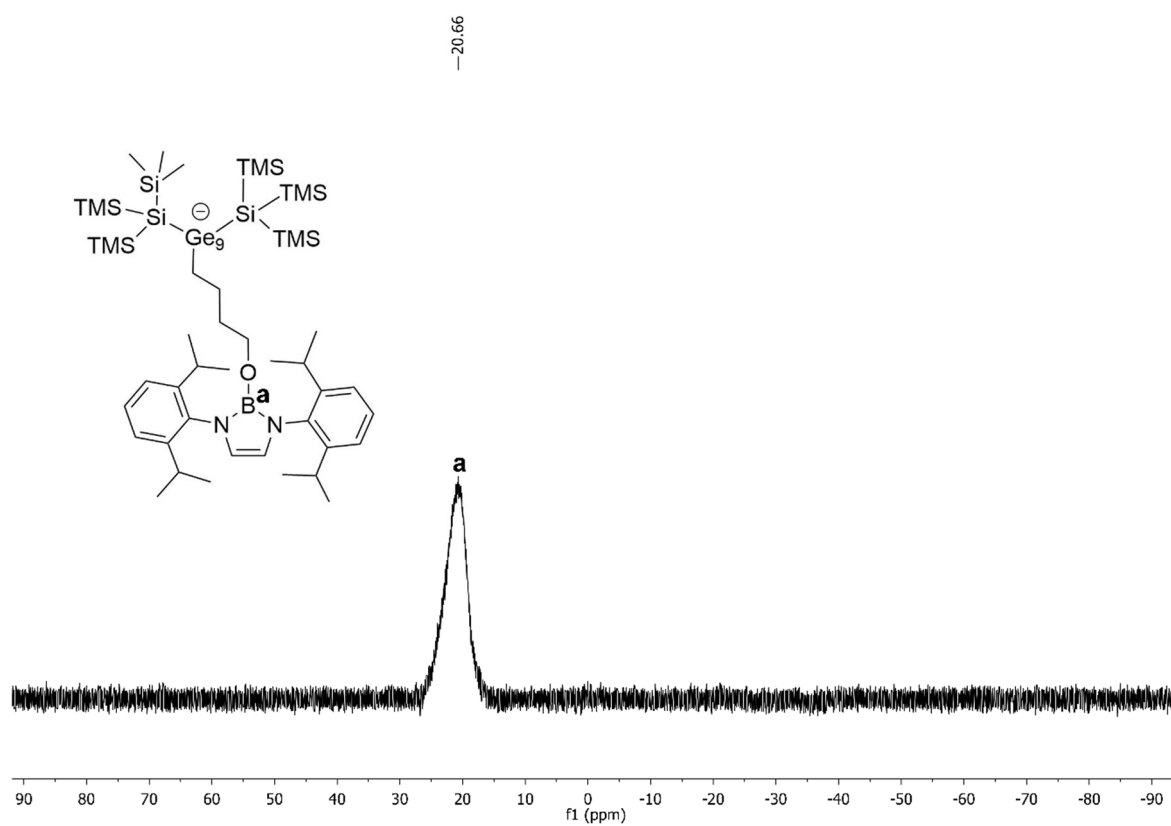
Figure S36.^{11}B NMR spectrum of compound **4** acquired in thf-d_8.
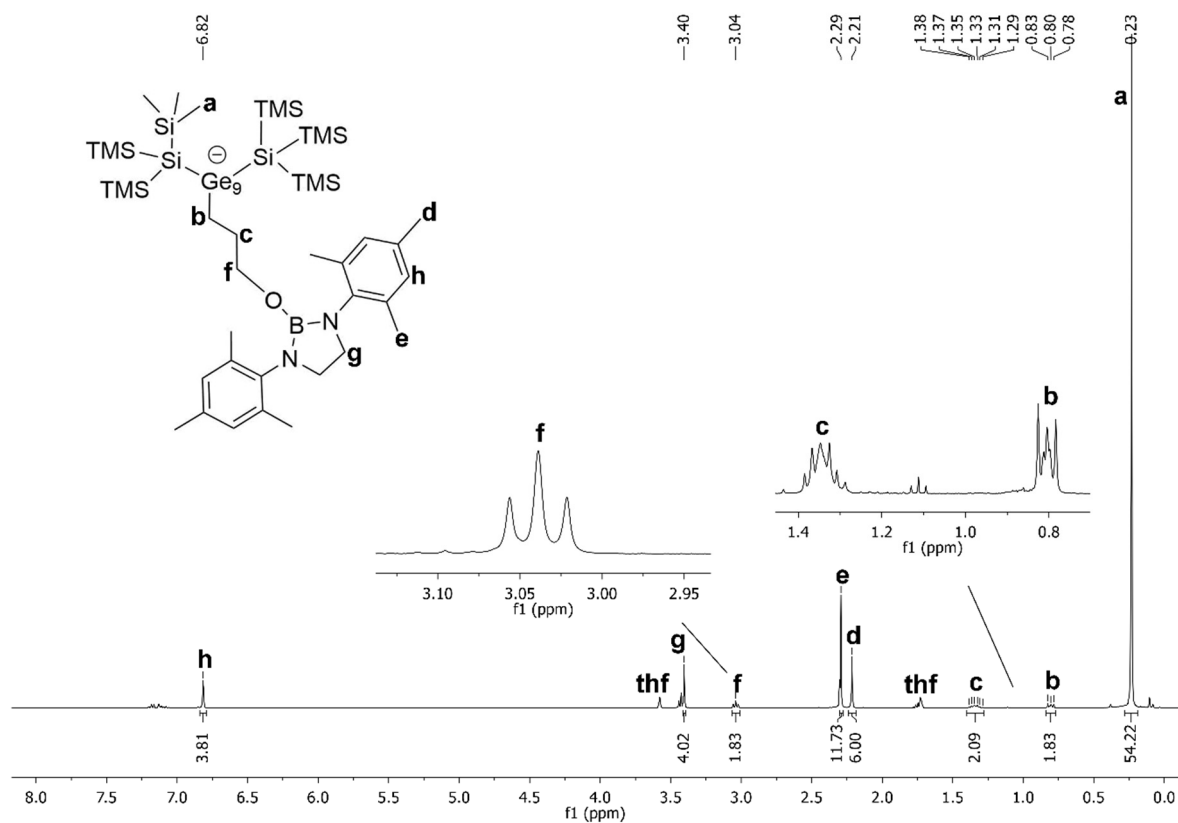
Figure S37. ^{1}H NMR spectrum of compound **5** acquired in thf-d_8.
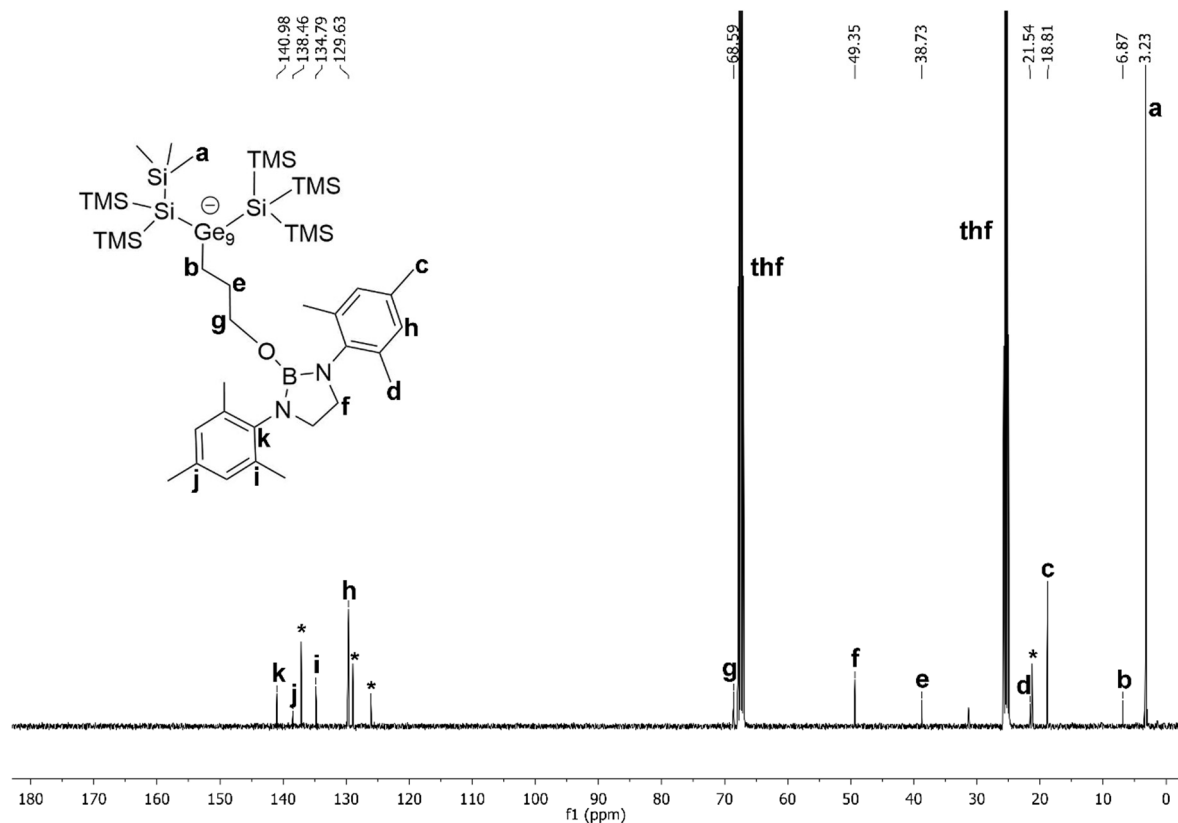
Figure S38. ^{13}C NMR spectrum of compound **5** acquired in thf-d_8. Asterisked signal is caused by unknown impurity.
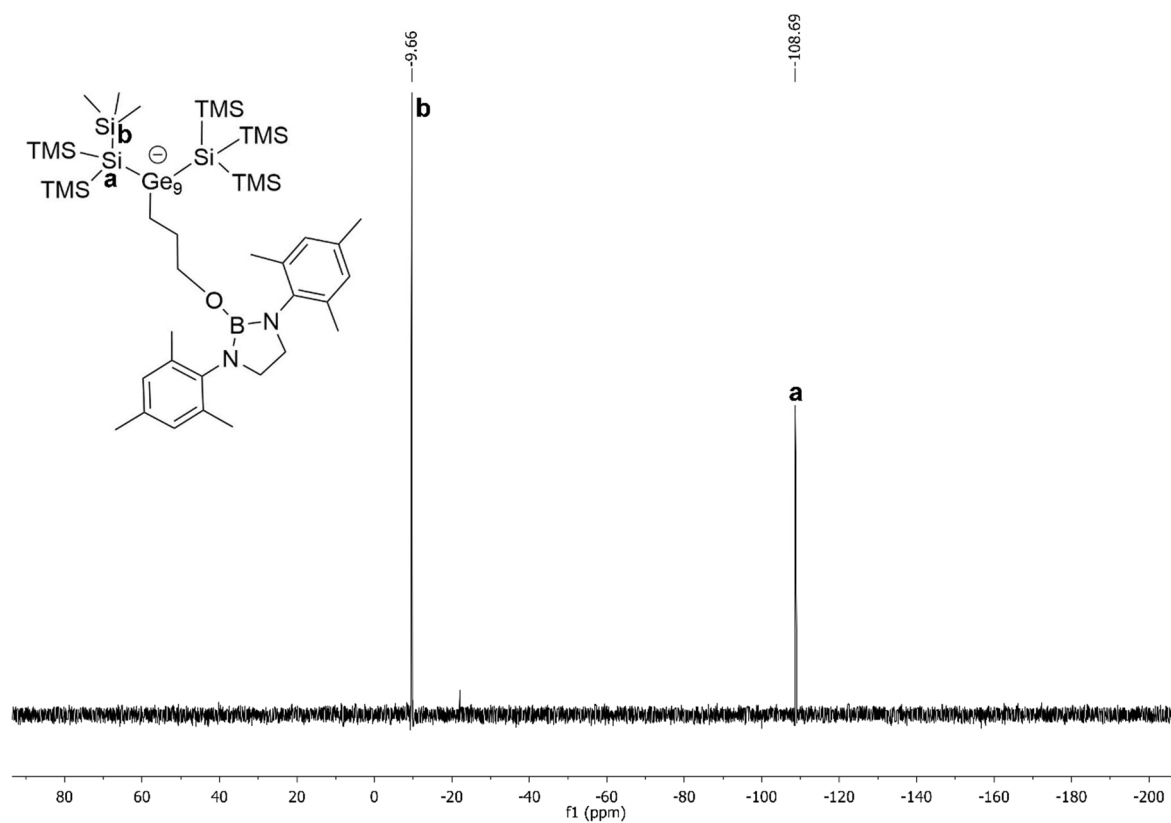
Figure S39. ^{29}Si-INEPT NMR spectrum of compound **5** acquired in thf-d_8.
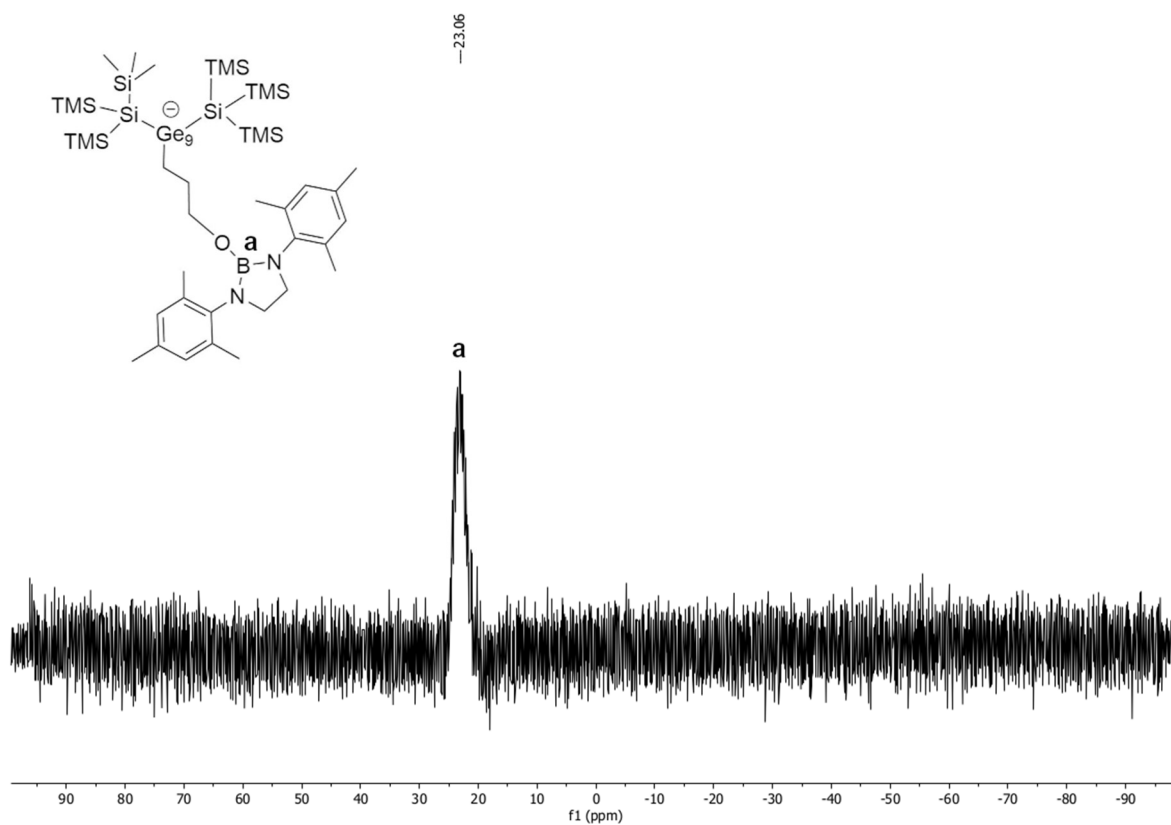
Figure S40. ^{11}B- NMR spectrum of compound **5** acquired in thf.
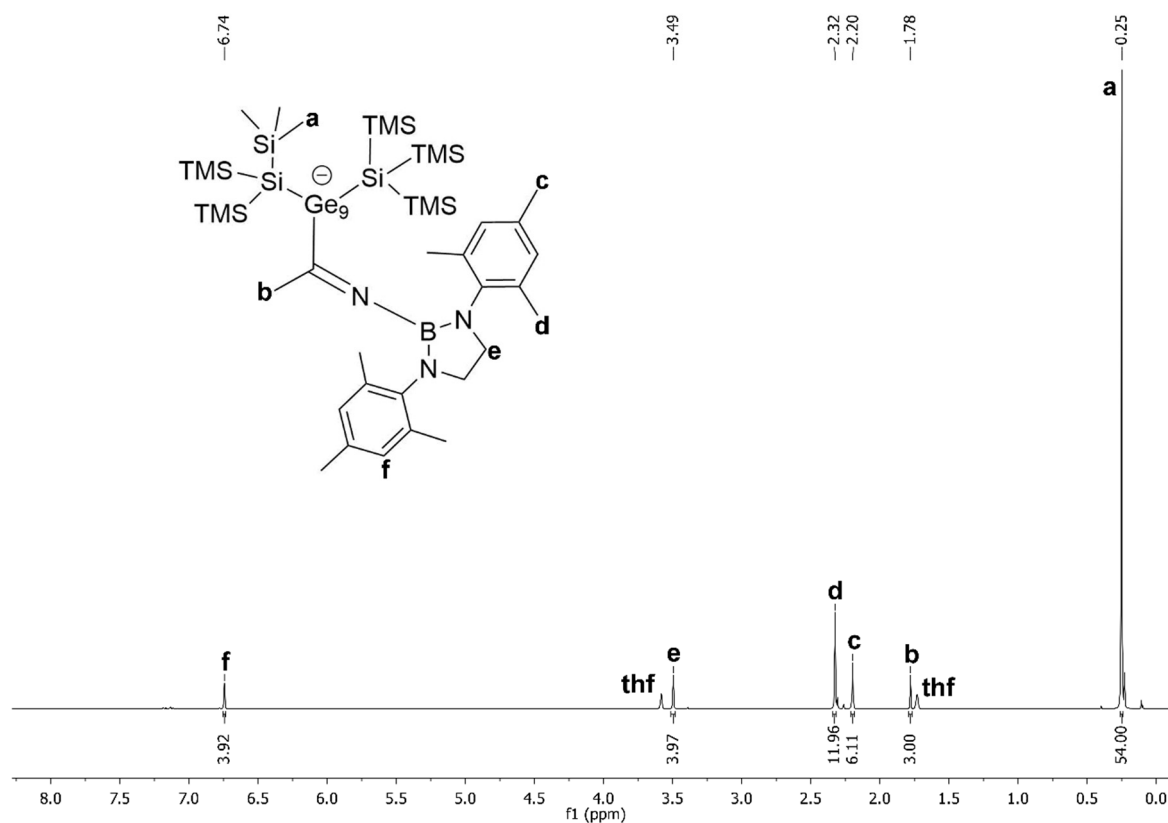
Figure S41.^{1}H NMR spectrum of compound **6** acquired in thf-d_8.
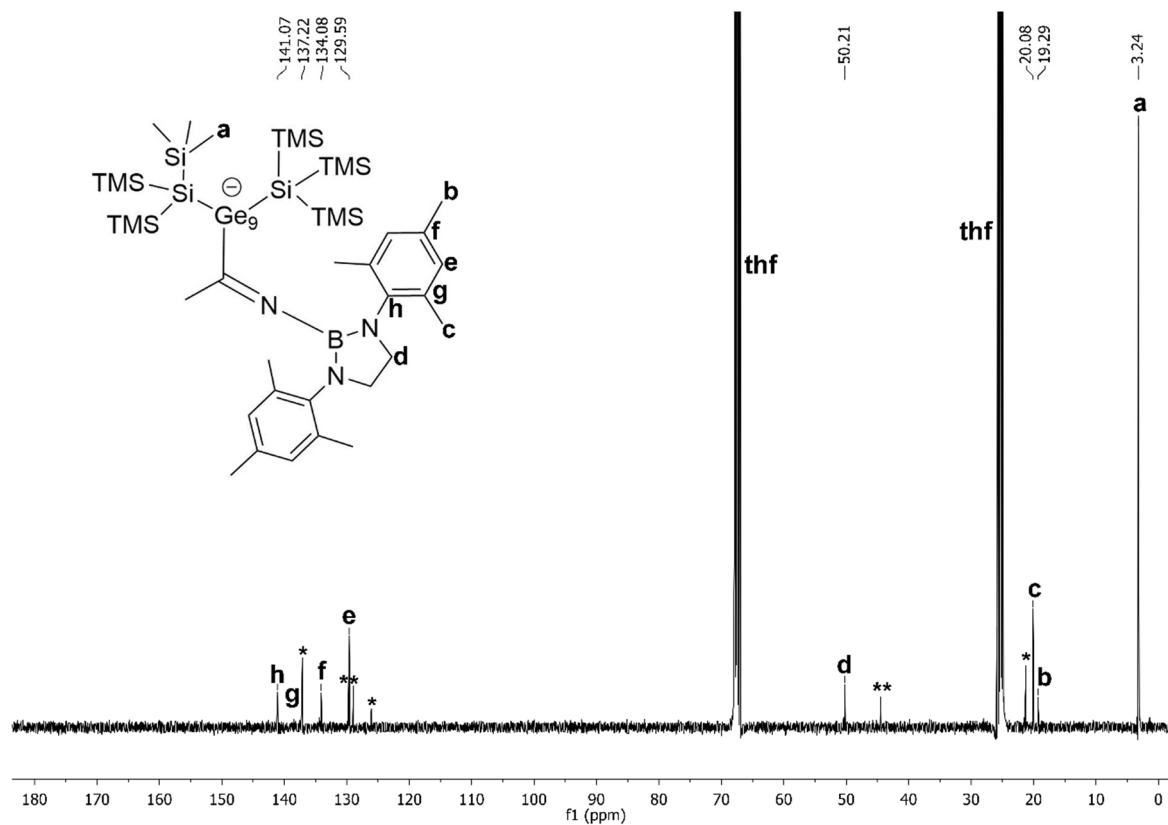
Figure S42.^{13}C NMR spectrum of compound **6** acquired in thf-d_8.* toluene; ** unknown impurity.
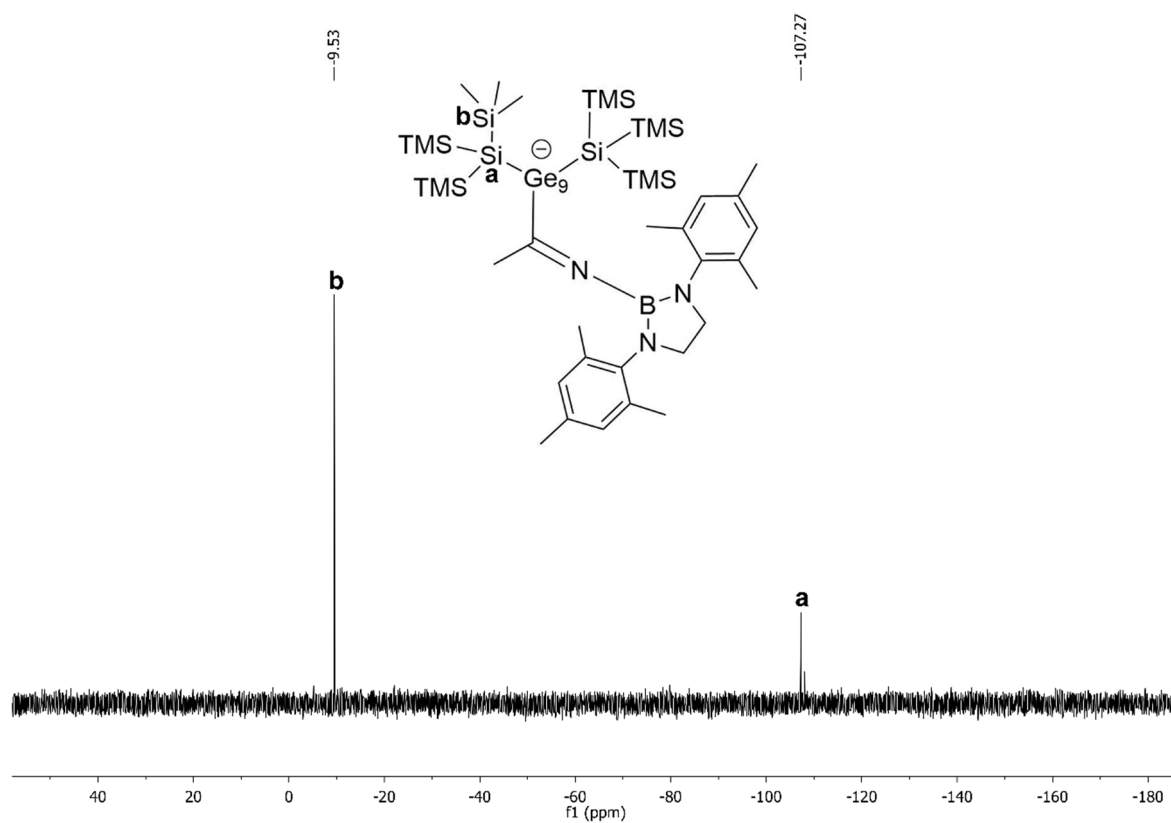
Figure S43. ^{29}Si-INEPT NMR spectrum of compound **6** acquired in thf-d_8.
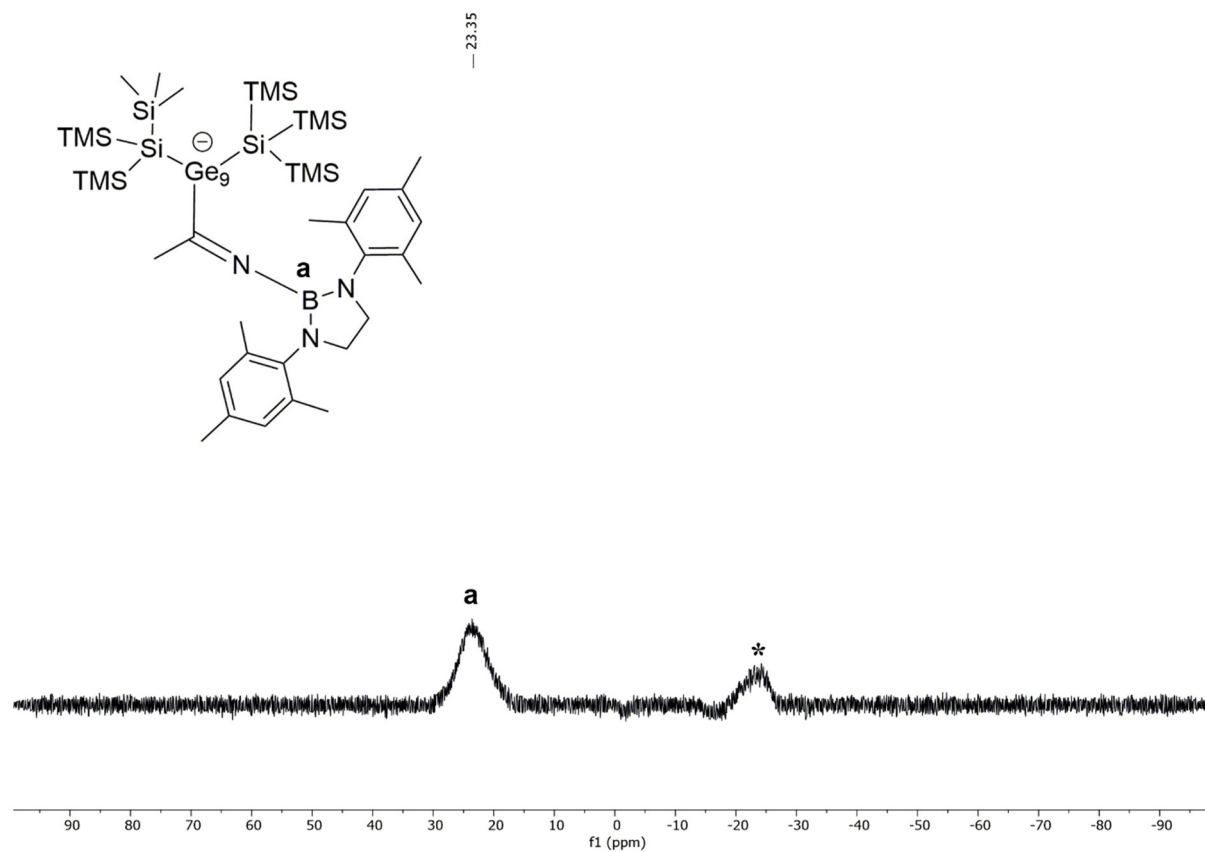
Figure S44: ^{11}B NMR spectrum of compound **6** acquired in thf-d_8. Asterisked signal is caused by glass of NMR tube.

ESI MS spectra

Table S8. Overview of performed ESI MS investigations of reactions of the cluster [Ge$_9${Si(TMS)$_3$}$_2$]$^{2-}$ with different boranes in thf (deuterated, non-deuterated), tmo and MeCN (deuterated, non-deuterated).

	thf	tmo	MeCN
DAB$^{o\text{-tol}}$-Br	deuterated and non-deuterated	-	-
DAB^{Mes}-Br	deuterated and non-deuterated	non-deuterated	deuterated and non-deuterated
DAB(II)^{Dipp}-Br	deuterated and non-deuterated	non-deuterated	deuterated and non-deuterated
DAB^{Dipp}-Br	deuterated and non-deuterated	non-deuterated	deuterated and non-deuterated
DAB$^{o\text{-xyl}}$-Br	non-deuterated	non-deuterated	non-deuterated
(^{i}Pr$_2$N)$_2$B-Br	deuterated and non-deuterated	no insertion of tmo between cluster and borane observed	deuterated and non-deuterated
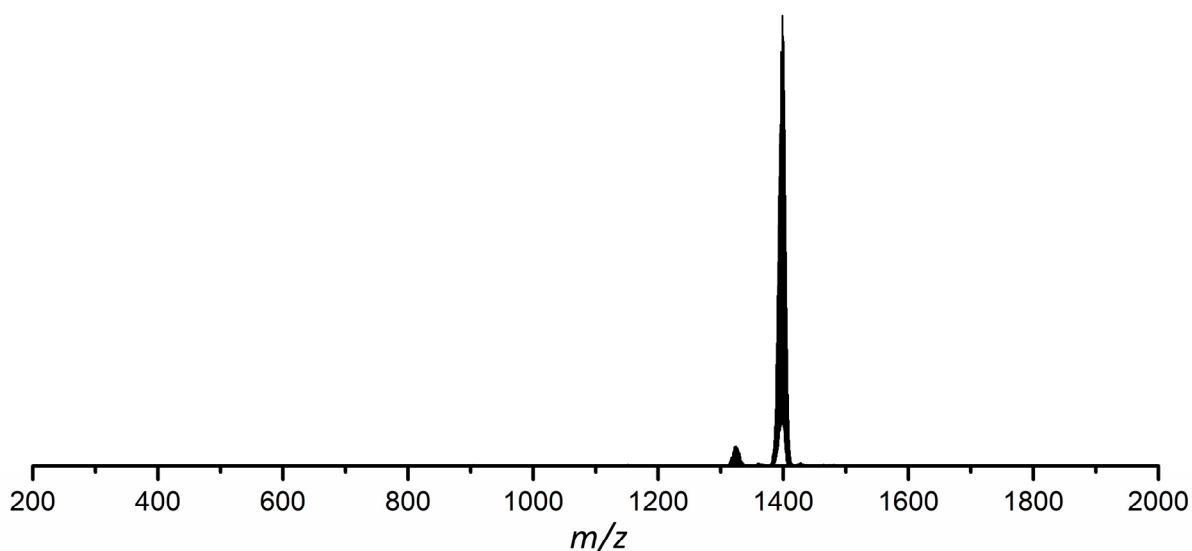
Figure S45. ESI MS spectrum (negative-ion mode, 3500 V, 300 °C) of a thf solution of [Ge$_9${Si(TMS)$_3$}$_2$DAB$^{o\text{-tol}}$]$^-$ (**1a**). The molecule peak of **1a** is detected at *m/z* 1398.7. A detailed view of the signal of anion **1a** is provided in Figure S46.
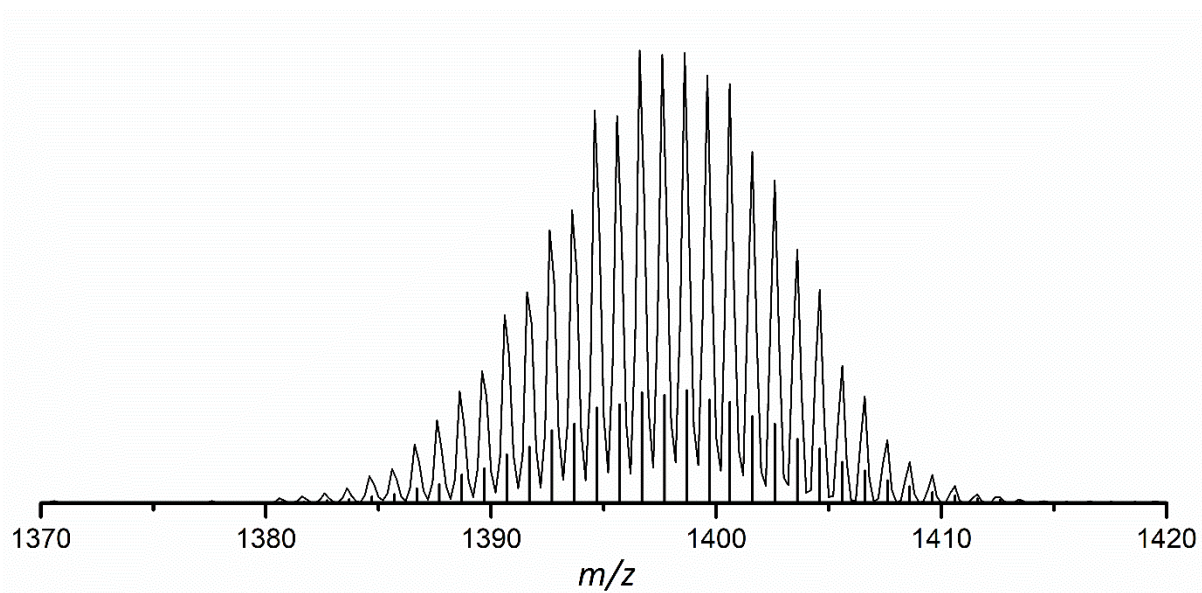
Figure S46. Detailed view on ESI MS signal of [Ge$_9${Si(TMS)$_3$}$_2$DAB$^{o\text{-tol}}$]$^-$ (**1a**) at *m/z* 1398.7.
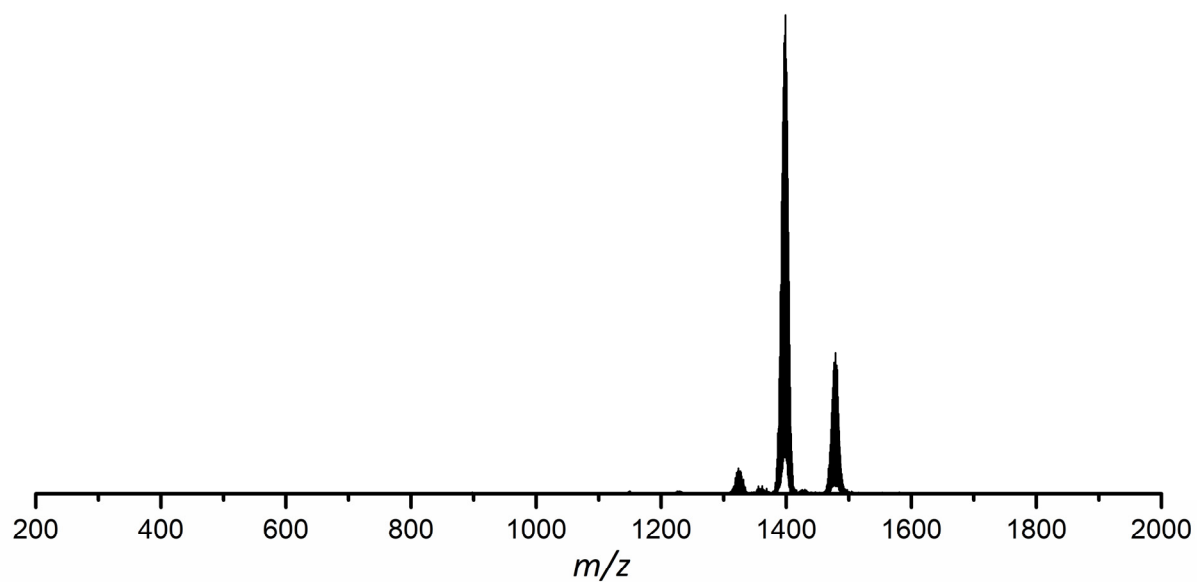
Figure S47. ESI MS spectrum (negative-ion mode, 3500 V, 300 °C) of thf diluted reaction mixture of [Ge$_9${Si(TMS)$_3$}$_2$]$^{2-}$ and DAB$^{o\text{-tol}}$Br in thf-*d$_8$*. Thf-*d$_8$* was added to a mixture of the reactants. The detected signals can be assigned to [Ge$_9${Si(TMS)$_3$}$_2$DAB$^{o\text{-tol}}$]$^-$ (**1a**; *m/z* 1398.7) and [Ge$_9${Si(TMS)$_3$}$_2$(CD$_2$)$_4$O-DAB$^{o\text{-tol}}$]$^-$ (**2a-*d$_8$***; *m/z* 1478.8).
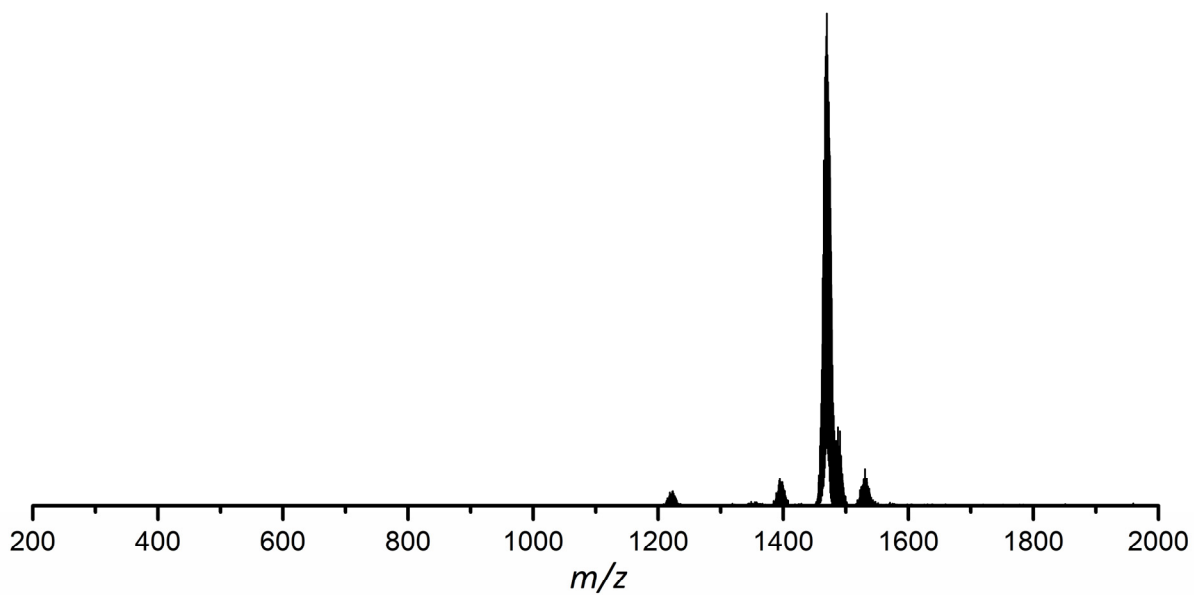
Figure S48. ESI MS spectrum (negative-ion mode, 3500 V, 300 °C) of a thf solution of $[Ge_9\{Si(TMS)_3\}_2(CH_2)_4O\text{-}DAB^{o\text{-}tol}]^-$ (**2a**). The molecule peak of **2a** is detected at *m/z* 1470.8. A detailed view of the signal of anion **2a** is provided in Figure S49.
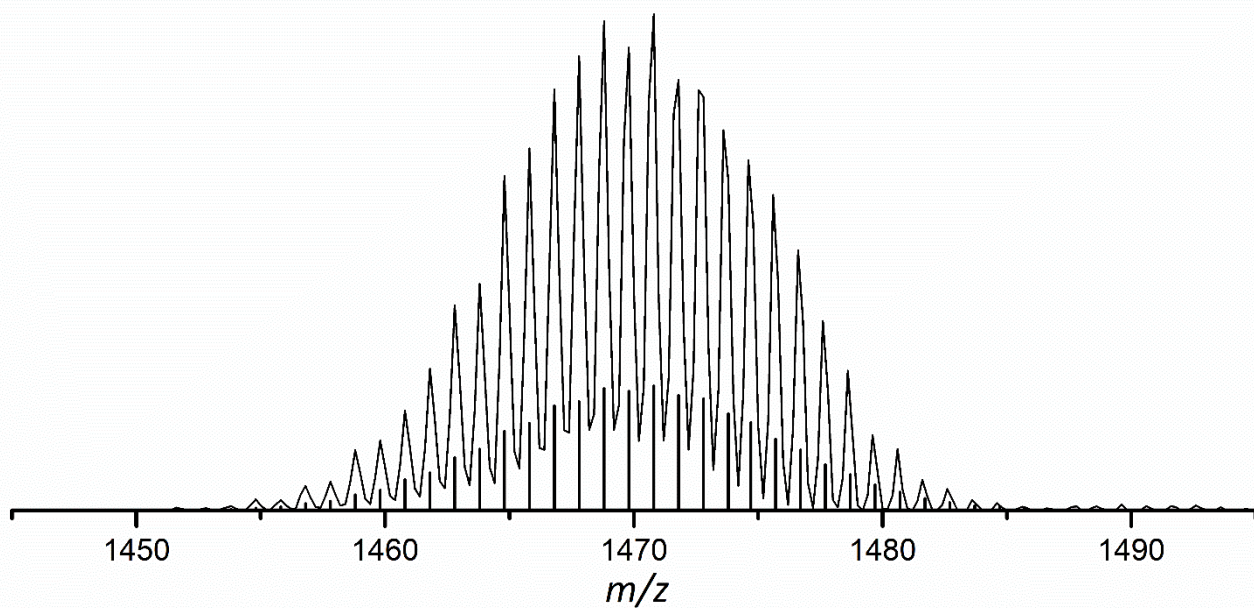
Figure S49. Detailed view on ESI MS signal of $[Ge_9\{Si(TMS)_3\}_2(CH_2)_4O\text{-}DAB^{o\text{-}tol}]^-$ (**2a**) at *m/z* 1470.8.
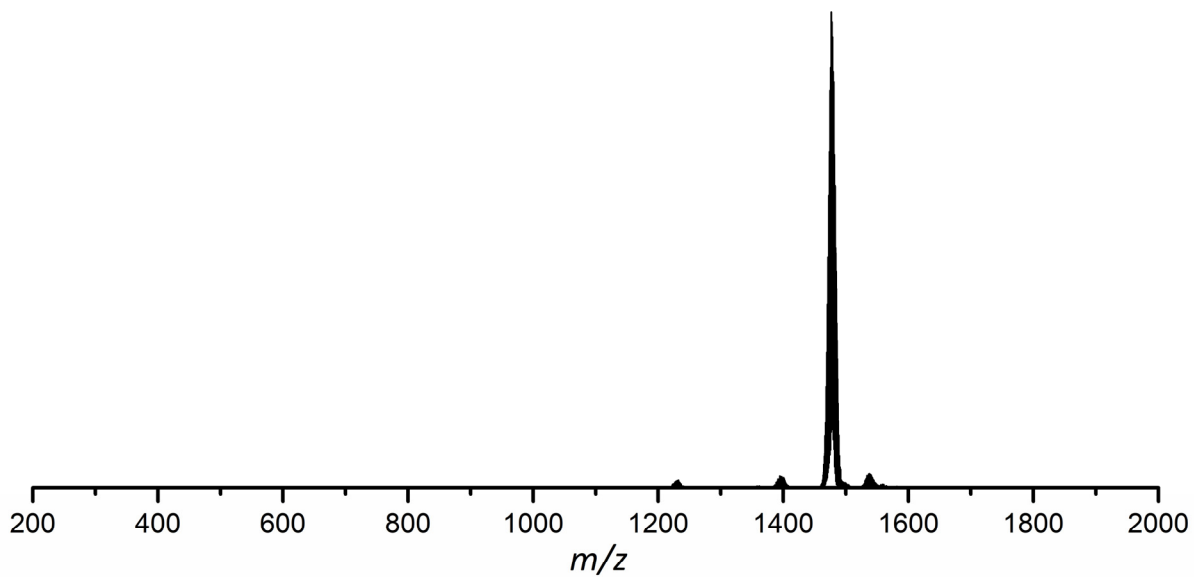
Figure S50. ESI MS spectrum (negative-ion mode, 3500 V, 300 °C) of a thf solution of $[Ge_9\{Si(TMS)_3\}_2(CD_2)_4O\text{-}DAB^{o\text{-}tol}]^-$ (**2a-d_8**). The molecule peak of **2a-d_8** is detected at m/z 1478.8. A detailed view of the signal of anion **2a-d_8** is provided in Figure S51.
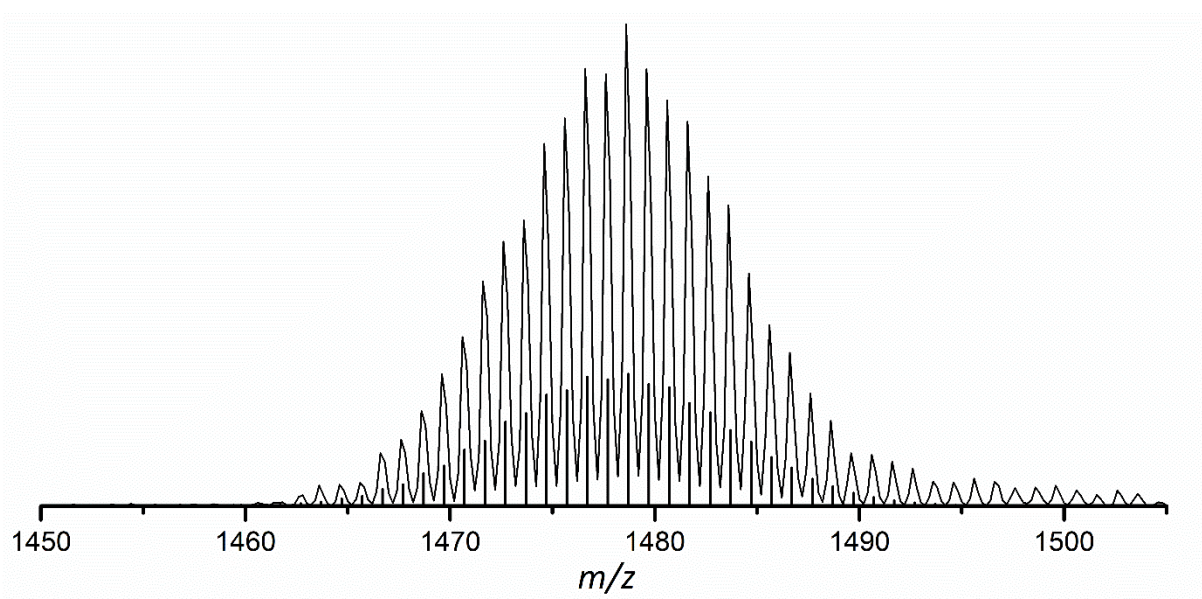
Figure S51. Detailed view on ESI MS signal of $[Ge_9\{Si(TMS)_3\}_2(CD_2)_4O\text{-}DAB^{o\text{-}tol}]^-$ (**2a-d_8**) at m/z 1478.8.
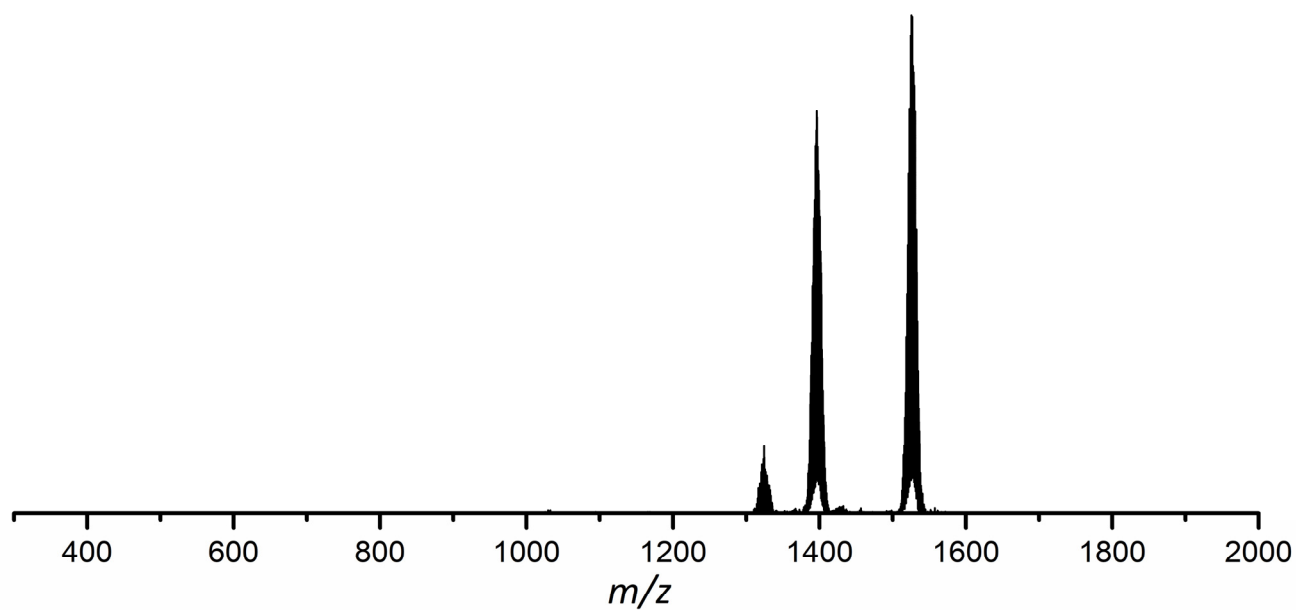
Figure S52. ESI MS spectrum (negative-ion mode, 3500 V, 300 °C) of a thf solution of [Ge$_9$\{Si(TMS)$_3$\}$_2$(CH$_2$)$_4$O-DAB^{Mes}]$^-$ (**3a**). The molecule peak of **3a** is detected at *m/z* 1526.8. A detailed view of the signal of anion **3a** is provided in Figure S53. The signal detected at *m/z* 1396 can be assigned to [Ge$_9$\{Si(TMS)$_3$\}$_3$]$^-$, which is formed during the ionization process in the mass spectrometer.
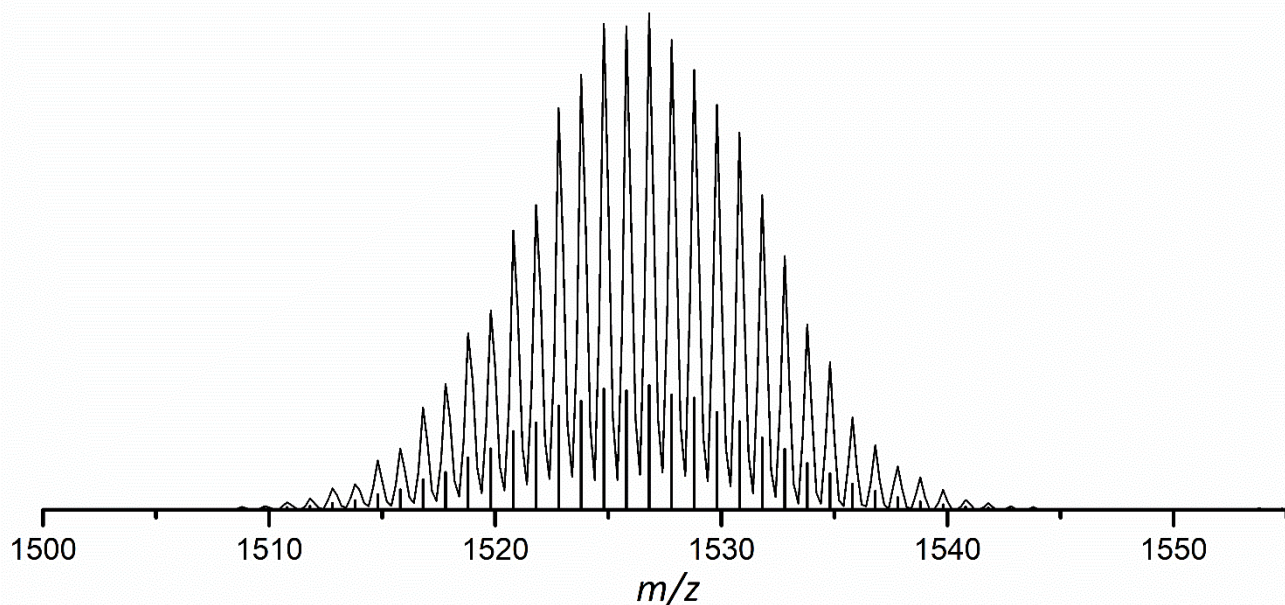
Figure S53. Detailed view on ESI MS signal of [Ge$_9$\{Si(TMS)$_3$\}$_2$(CH$_2$)$_4$O-DAB^{Mes}]$^-$ (**3a**) at *m/z* 1526.8.
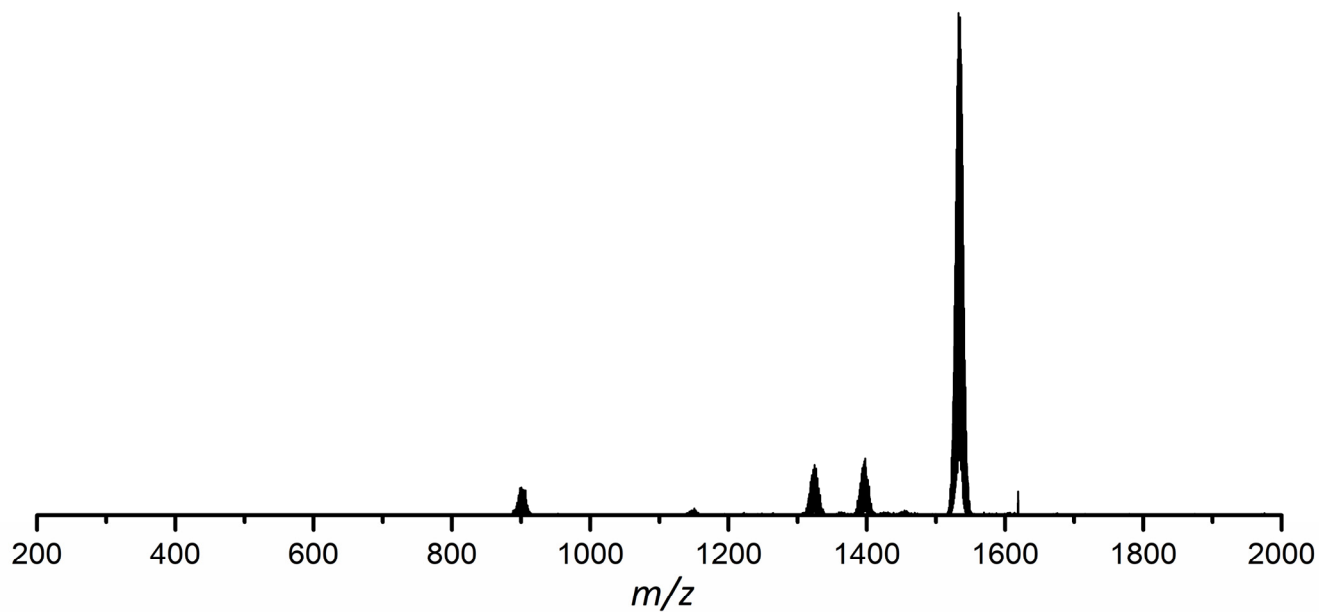
Figure S54. ESI MS spectrum (negative-ion mode, 3500 V, 300 °C) of a thf solution of [Ge$_9${Si(TMS)$_3$}$_2$(CD$_2$)$_4$O-DAB^{Mes}]$^-$ (**3a-d_8**). The molecule peak of **3a-d_8** is detected at m/z 1534.8. A detailed view of the signal of anion **3a-d_8** is provided in Figure S55.
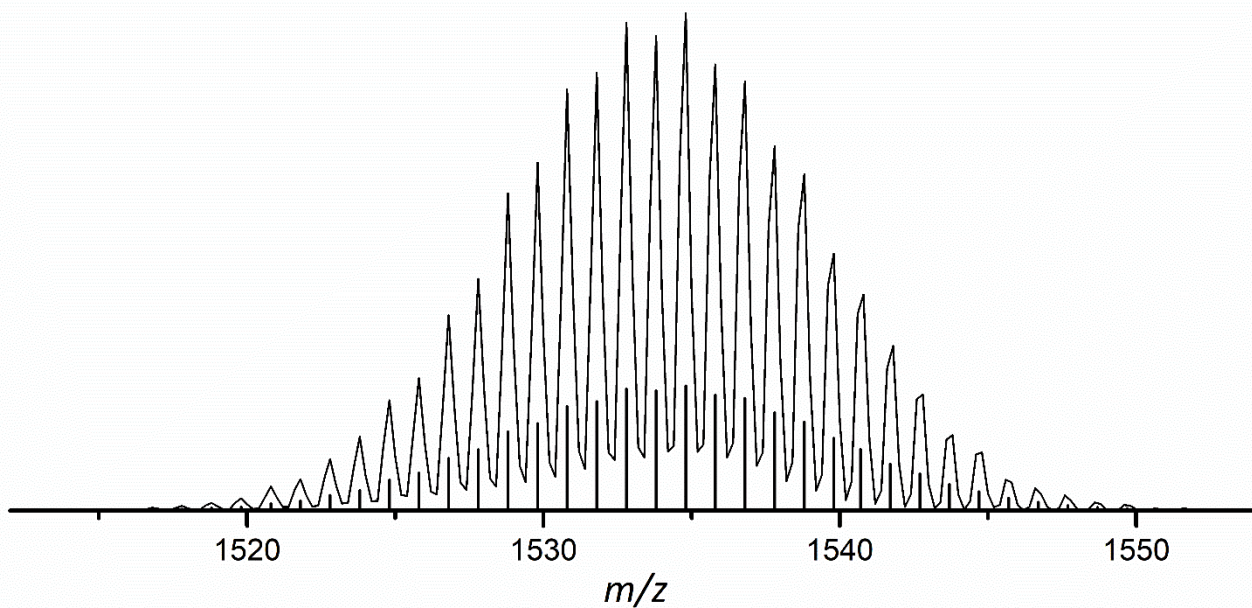
Figure S55. Detailed view on ESI MS signal of [Ge$_9${Si(TMS)$_3$}$_2$(CD$_2$)$_4$O-DAB^{Mes}]$^-$ (**3a-d_8**) at m/z 1534.8.
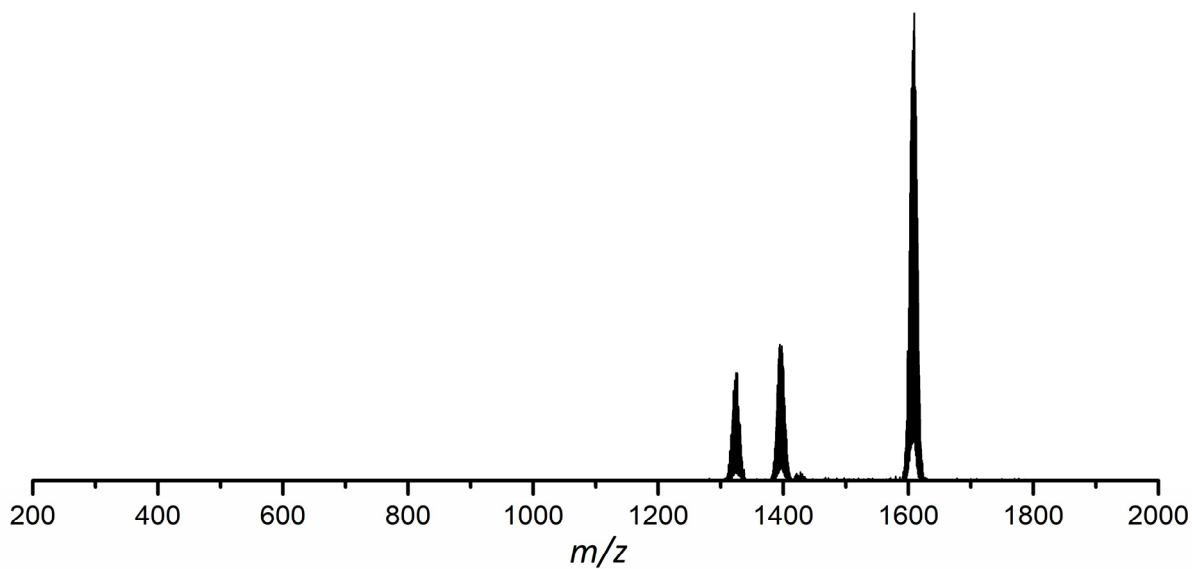
Figure S56. ESI MS spectrum (negative-ion mode, 3500 V, 300 °C) of a thf solution of [Ge$_9${Si(TMS)$_3$}$_2$(CH$_2$)$_4$O-DAB(II)^{Dipp}]$^-$ (**4a**). The molecule peak of **4a** is detected at *m/z* 1608.8. A detailed view of the signal of anion **4a** is provided in Figure S57. The signal detected at *m/z* 1396 can be assigned to [Ge$_9${Si(TMS)$_3$}$_3$]$^-$, which is formed during the ionization process in the mass spectrometer.
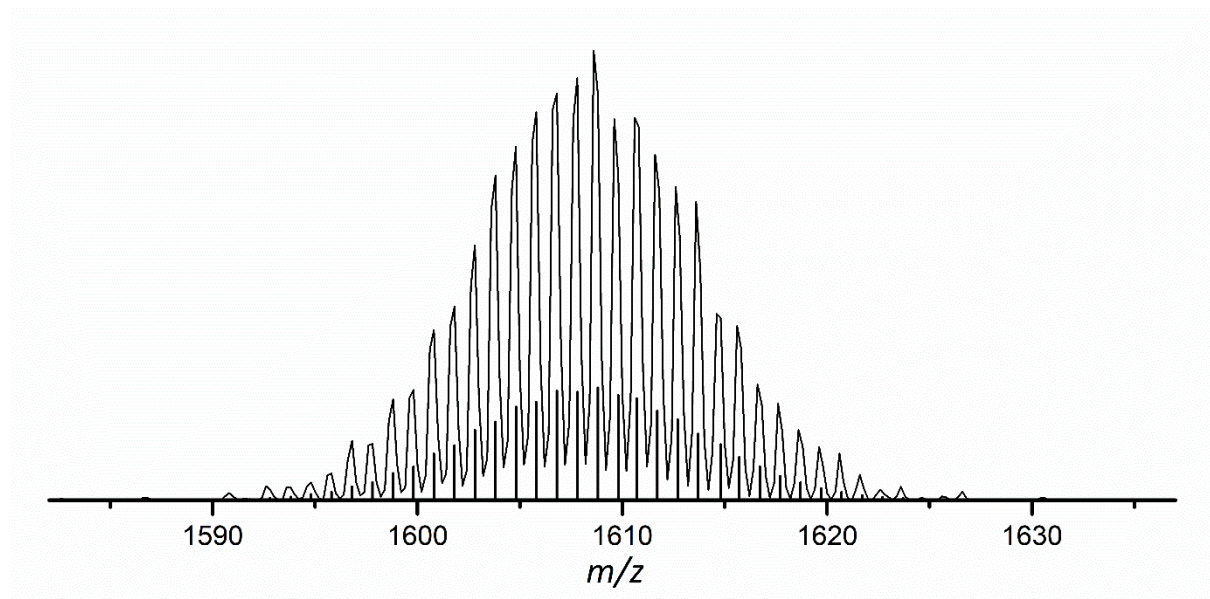
Figure S57. Detailed view on ESI MS signal of [Ge$_9${Si(TMS)$_3$}$_2$(CH$_2$)$_4$O-DAB(II)^{Dipp}]$^-$ (**4a**) at *m/z* 1608.8.
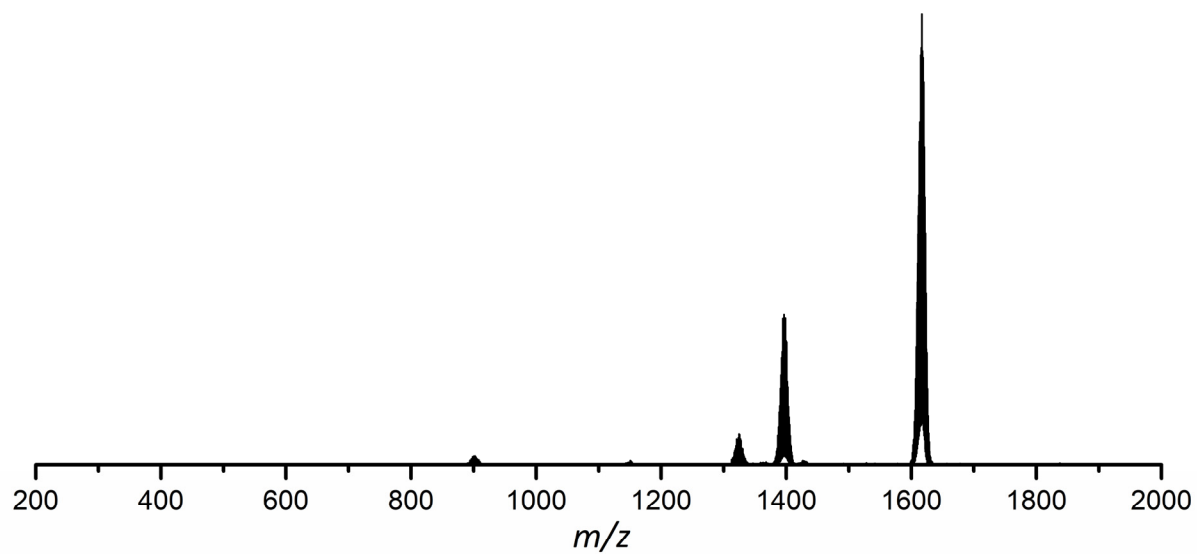
Figure S58. ESI MS spectrum (negative-ion mode, 3500 V, 300 °C) of a thf solution of [Ge$_9${Si(TMS)$_3$}$_2$(CD$_2$)$_4$O-DAB(II)^{Dipp}]$^-$ (**4a-d$_8$**). The molecule peak of **4a-d$_8$** is detected at m/z 1616.8. A detailed view of the signal of anion **4a-d$_8$** is provided in Figure S59. The signal detected at m/z 1396 can be assigned to [Ge$_9${Si(TMS)$_3$}$_3$]$^-$, which is formed during the ionization process in the mass spectrometer.
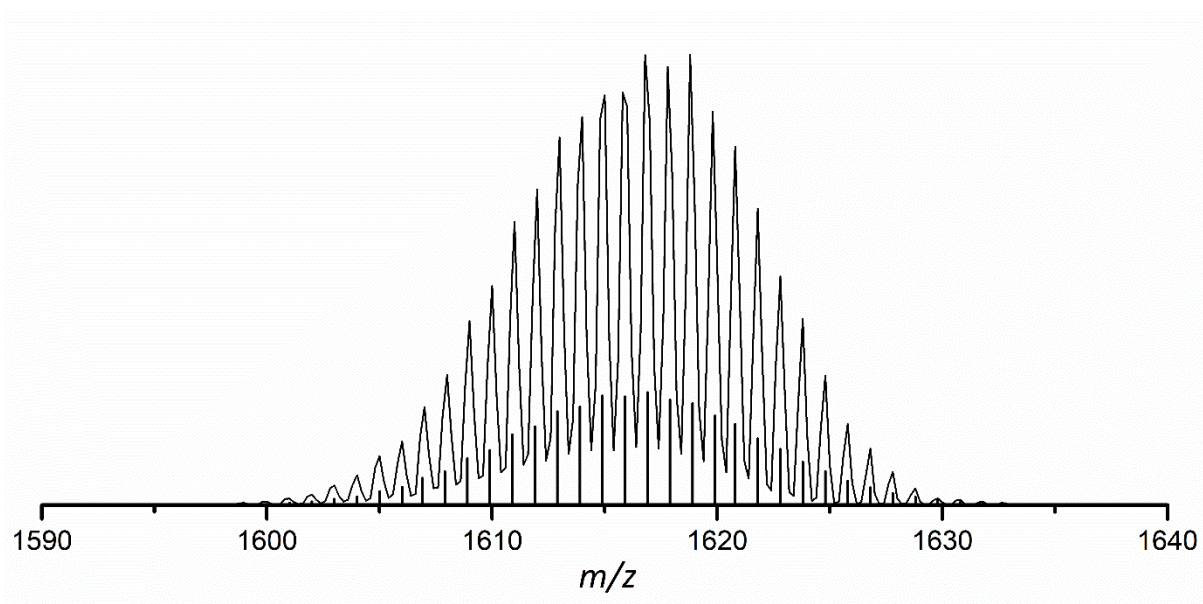
Figure S59. Detailed view on ESI MS signal of [Ge$_9${Si(TMS)$_3$}$_2$(CD$_2$)$_4$O-DAB(II)^{Dipp}]$^-$ (**4a-d$_8$**) at m/z 1616.8.
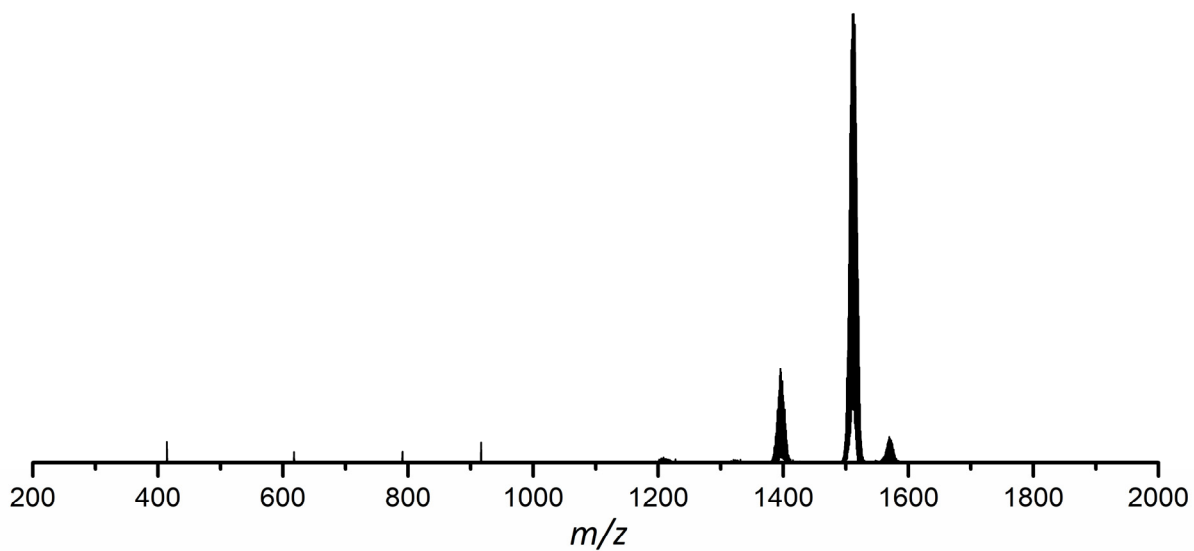
Figure S60. ESI MS spectrum (negative-ion mode, 3500 V, 300 °C) of a thf solution of $[Ge_9\{Si(TMS)_3\}_2(CH_2)_3O\text{-}DAB^{Mes}]^-$ (**5a**). The molecule peak of **5a** is detected at m/z 1512.8. A detailed view of the signal of anion **5a** is provided in Figure S61. The signal detected at m/z 1396 can be assigned to $[Ge_9\{Si(TMS)_3\}_3]^-$, which is formed during the ionization process in the mass spectrometer.
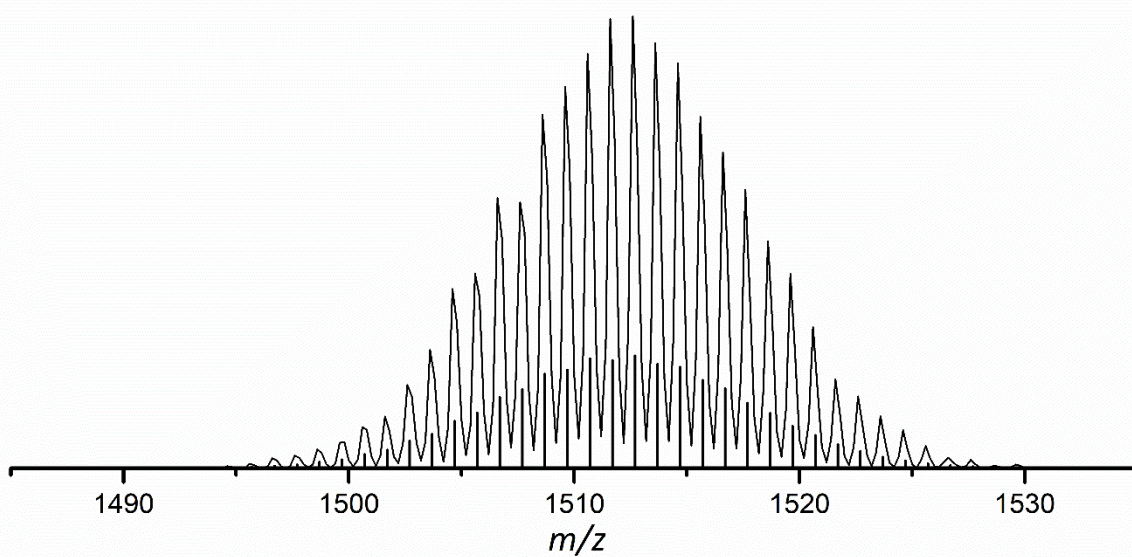
Figure S61. Detailed view on ESI MS signal of $[Ge_9\{Si(TMS)_3\}_2(CH_2)_3O\text{-}DAB^{Mes}]^-$ (**5a**) at m/z 1512.8.
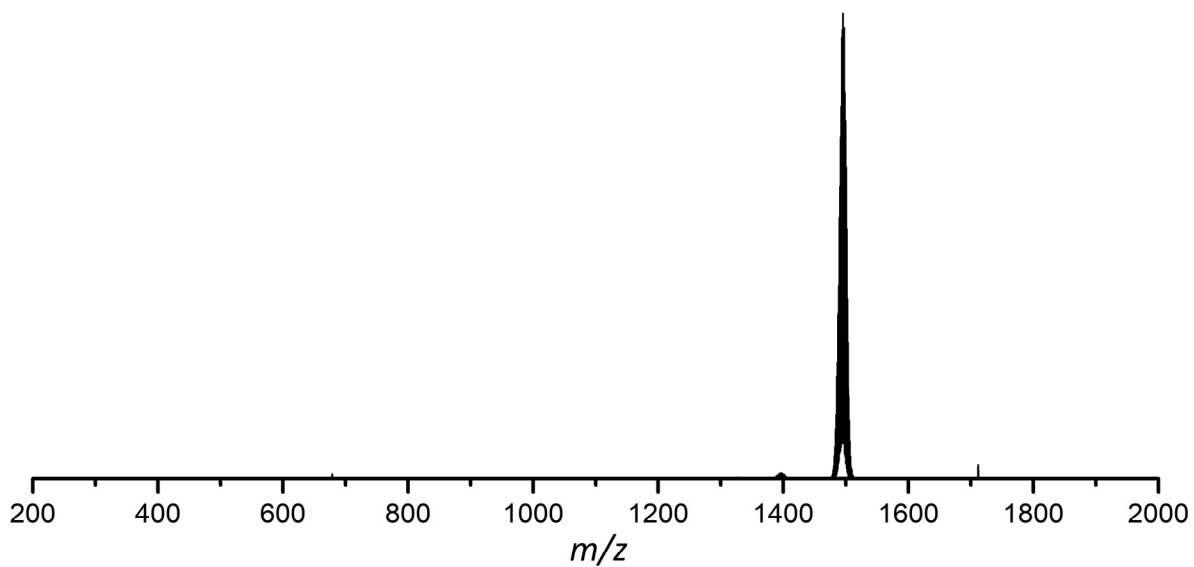
Figure S62. ESI MS spectrum (negative-ion mode, 3500 V, 300 °C) of a MeCN solution of [Ge$_9${Si(TMS)$_3$}$_2$CH$_3$C=N-DAB^{Mes}]$^-$ (**6a**). The molecule peak of **6a** is detected at *m/z* 1495.8. A detailed view of the signal of anion **6a** is provided in Figure S63.
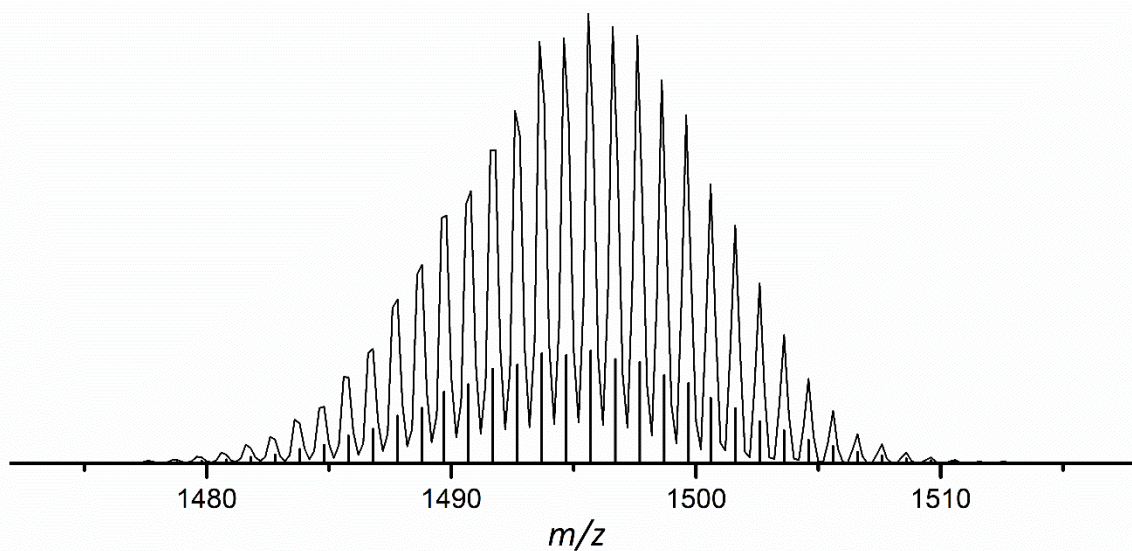
Figure S63. Detailed view on ESI MS signal of [Ge$_9${Si(TMS)$_3$}$_2$CH$_3$C=N-DAB^{Mes}]$^-$ (**6a**) at *m/z* 1495.8.
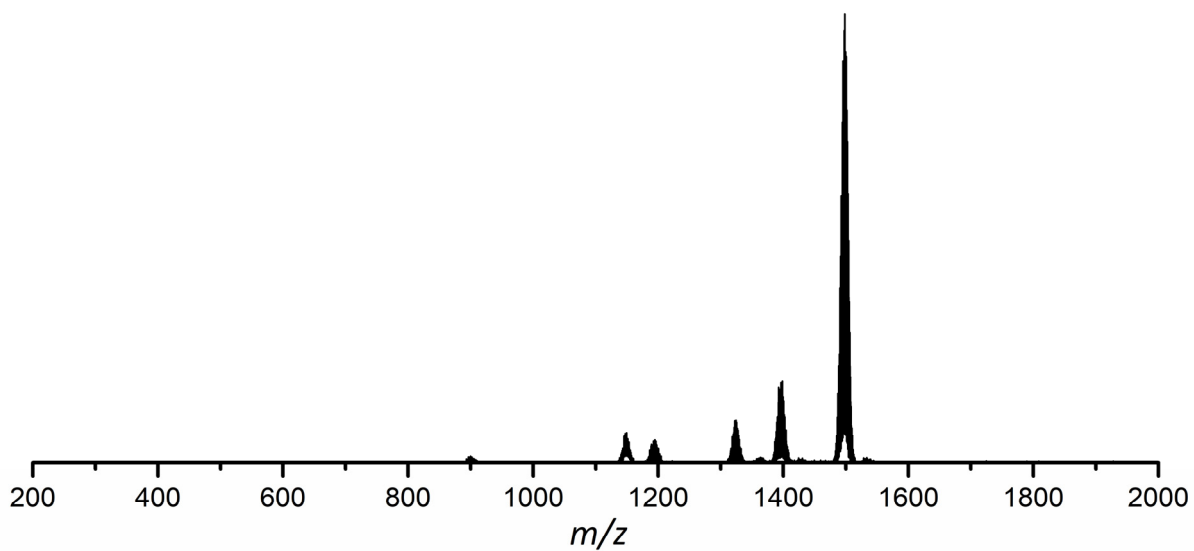
Figure S64. ESI MS spectrum (negative-ion mode, 3500 V, 300 °C) of a MeCN solution of [Ge$_9${Si(TMS)$_3$}$_2$CD$_3$C=N-DAB^{Mes}]$^-$ (**6a-d_3**). The molecule peak of **6a-d_3** is detected at m/z 1498.8. A detailed view of the signal of anion **6a-d_3** is provided in Figure S65.
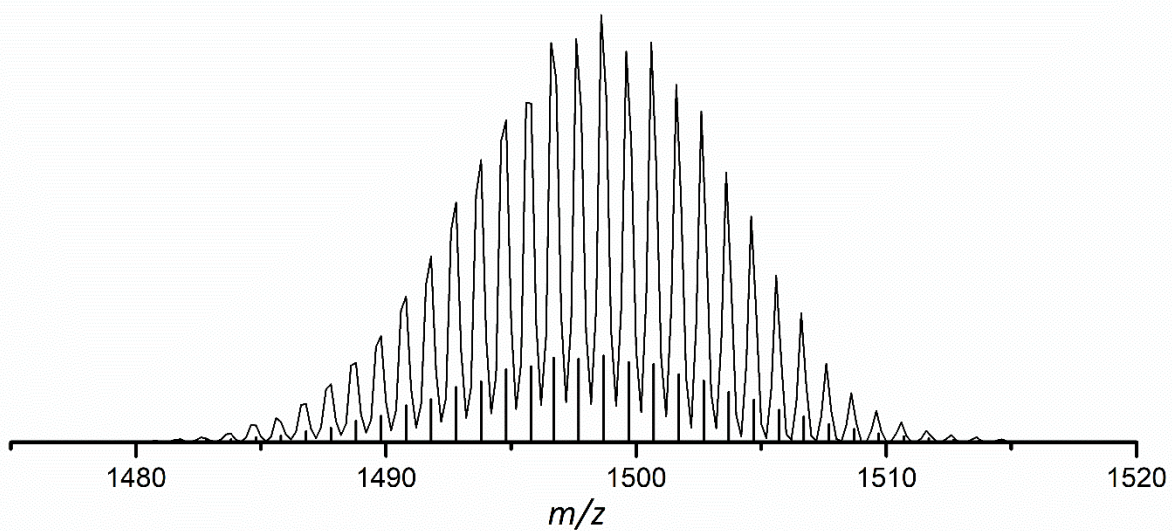
Figure S65. Detailed view on ESI MS signal of [Ge$_9${Si(TMS)$_3$}$_2$CD$_3$C=N-DAB^{Mes}]$^-$ (**6a-d_3**) at m/z 1498.8.
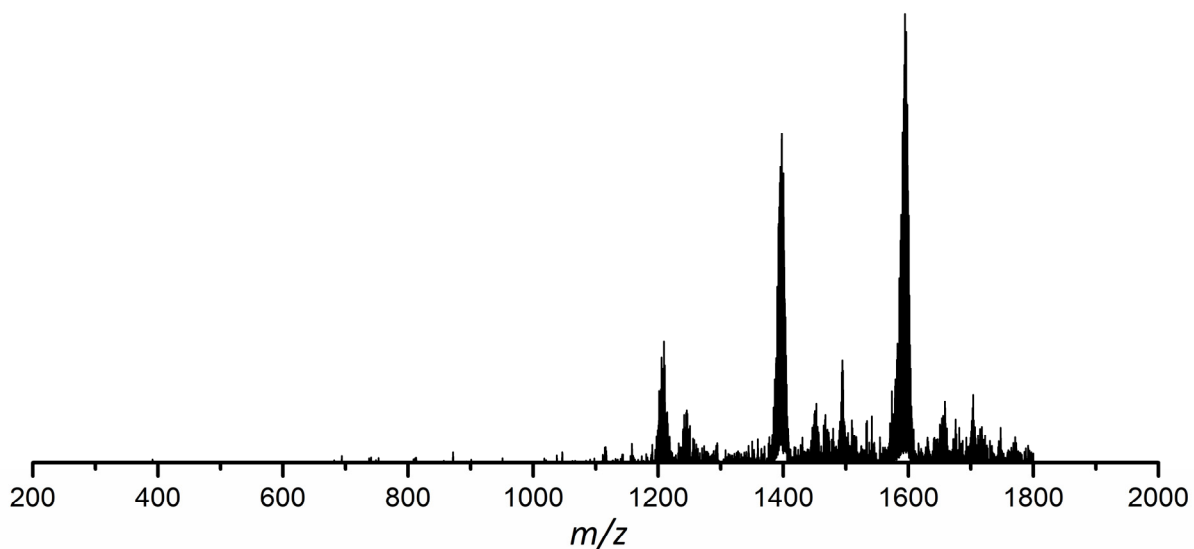
Figure S66. ESI MS spectrum (negative-ion mode, 3500 V, 300 °C) of a thf solution of [Ge$_9${Si(TMS)$_3$}$_2$(CH$_2$)$_3$O-DAB(II)^{Dipp}]$^-$. The molecule peak is detected at *m/z* 1594.8. A detailed view of the signal is provided in Figure S67. The signal detected at *m/z* 1396 can be assigned to [Ge$_9${Si(TMS)$_3$}$_3$]$^-$, which is formed during the ionization process in the mass spectrometer.
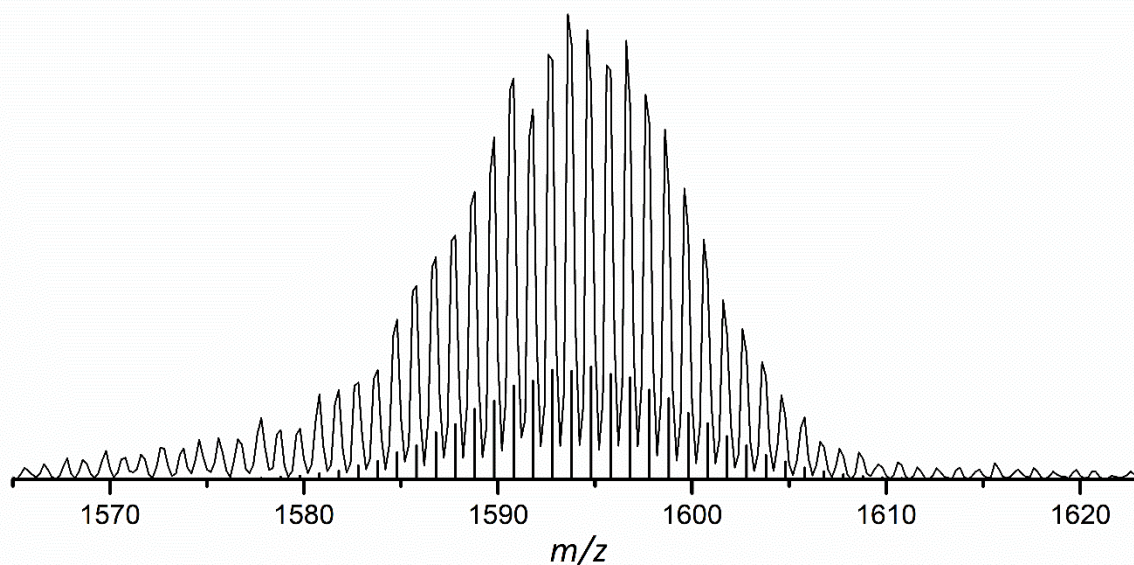
Figure S67. Detailed view on ESI MS signal of [Ge$_9${Si(TMS)$_3$}$_2$(CH$_2$)$_3$O-DAB(II)^{Dipp}]$^-$ at *m/z* 1594.8.
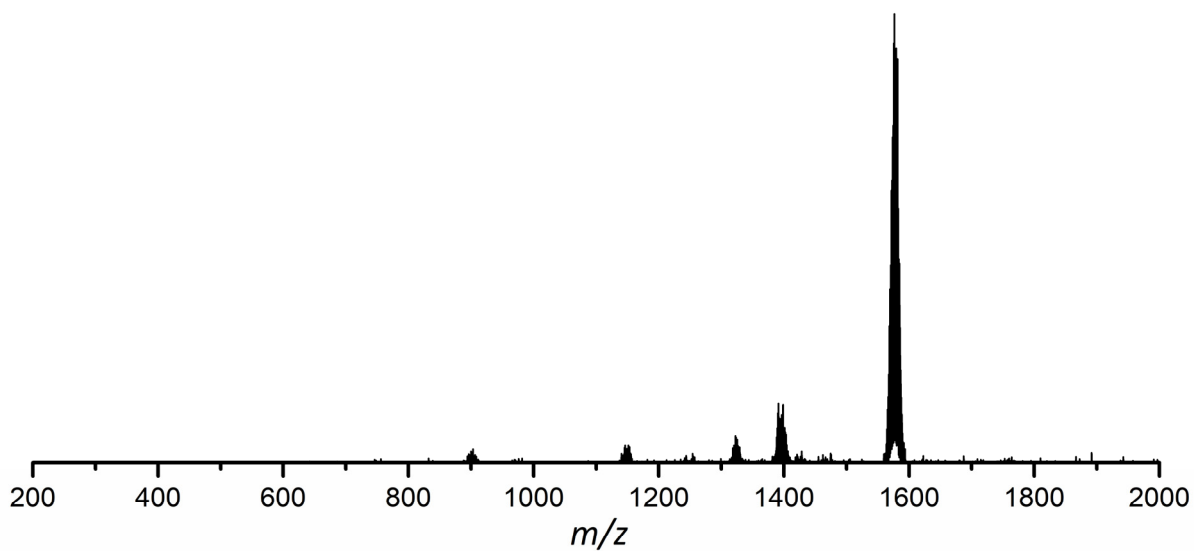
Figure S68. ESI MS spectrum (negative-ion mode, 3500 V, 300 °C) of a MeCN solution of [Ge$_9${Si(TMS)$_3$}$_2$CH$_3$C=N-DAB(II)^{Dipp}]⁻. The molecule peak is detected at *m/z* 1577.8. A detailed view of the signal is provided in Figure S69.
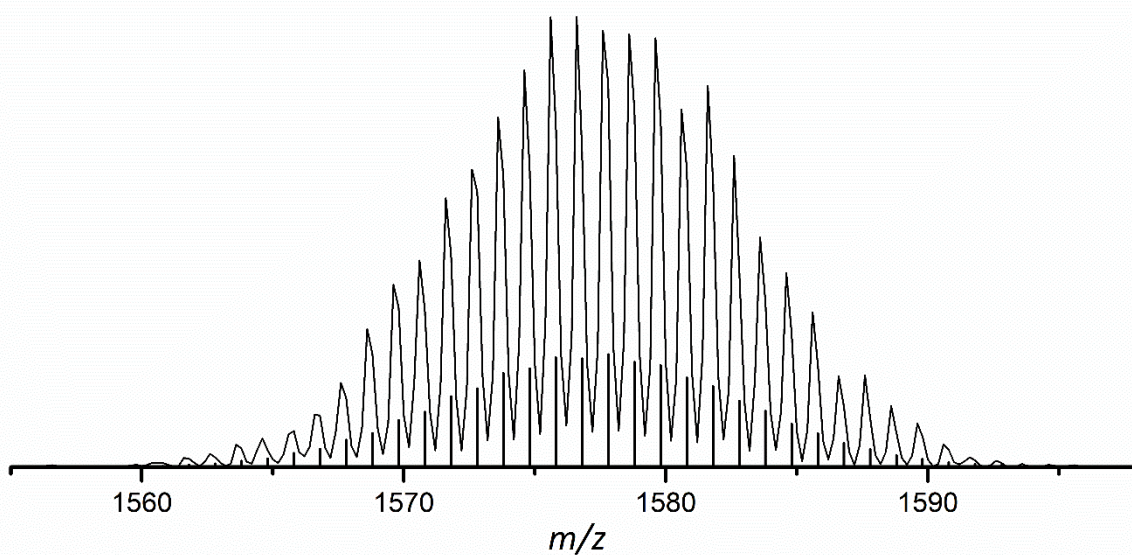
Figure S69. Detailed view on ESI MS signal of [Ge$_9${Si(TMS)$_3$}$_2$CH$_3$C=N-DAB(II)^{Dipp}]⁻ at *m/z* 1577.8.
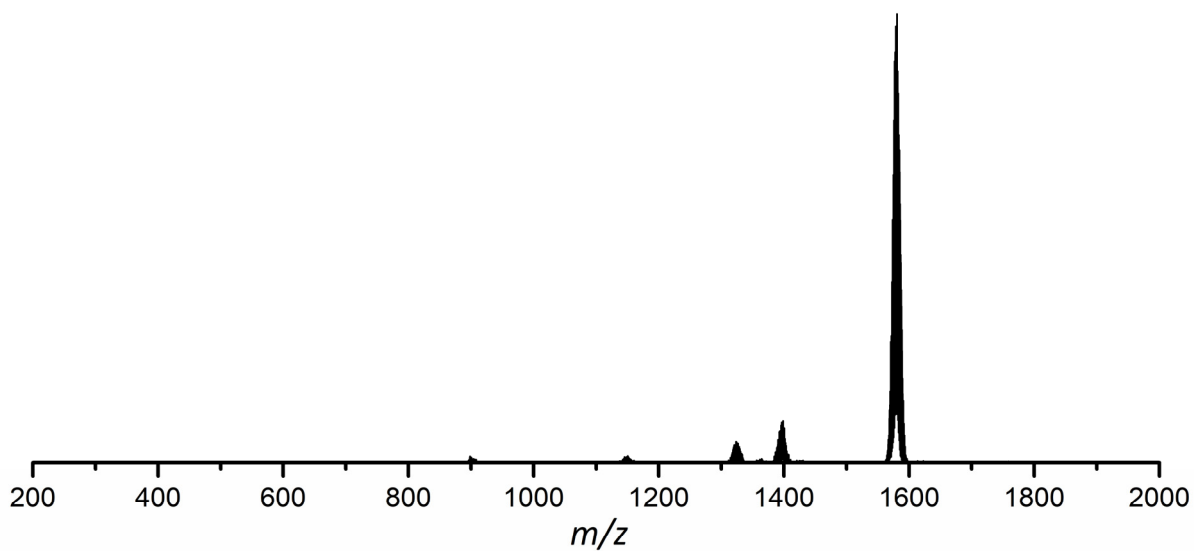
Figure S70. ESI MS spectrum (negative-ion mode, 3500 V, 300 °C) of a MeCN solution of $[Ge_9\{Si(TMS)_3\}_2CD_3C=N\text{-}DAB(II)^{Dipp}]^-$. The molecule peak is detected at *m/z* 1580.8. A detailed view of the signal is provided in Figure S71.
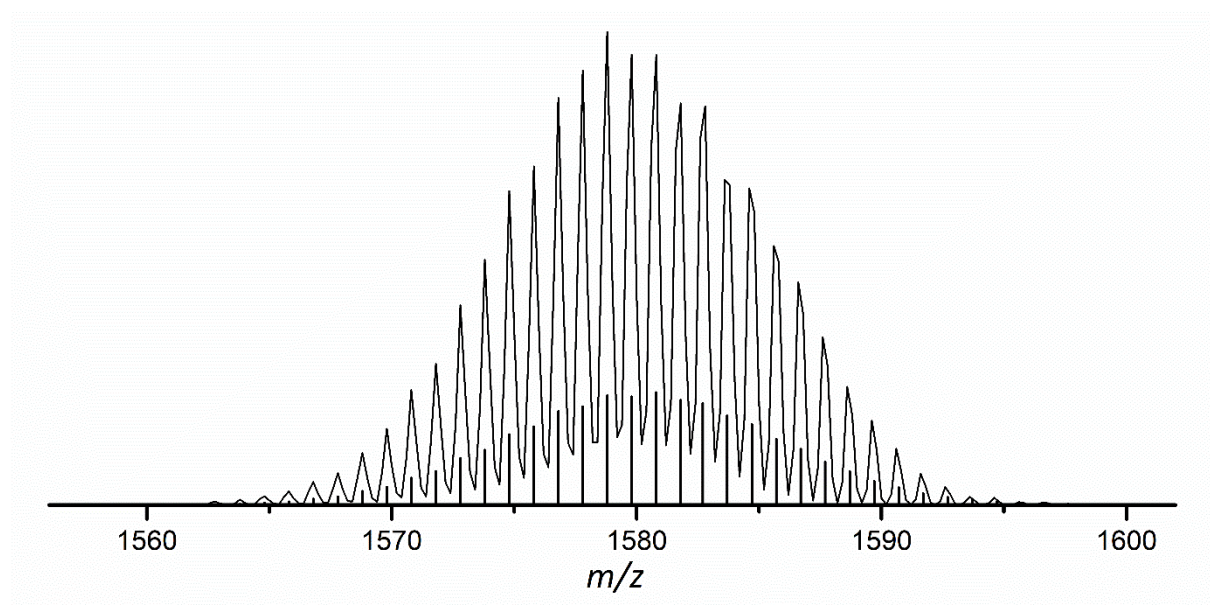
Figure S71. Detailed view on ESI MS signal of $[Ge_9\{Si(TMS)_3\}_2CD_3C=N\text{-}DAB(II)^{Dipp}]^-$ at *m/z* 1580.8.
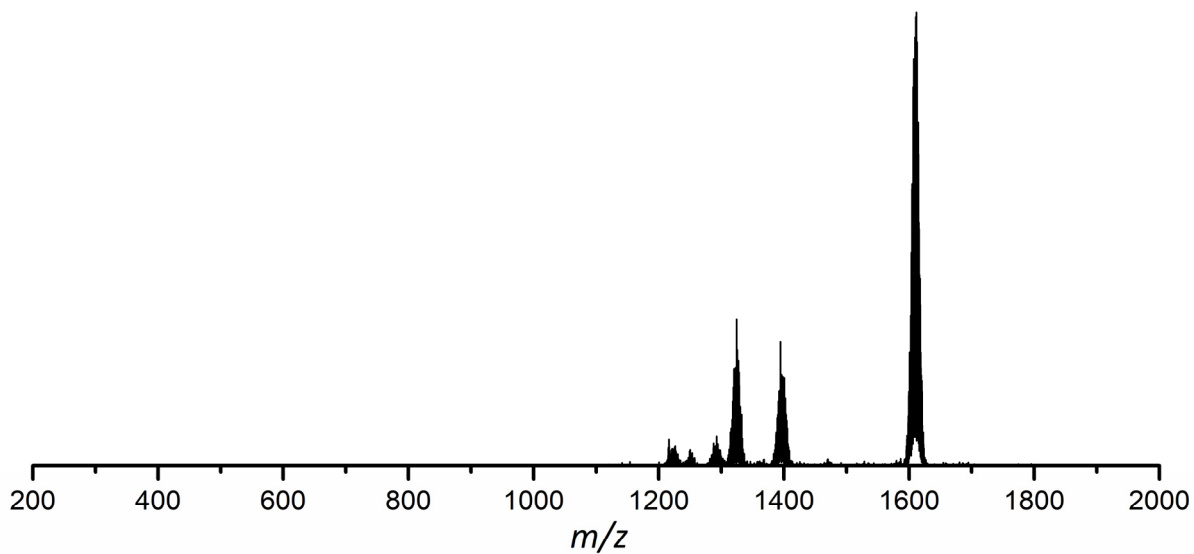
Figure S72. ESI MS spectrum (negative-ion mode, 3500 V, 300 °C) of a thf solution of [Ge$_9${Si(TMS)$_3$}$_2$(CH$_2$)$_4$O-DAB^{Dipp}]$^-$. The molecule peak is detected at *m/z* 1610.8. A detailed view of the signal is provided in Figure S73. The signal detected at *m/z* 1396 can be assigned to [Ge$_9${Si(TMS)$_3$}$_3$]$^-$, which is formed during the ionization process in the mass spectrometer.
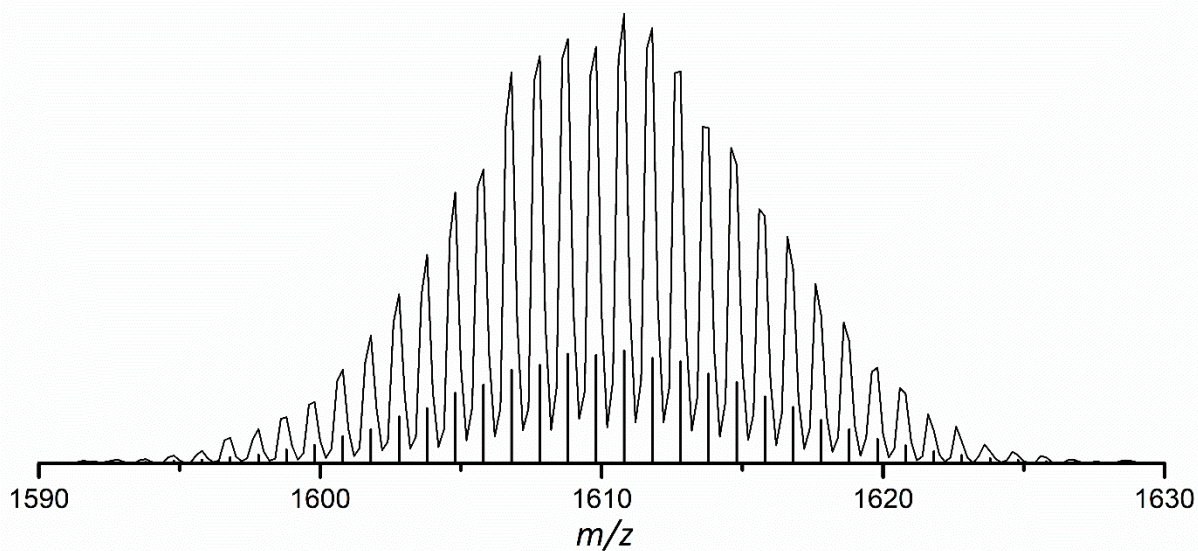
Figure S73. Detailed view on ESI MS signal of [Ge$_9${Si(TMS)$_3$}$_2$(CH$_2$)$_4$O-DAB^{Dipp}]$^-$ at *m/z* 1610.8.
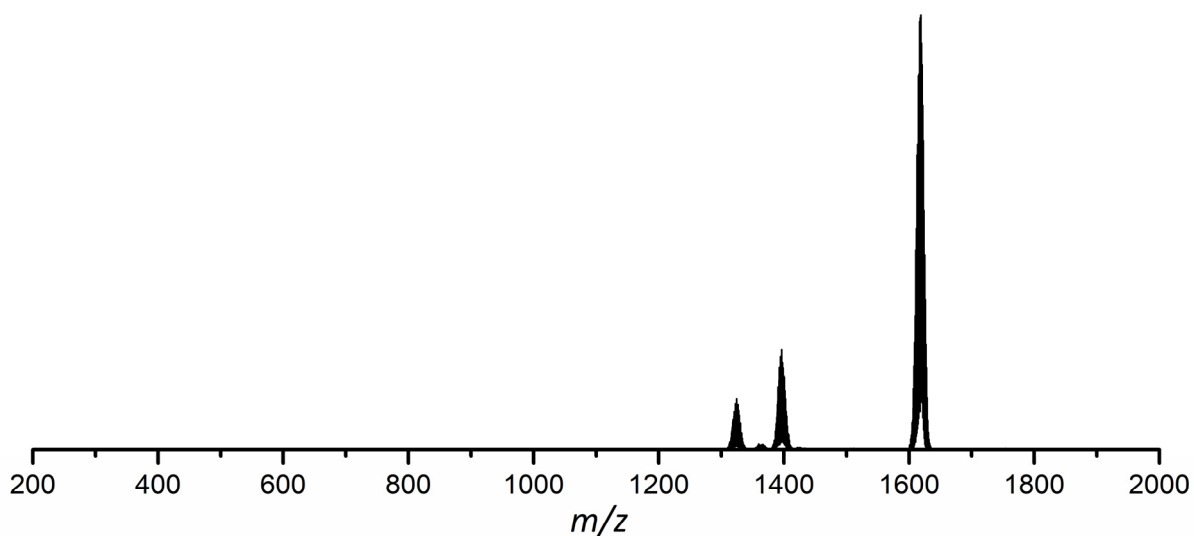
Figure S74. ESI MS spectrum (negative-ion mode, 3500 V, 300 °C) of a thf solution of $[Ge_9\{Si(TMS)_3\}_2(CD_2)_4O\text{-}DAB^{Dipp}]^-$. The molecule peak is detected at *m/z* 1618.8. A detailed view of the signal is provided in Figure S75. The signal detected at *m/z* 1396 can be assigned to $[Ge_9\{Si(TMS)_3\}_3]^-$, which is formed during the ionization process in the mass spectrometer.
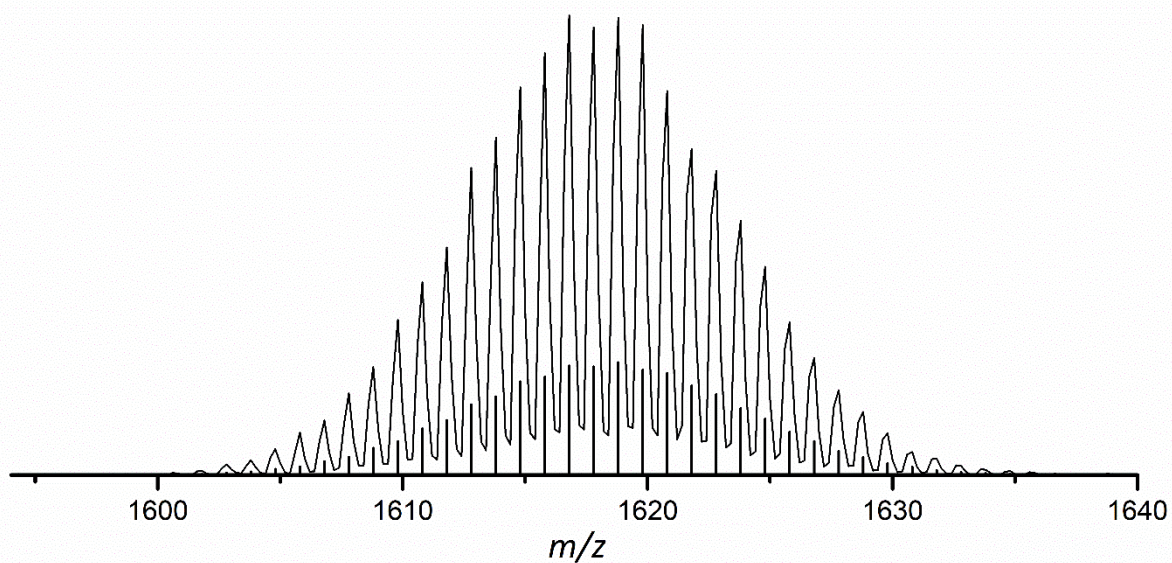
Figure S75. Detailed view on ESI MS signal of $[Ge_9\{Si(TMS)_3\}_2(CD_2)_4O\text{-}DAB^{Dipp}]^-$ at *m/z* 1618.8.
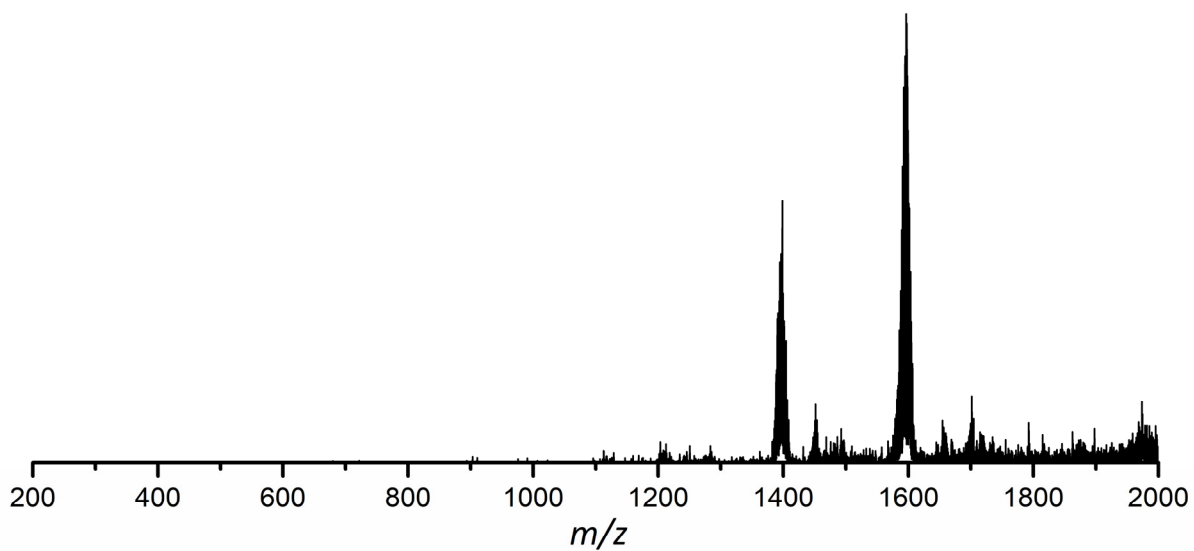
Figure S76. ESI MS spectrum (negative-ion mode, 3500 V, 300 °C) of a thf solution of [Ge$_9${Si(TMS)$_3$}$_2$(CH$_2$)$_3$O-DAB^{Dipp}]$^-$. The molecule peak is detected at *m/z* 1596.8. A detailed view of the signal is provided in Figure S77. The signal detected at *m/z* 1396 can be assigned to [Ge$_9${Si(TMS)$_3$}$_3$]$^-$, which is formed during the ionization process in the mass spectrometer.
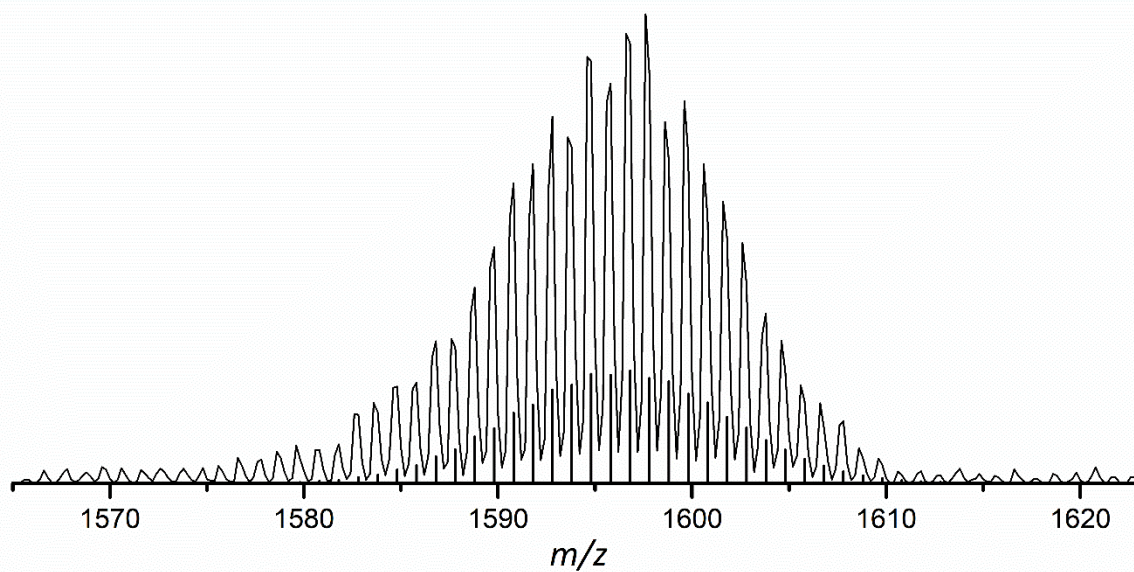
Figure S77. Detailed view on ESI MS signal of [Ge$_9${Si(TMS)$_3$}$_2$(CH$_2$)$_3$O-DAB^{Dipp}]$^-$ at *m/z* 1596.8.
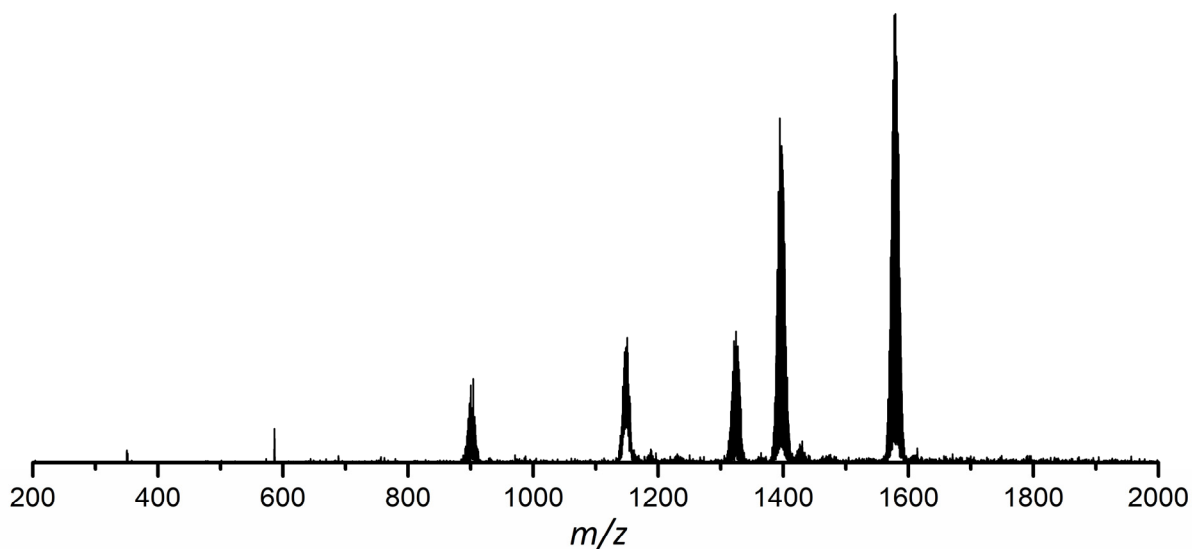
Figure S78. ESI MS spectrum (negative-ion mode, 3500 V, 300 °C) of a thf solution of [Ge$_9$\{Si(TMS)$_3$\}$_2$CH$_3$C=N-DAB^{Dipp}]$^-$. The molecule peak is detected at *m/z* 1579.8. A detailed view of the signal is provided in Figure S79. The signal detected at *m/z* 1396 can be assigned to [Ge$_9$\{Si(TMS)$_3$\}$_3$]$^-$, which is formed during the ionization process in the mass spectrometer.
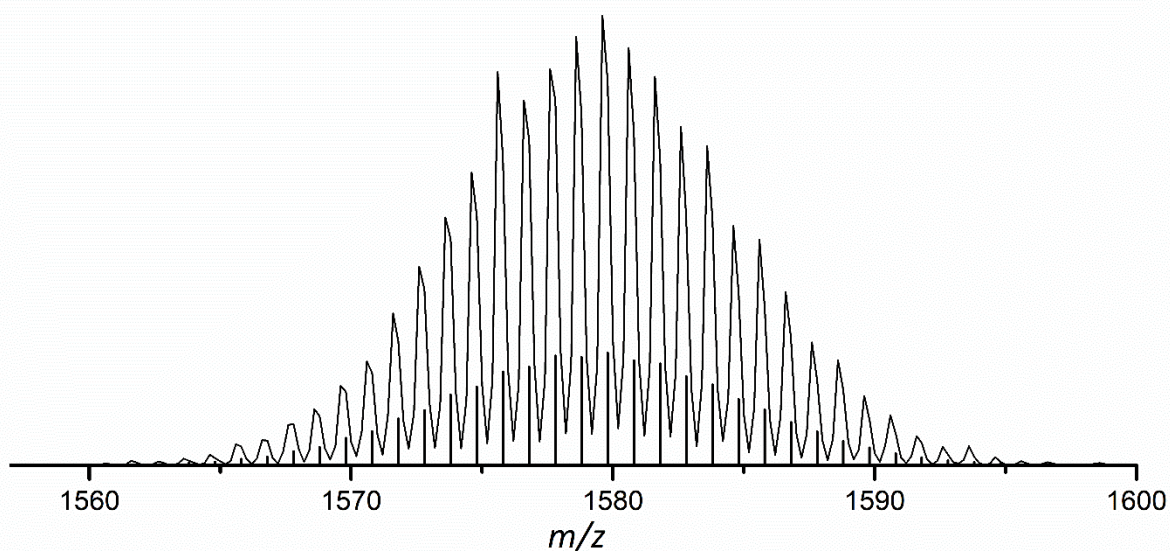
Figure S79. Detailed view on ESI MS signal of [Ge$_9$\{Si(TMS)$_3$\}$_2$CH$_3$C=N-DAB^{Dipp}]$^-$ at *m/z* 1579.8.
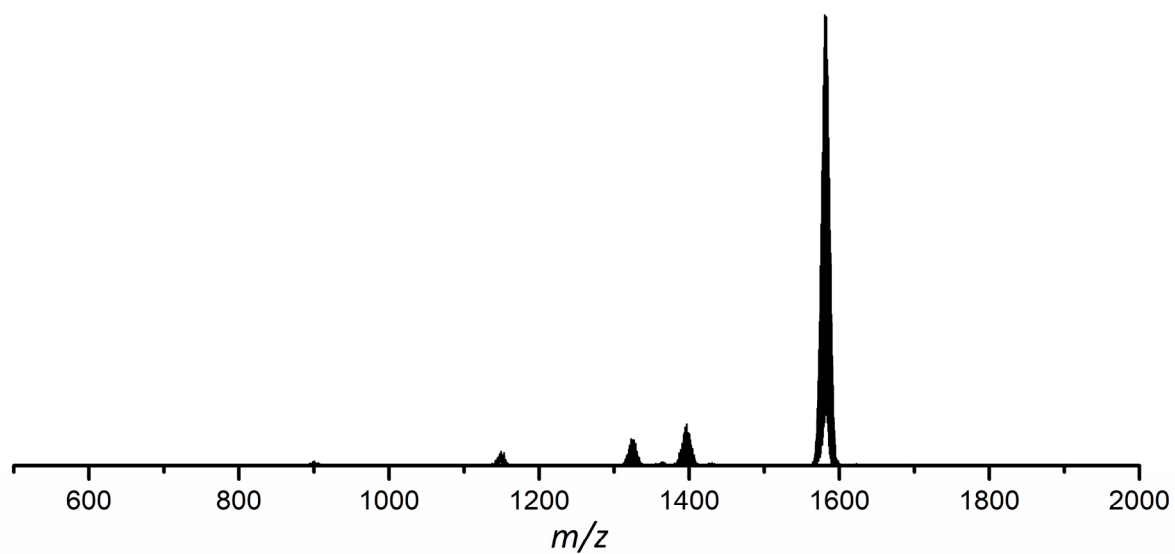
Figure S80. ESI MS spectrum (negative-ion mode, 3500 V, 300 °C) of a thf solution of [Ge$_9$\{Si(TMS)$_3$\}$_2$CD$_3$C=N-DAB^{Dipp}]$^-$. The molecule peak is detected at *m/z* 1582.8. A detailed view of the signal is provided in Figure S81. The signal detected at *m/z* 1396 can be assigned to [Ge$_9$\{Si(TMS)$_3$\}$_3$]$^-$, which is formed during the ionization process in the mass spectrometer.
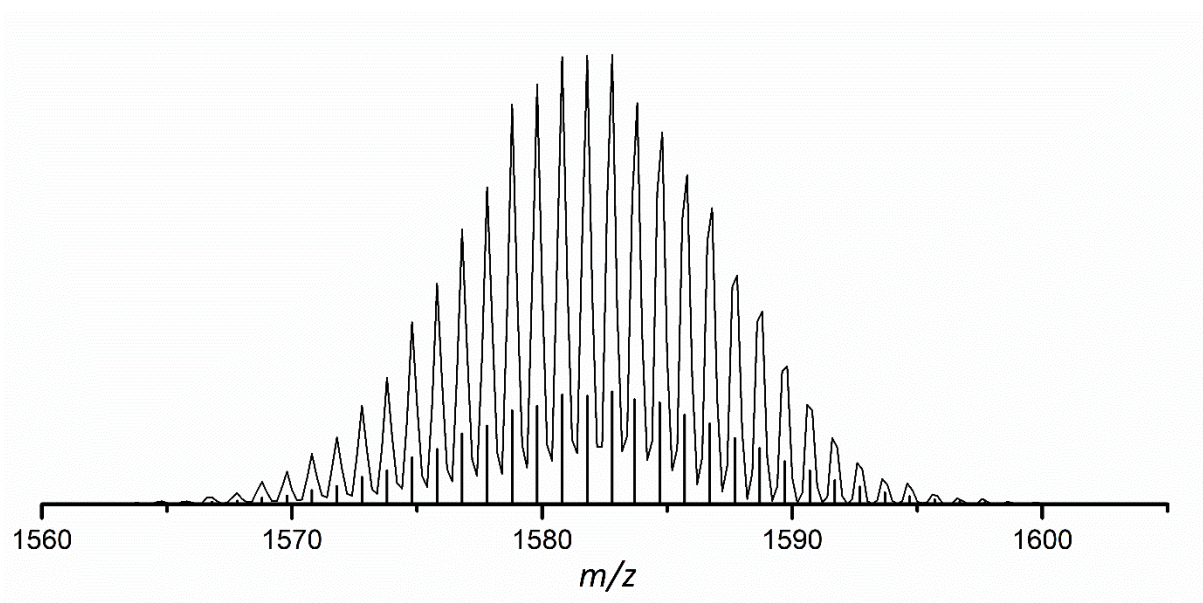
Figure S81. Detailed view on ESI MS signal of [Ge$_9$\{Si(TMS)$_3$\}$_2$CD$_3$C=N-DAB^{Dipp}]$^-$ at *m/z* 1582.8.
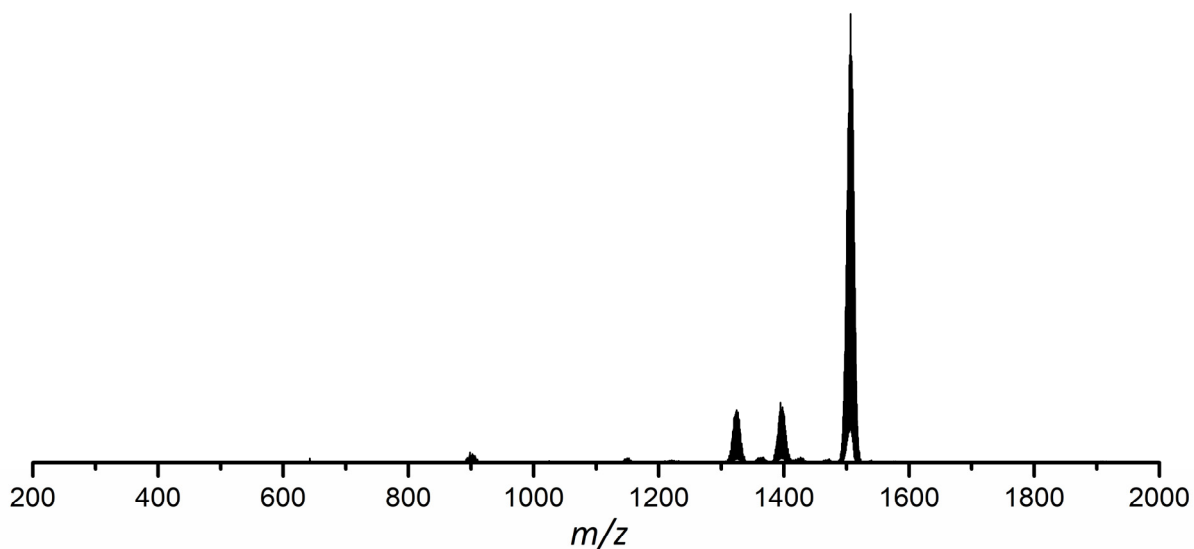
Figure S82. ESI MS spectrum (negative mode, 3500 V, 300 °C) of a thf solution of [Ge$_9${Si(TMS)$_3$}$_2$(CH$_2$)$_4$O-DAB^{o-xyl}]$^-$. The molecule peak is detected at m/z 1506.8. A detailed view of the signal is provided in Figure S83. The signal detected at m/z 1396 can be assigned to [Ge$_9${Si(TMS)$_3$}$_3$]$^-$, which is formed during the ionization process in the mass spectrometer.
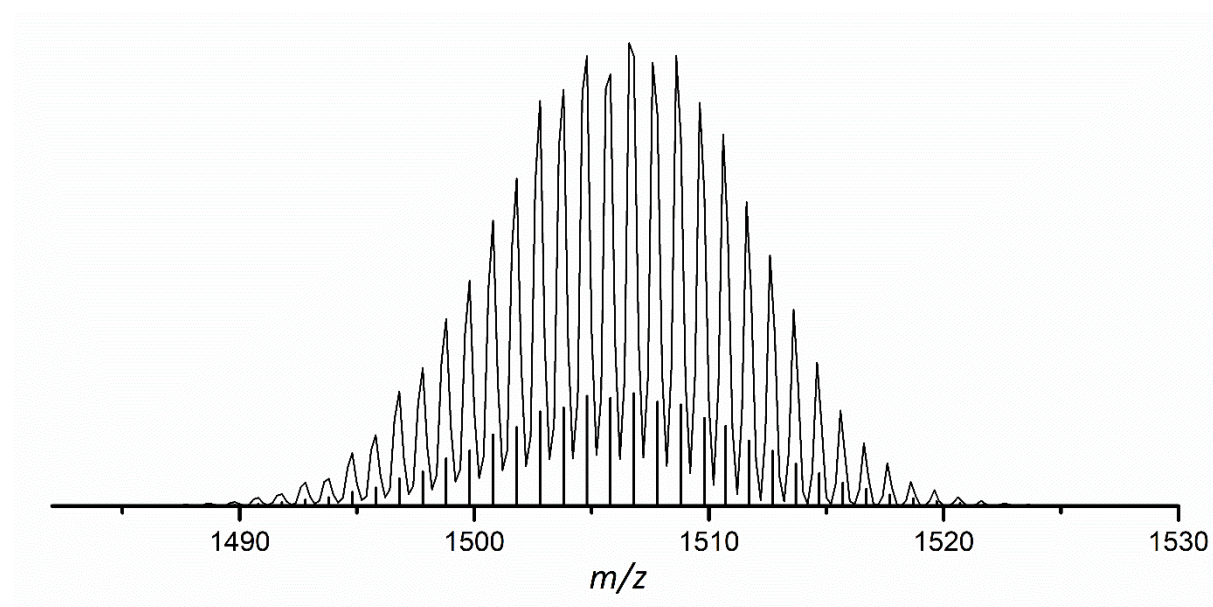
Figure S83. Detailed view on ESI MS signal of [Ge$_9${Si(TMS)$_3$}$_2$(CH$_2$)$_4$O-DAB^{o-xyl}]$^-$ at m/z 1506.8.
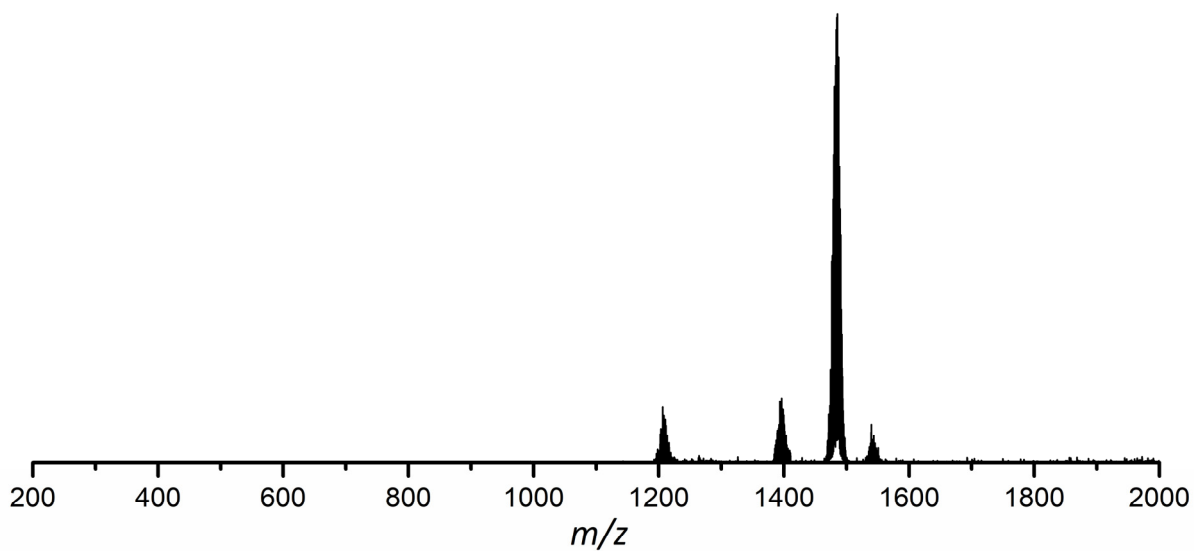
Figure S84. ESI MS spectrum (negative-ion mode, 3500 V, 300 °C) of a thf solution of [Ge$_9${Si(TMS)$_3$}$_2$(CH$_2$)$_3$O-DAB$^{o\text{-}xyl}$]$^-$. The molecule peak is detected at *m/z* 1484.8. A detailed view of the signal is provided in Figure S85. The signal detected at *m/z* 1396 can be assigned to [Ge$_9${Si(TMS)$_3$}$_3$]$^-$, which is formed during the ionization process in the mass spectrometer.
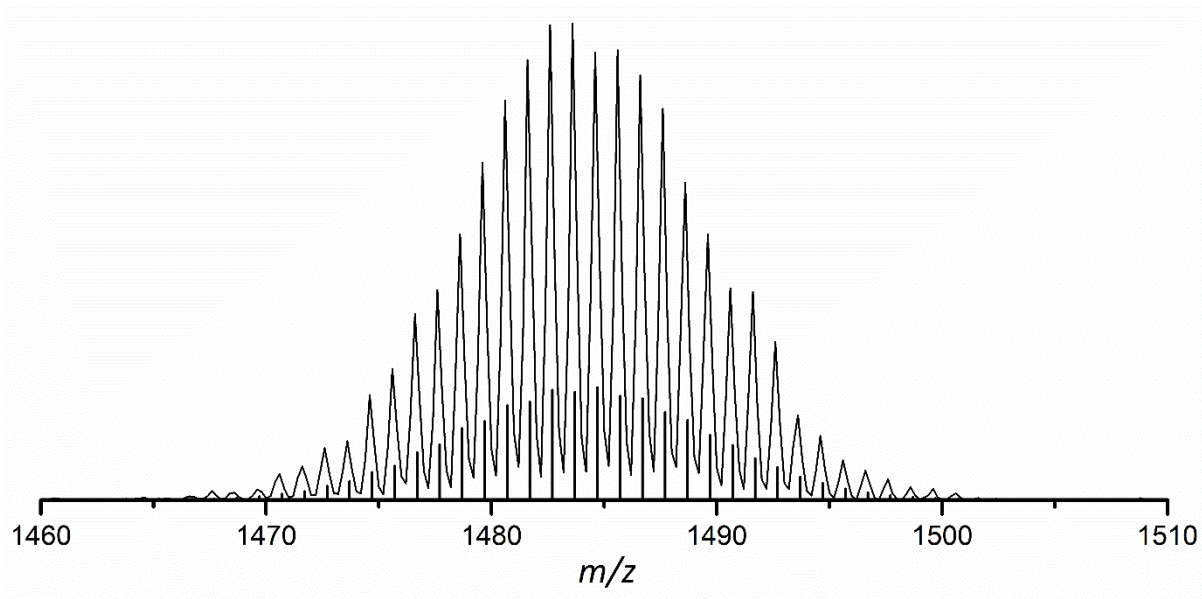
Figure S85. Detailed view on ESI MS signal of [Ge$_9${Si(TMS)$_3$}$_2$(CH$_2$)$_3$O-DAB$^{o\text{-}xyl}$]$^-$ at *m/z* 1484.8.
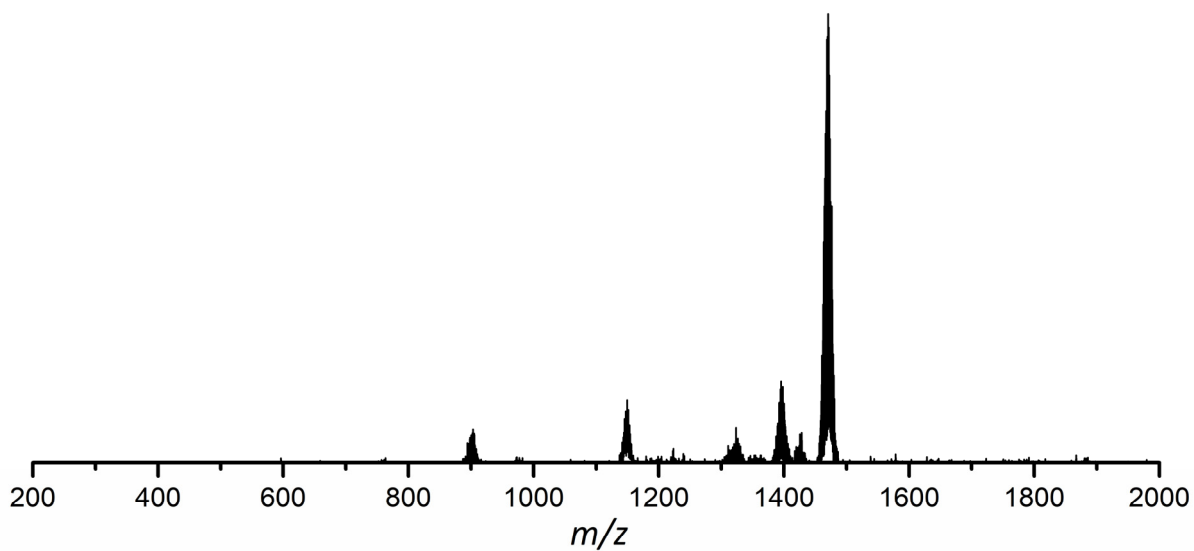
Figure S86. ESI MS spectrum (negative-ion mode, 3500 V, 300 °C) of a thf solution of [Ge$_9${Si(TMS)$_3$}$_2$CD$_3$C=N-DAB$^{o\text{-xyl}}$]$^-$. The molecule peak is detected at *m/z* 1470.8. A detailed view of the signal is provided in Figure S87. The signal detected at *m/z* 1396 can be assigned to [Ge$_9${Si(TMS)$_3$}$_3$]$^-$, which is formed during the ionization process in the mass spectrometer.
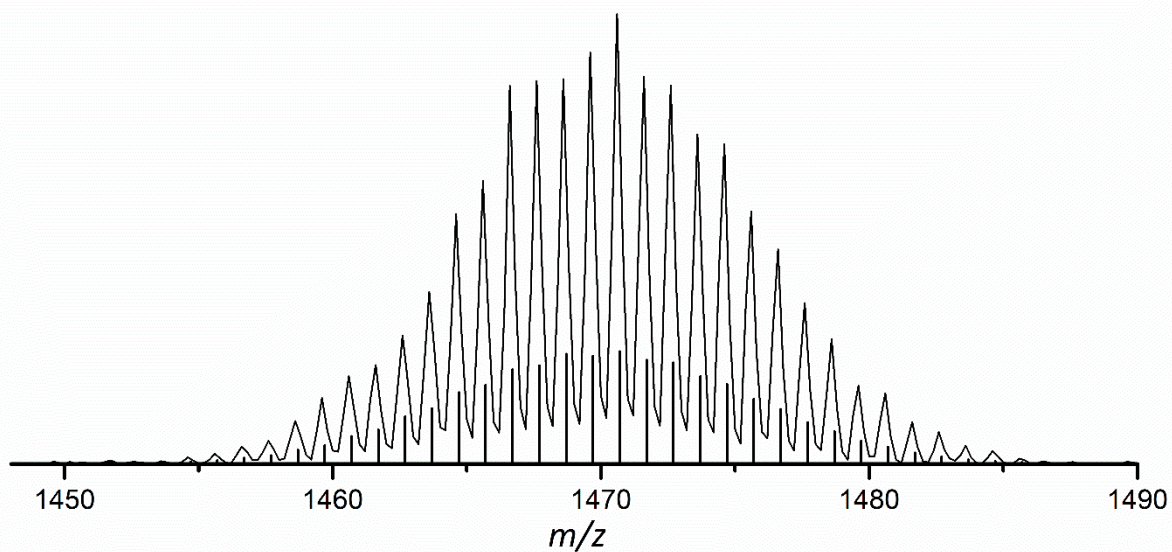
Figure S87. Detailed view on ESI MS signal of [Ge$_9${Si(TMS)$_3$}$_2$CD$_3$C=N-DAB$^{o\text{-xyl}}$]$^-$ at *m/z* 1470.8.
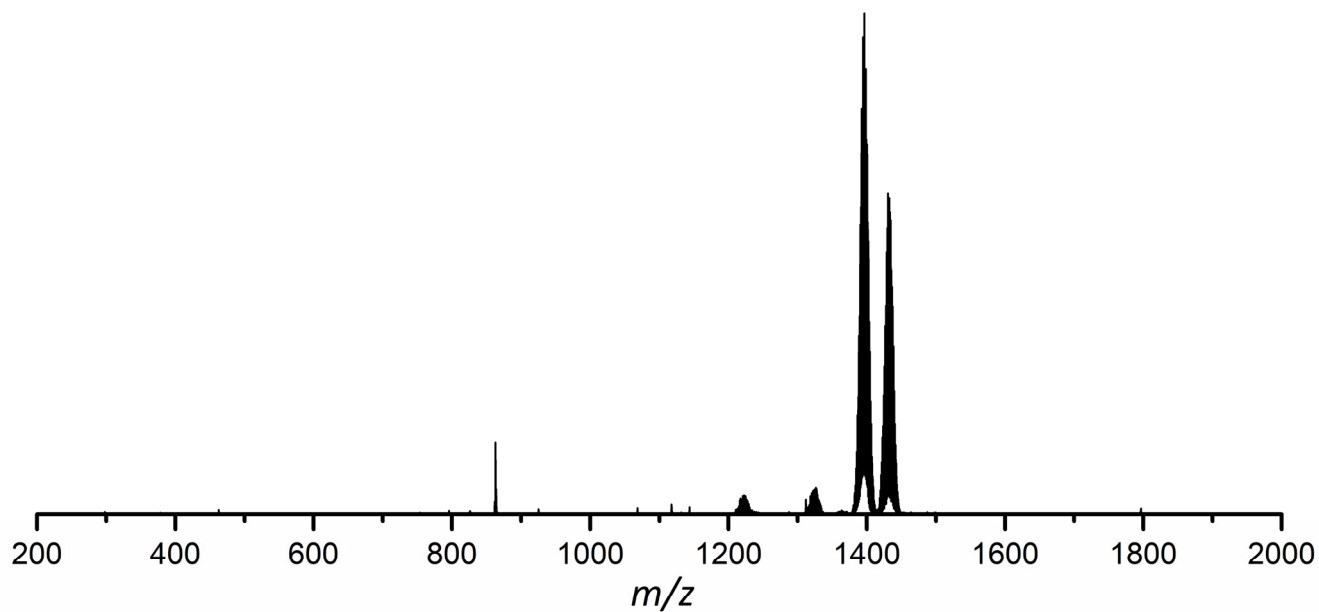
Figure S88. ESI MS spectrum (negative-ion mode, 3500 V, 300 °C) of a thf solution of $[Ge_9\{Si(TMS)_3\}_2(CH_2)_4O\text{-}B(N^iPr_2)_2]^-$. The molecule peak is detected at *m/z* 1432.8. A detailed view of the signal is provided in Figure S89. The signal detected at *m/z* 1396 can be assigned to $[Ge_9\{Si(TMS)_3\}_3]^-$, which is formed during the ionization process in the mass spectrometer.
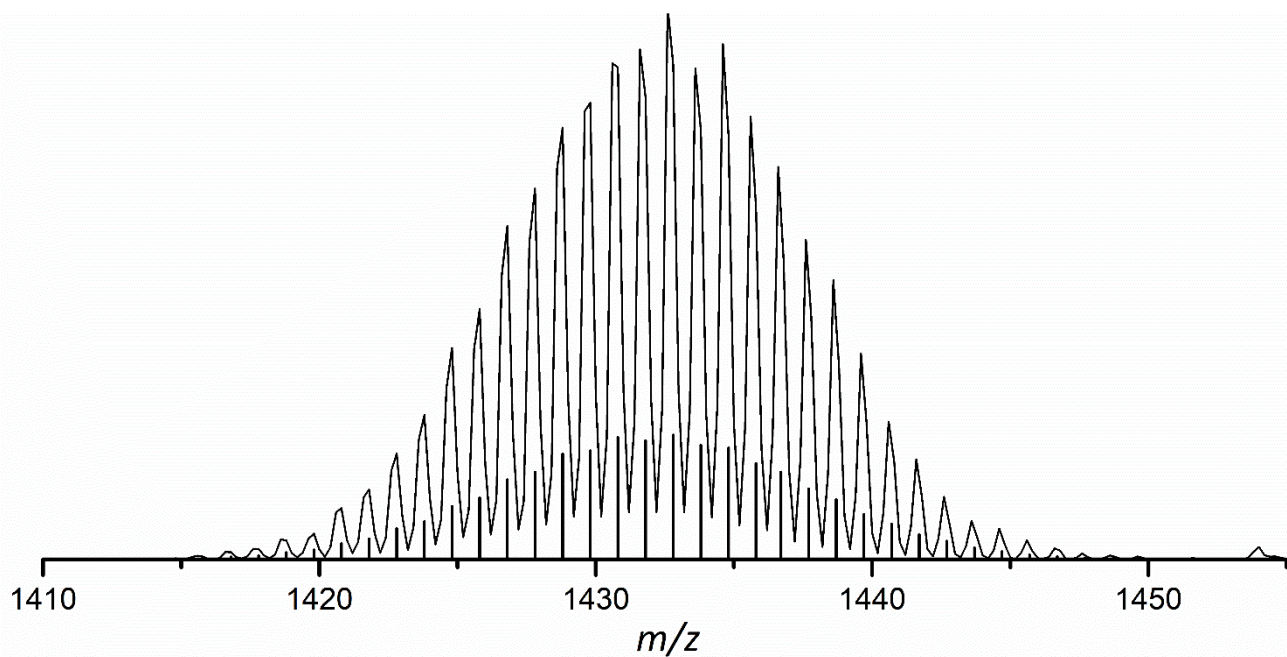
Figure S89. Detailed view on ESI MS signal of $[Ge_9\{Si(TMS)_3\}_2(CH_2)_4O\text{-}B(N^iPr_2)_2]^-$ at *m/z* 1432.8.
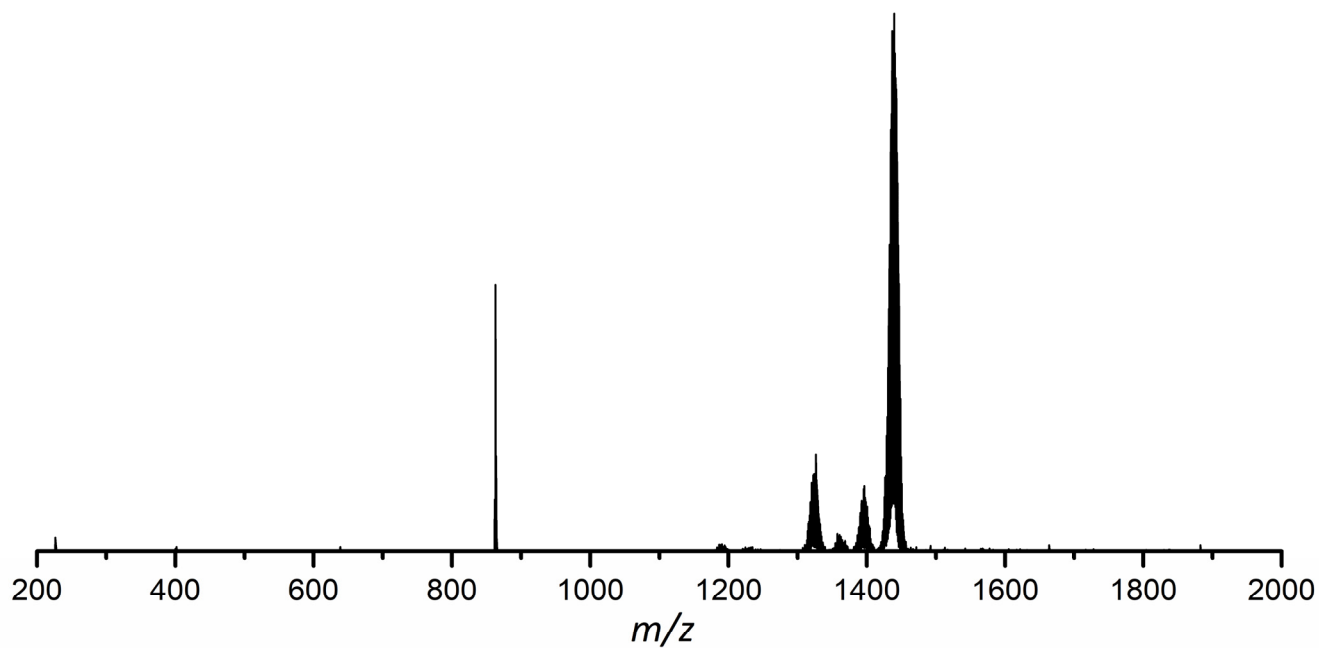
Figure S90. ESI MS spectrum (negative-ion mode, 3500 V, 300 °C) of a thf solution of $[Ge_9\{Si(TMS)_3\}_2(CD_2)_4O\text{-}B(N^iPr_2)_2]^-$. The molecule peak is detected at m/z 1440.8. A detailed view of the signal is provided in Figure S91. The signal detected at m/z 1396 can be assigned to $[Ge_9\{Si(TMS)_3\}_3]^-$, which is formed during the ionization process in the mass spectrometer.
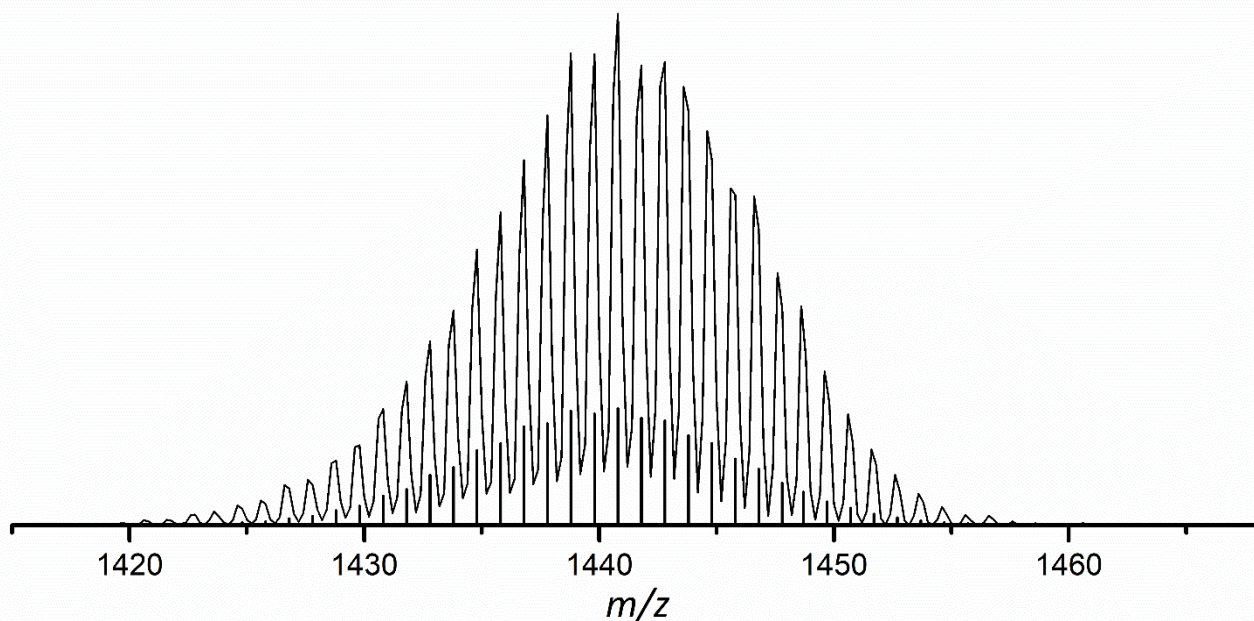
Figure S91. Detailed view on ESI MS signal of $[Ge_9\{Si(TMS)_3\}_2(CD_2)_4O\text{-}B(N^iPr_2)_2]^-$ at m/z 1440.8.
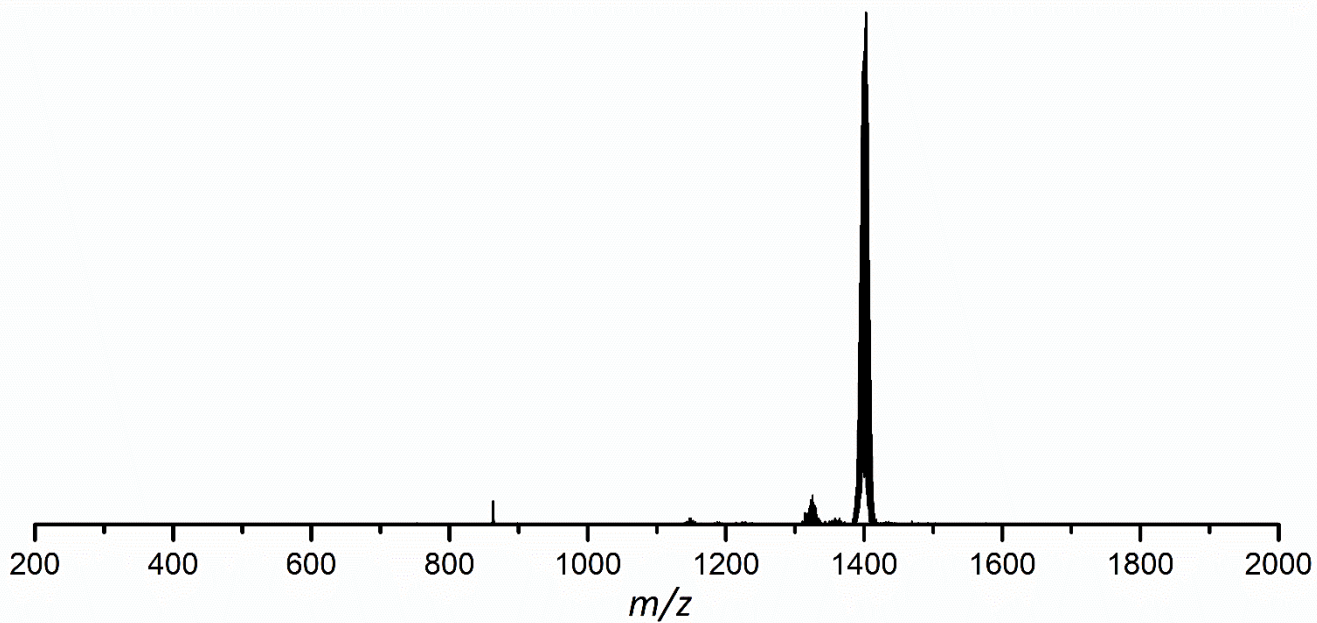
Figure S92. ESI MS spectrum (negative-ion mode, 3500 V, 300 °C) of a thf solution of [Ge$_9${Si(TMS)$_3$}$_2$CH$_3$C=N-B(N^{i}Pr$_2$)$_2$]$^-$. The molecule peak is detected at *m/z* 1401.8. A detailed view of the signal is provided in Figure S93.
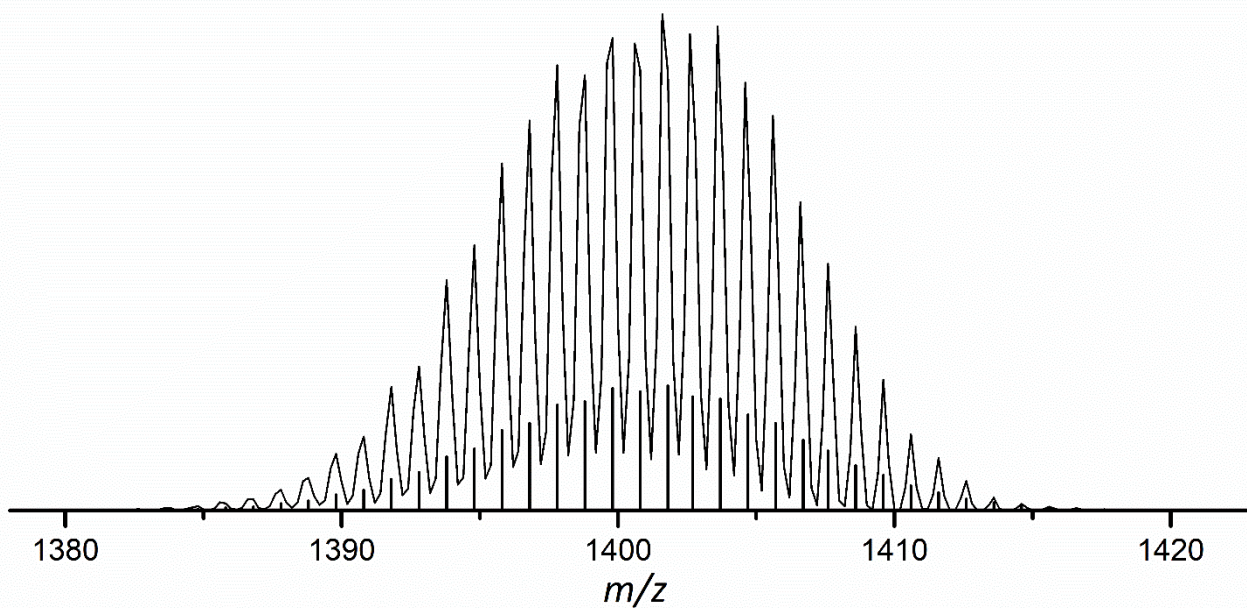
Figure S93. Detailed view on ESI MS signal of [Ge$_9${Si(TMS)$_3$}$_2$CH$_3$C=N-B(N^{i}Pr$_2$)$_2$]$^-$ at *m/z* 1401.8.
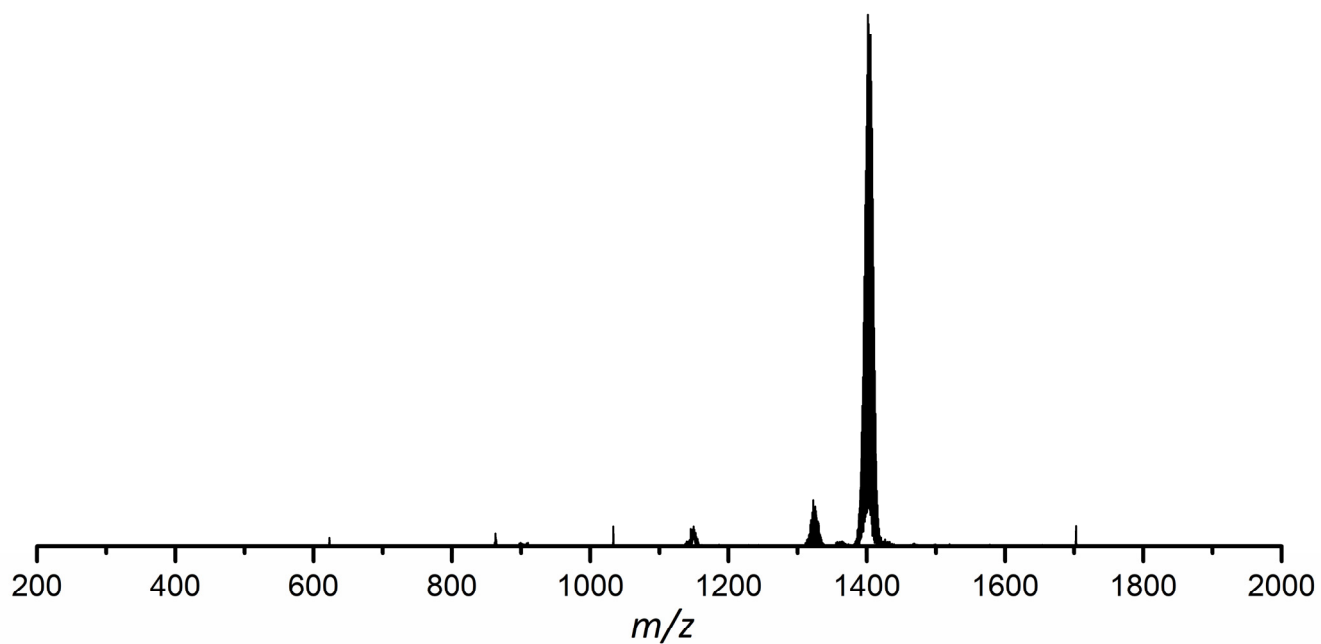
Figure S94. ESI MS spectrum (negative-ion mode, 3500 V, 300 °C) of a thf solution of [Ge$_9${Si(TMS)$_3$}$_2$CD$_3$C=N-B(N^{i}Pr$_2$)$_2$]$^-$. The molecule peak is detected at *m/z* 1404.8. A detailed view of the signal is provided in Figure S95.
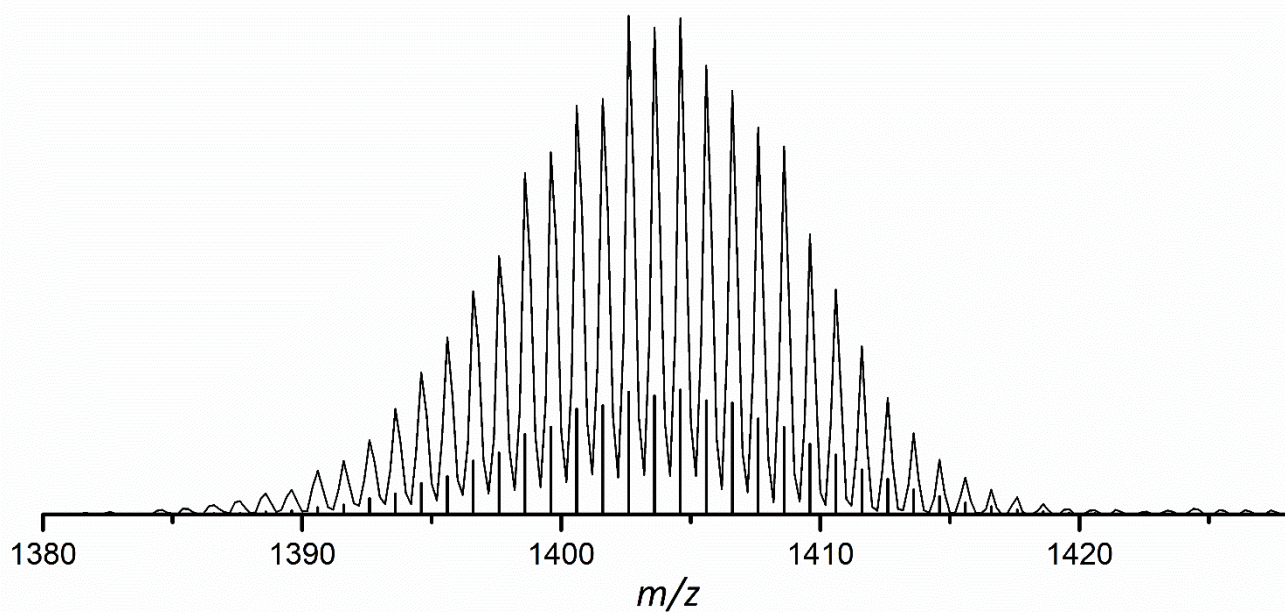
Figure S95. Detailed view on ESI MS signal of [Ge$_9${Si(TMS)$_3$}$_2$CD$_3$C=N-B(N^{i}Pr$_2$)$_2$]$^-$ at *m/z* 1404.8.

References

1   O. Kysliak and A. Schnepf, *Dalton Trans.*, 2016, **45**, 2404.
2   Y. Segawa, Y. Suzuki, M. Yamashita and K. Nozaki, *J. Am. Chem. Soc.*, 2008, **130**, 16069.
3   P. Chavant and M. Vaultier, *J. Organomet. Chem.*, 1993, **455**, 37.
4   G. M. Sheldrick, *Acta Crystallogr. Sec. C. Struct. Chem.*, 2015, **71**, 3.
5   A. L. Spek, *Acta Crystallogr. Sect. D. Biol. Crystallogr.*, 2009, **65**, 148.
6   G. R. Fulmer, A. J. Miller, N. H. Sherden, H. E. Gottlieb, A. Nudelman, B. M. Stoltz, J. E. Bercaw and K. I. Goldberg, *Organometallics*, 2010, **29**, 2176.